Growth and Characterisation of Radio Frequency Magnetron Sputtered Indium Tin Oxide Thin Films

Thesis submitted to
COCHIN UNIVERSITY OF SCIENCE AND TECHNOLOGY
in partial fulfillment of the requirements
for the award of the degree of
DOCTOR OF PHILOSOPHY

Nisha M.

Department of Physics
Cochin University of Science And Technology
Cochin – 682 022, Kerala, India

December 2006

Growth and Characterisation of Radio Frequency Magnetron Sputtered Indium Tin Oxide Thin Films

Ph.D thesis in the field of material science

Author:

Nisha M.
Optoelectronics Device Laboratory
Department of Physics
Cochin University of Science and Technology
Cochin – 682 022, Kerala, India
email: nishamadav@yahoo.com

Supervisor:

Dr. M.K. Jayaraj
Reader
Optoelectronics Device Laboratory
Department of Physics
Cochin University of Science and Technology
Cochin – 682 022, Kerala, India
email: mkj@cusat.ac.in

December 2006

Dr. M.K. Jayaraj
Reader
Department of Physics
Cochin University of Science and Technology
Cochin – 682 022

12th December 2006

Certificate

Certified that the work presented in this thesis entitled "*Growth and Characterisation of Radio Frequency Magnetron Sputtered Indium Tin Oxide Thin Films*" is based on the authentic record of research done by *Mrs. Nisha M.* under my guidance in the Department of Physics, Cochin University of Science and Technology, Cochin – 682 022 and has not been included in any other thesis submitted for the award of any degree.

Dr. M.K. Jayaraj
(Supervising Guide)

Phone : +91 484 2577404 extn 33 Fax: 91 484 2577595 email: mkj@cusat.ac.in

Declaration

Certified that the work presented in this thesis entitled "*Growth and Characterisation of Radio Frequency Magnetron Sputtered Indium Tin Oxide Thin Films*" is based on the original research work done by me under the supervision and guidance of Dr. M.K. Jayaraj, Reader, Department of Physics, Cochin University of Science and Technology, Cochin-682022 has not been included in any other thesis submitted previously for the award of any degree.

Cochin – 22
12th December 2006

Nisha M.

Acknowledgements

I wish to express my deepest sense of gratitude to the man who inspired and guided me to the art of experimenting: Dr.M.K.Jayaraj, my guide and supervisor. Among all the responsibilities and duties, he found time to share his expertise and knowledge, with us. I am deeply indebted to him for his gentle and inspiring guidance, forbearance, constant encouragement and support,

I extend my sincere thanks to Prof. V.C.Kuriakose, the Head of the Department of Physics and all other former Heads of the Department for allowing me to use the facilities. With a sense of gratitude, I remember all other faculty members of the Department of Physics. I am thankful to all the office and library staff of the Department of Physics and the technical staff at USIC for all the help and cooperation.

I am very much obliged and thankful to the Principal and colleagues of GHSS Ala and GHSS Muppathadam for all the support and encouragements to complete my thesis work.

I specially appreciate the sincere support of Dr Aldrin and Mr.Manoj for all the guidance given throughout the research work.

I would like to express my sincere appreciation to my colleagues in the OED lab Asha, Reshmi, Rahana, Joshy Sir, Ajimsha, Mini, Anoop, Anila teacher, Vanaja Madam, Saji, Aneesh, Ratheesh, Arun, Vineetha and Sasankan for all the help they had extended.

I am also thankful to Anusha, Vineeth, Jerome Sir, Meenu,, Sanjay Pramod and Sreejith for their valuble help during various stages of my work.

I thank my husband , Rajesh for his patience and support.

I record my deep and utmost gratitude to my parents and sister and brother in law for their selfless support, motivation, encouragements, patience and tolerance during the entire period of my work.

I thank all my well wishers.

Finally I thank God almighty

Nisha M.

Contents

Preface

Chapter1
Transparent Conducting Oxides

1.1 Introduction 5
1.2 Historical development of TCOs 6
1.3 Mechanism behind simultaneous transparency and conductivity 7
1.4 Correlation of optical and electrical properties 8
1.5 Properties of transparent conductors 10
    1.5.1 Electrical properties 10
    1.5.2 Optical properties and plasma frequency 11
    1.5.3 Optical and electrical performance of transparent conductors 12
    1.5.4 Work function 14
    1.5.5 Thermal stability 14
    1.5.6 Minimum deposition temperature 14
    1.5.7 Diffusion barrier between transparent conductors and sodium containing glass substrates 15
    1.5.8 Etching patterns 15
    1.5.9 Chemical durability 15
    1.5.10 Mechanical hardness 15
    1.5.11 Production costs 16
    1.5.12 Toxicity 16
1.6 Types of transparent conducting oxides 16
1.7 Applications of TCOs 22
1.8 Latest developments in transparent electronics 24
1.9 Conclusion 25
References 26

Chapter 2
Indium Tin Oxide: An Overview of the Present Status

2.1 Introduction 33
2.2 Crystal structure of ITO 34
2.3 Elecronic band structure of ITO 35
2.4 Optical properties of ITO 39
2.5 Electrical properties of ITO thin films 41
2.6 Work function of ITO 43
2.7 Parameters influencing the properties of ITO thin films 45
2.8 Deposition methods for ITO thin films 48
2.8.1 Chemical vapour deposition (CVD) 50
2.8.2 Vacuum evaporation 50
2.8.3 Electron beam evaporation 51
2.8.4 Sputtering 53
2.8.5 Pulsed laser deposition 55
2.9 Conclusion 57
References 58

Chapter 3
Deposition and Characterization Techniques

3.1 Introduction 67
3.2 Thin film preparation techniques 67
3.2.1 Vacuum evaporation 68
3.2.2 Sputtering 69
3.2.3 Pulsed laser deposition 75
3.2.4 Chemical vapour deposition 76
3.2.5 Spray pyrolysis 77
3.3 Characterization tools 78
3.3.1 Thin film thickness 78
3.3.1a Optical interference method 78
3.3.2 Surface morphology 79
3.3.3 Energy disperive X-ray analysis 80
3.3.4 X-ray diffraction studies 81
3.3.5 Optical characterization 82
3.3.5a Determination of optical bandgap 82

3.3.5bDeteermination of optical constants 83
3.3.6 Electrical characterization 86
3.3.6a Resistivity by two-probe method 86
3.3.6bHall measurement 86
3.4 Plasma studies 88
3.4.1 Introduction 88
3.4.2 Different types of plasma 92
3.4.2a Weakly ionized plasma 92
3.4.2b Strongly ionized plasma 92
3.4.2c Hot plasma 92
3.4.2d Cold plasma 93
3.5 Plasma diagnostics 93
3.5.1 Langmuir probe 94
3.5.1a Theory of Langmuir probe 95
3.5.1b Specifics of Langmuir probe 100
3.5.1c Practical complications 100
3.5.2Optical emission spectroscopy 101
3.5.2a Charge coupled device 101
3.5.2b Spectrometer 104
3.5.2c Monochromator calibration 106
3.5.2d OES recording 107
References 108

Chapter 4
Influence of Annealing and Substrate Temperature on the Properties of ITO Thin Films

4.1 Introduction 115
4.2 Experimental 115
4.3 Results and discussion 117
4.3.1 Influence of annealing temperature 117
4.3.2 Influence of substrate temperature 124
4.4 Comparison of post annealing and substrate temperature on the properties of ITO thin films 139
4.5 Conclusion 140
References 141

Chapter 5
Influence of RF Power on the Properties of ITO Thin Films

5.1 Introduction 147
5.2 Experimental 147
    5.2.1 Thin film deposition 147
    5.2.2 Plasma diagnostics 149
5.3 Structural characterization 150
5.4 Optical characterization 158
5.5 Electrical characterization 160
5.6 Plasma characterization 164
    5.6.1 Langmuir probe 164
        5.6.1a Ion density 166
        5.6.1b Electron temperature 168
    5.6.2 Optical emission spectral studies 170
5.7 Conclusion 171
References 173

Chapter 6
Influence of Bias Voltage on the Properties of ITO Thin Films Deposited on Flexible Substrates

6.1 Introduction 179
6.2 Experimental 179
6.3 Results and discussion 180
    6.3.1 Structural characterization 180
    6.3.2 Electrical characterization 182
    6.3.3 Langmuir probe analysis 185
    6.3.4 Optical emission spectral studies 190
6.4 Conclusion 191
References 193

Chapter 7

Summary and Outlook 197

Preface

The increasing interest in the interaction of light with electricity and electronically active materials made the materials and techniques for producing semitransparent electrically conducting films particularly attractive. Transparent conductors have found major applications in a number of electronic and optoelectronic devices including resistors, transparent heating elements, antistatic and electromagnetic shield coatings, transparent electrode for solar cells, antireflection coatings, heat reflecting mirrors in glass windows and many other. Tin doped indium oxide (indium tin oxide or ITO) is one of the most commonly used transparent conducting oxides. At present and likely well into the future this material offers best available performance in terms of conductivity and transmittivity combined with excellent environmental stability, reproducibility and good surface morphology.

Although partial transparency, with a reduction in conductivity, can be obtained for very thin metallic films, high transparency and simultaneously high conductivity cannot be attained in intrinsic stoichiometric materials. The only way this can be achieved is by creating electron degeneracy in a wide bandgap (E_g > 3eV or more for visible radiation) material by controllably introducing non-stoichiometry and/or appropriate dopants. These conditions can be conveniently met for ITO as well as a number of other materials like Zinc oxide, Cadmium oxide etc.

ITO shows interesting and technologically important combination of properties viz high luminous transmittance, high IR reflectance, good electrical conductivity, excellent substrate adherence and chemical inertness. ITO is a key part of solar cells, window coatings, energy efficient buildings, and flat panel displays. In solar cells, ITO can be the transparent, conducting top layer that lets light into the cell to shine the junction and lets electricity flow out. Improving the ITO layer can help improve the solar cell efficiency. A transparent

conducting oxide is a material with high transparency in a derived part of the spectrum and high electrical conductivity. Beyond these key properties of transparent conducting oxides (TCOs), ITO has a number of other key characteristics. The structure of ITO can be amorphous, crystalline, or mixed, depending on the deposition temperature and atmosphere. The electro-optical properties are a function of the crystallinity of the material. In general, ITO deposited at room temperature is amorphous, and ITO deposited at higher temperatures is crystalline. Depositing at high temperatures is more expensive than at room temperature, and this method may not be compatible with the underlying devices.

The main objective of this thesis work is to optimise the growth conditions of Indium tin oxide thin films at low processing temperatures. The films are prepared by radio frequency magnetron sputtering under various deposition conditions. The films are also deposited on to flexible substrates by employing bias sputtering technique. The films thus grown were characterised using different tools. A powder x-ray diffractometer was used to analyse the crystalline nature of the films. The energy dispersive x-ray analysis (EDX) and scanning electron microscopy (SEM) were used for evaluating the composition and morphology of the films. Optical properties were investigated using the UV-VIS-NIR spectrophotometer by recording the transmission/absorption spectra. The electrical properties were studied using vander Pauw four probe technique. The plasma generated during the sputtering of the ITO target was analysed using Langmuir probe and optical emission spectral studies.

An overview of the developments in the filed of transparent conducting oxides is briefly presented in ***Chapter 1.*** The advantages of semiconducting transparent thin films as a potential candidate over other materials are discussed. The review gives an insight into the developments in the field of transparent conducting oxides and transparent electronics.

Tin doped indium oxide (ITO) thin films are having numerous applications in opto-electronic devices and are widely used as the transparent conducing electrode in solar cells. ***Chapter 2*** presents a detailed literature review on the material.

Chapter 3 deals with the various deposition methods and characterisation tools employed in the present study. The characterisation tools include both material characterisation and plasma characterisation.

Chapter 4 presents the comparative study on the influence of annealing and substrate temperature on the properties of ITO thin films. Indium tin oxide thin films were deposited by RF magnetron sputtering of ITO target. The influence of annealing temperature and substrate temperature on the properties of the films were investigated. The as deposited films showed (222) and (440) peaks of Indium oxide, and an enhancement in the (222) peak intensity were observed with increase in annealing temperature. The films deposited onto preheated substrates showed (400) diffraction peak along with (222) peak. The structural characteristics also showed a dependence on the oxygen partial pressure during sputtering. Oxygen deficient films showed (400) plane texturing while oxygen-incorporated films were preferentially oriented in the [111] direction. An annealing temperature of 250^0C resulted in films with maximum bandgap and minimum resistivity whereas a substrate temperature of 150^0C was sufficient to get films with low resistivity and high bandgap.

Chapter 5 gives a detailed description on the influence of RF power on the properties of ITO thin films. Highly transparent and conducting ITO thin films were deposited at room temperature by RF magnetron sputtering of ITO target (95wt%In_2O_3 and 5wt% SnO_2) in pure argon atmosphere. Thin films were deposited on glass substrate without any intentional heating at various RF

powers ranging from 20W to 50W and the influence of RF power on the structural, electrical and optical properties of the films were investigated. The influence of fluorine doping on the properties of ITO thin films was also investigated as a function of RF power. Enhancement of crystallinity and conductivity was observed with increase in RF power. Film deposited on glass substrates at an RF power of 50W was oriented in the (100) direction and it showed a minimum resistivity of $1.27 \times 10^{-3} \Omega cm$. It has been observed that the film properties are greatly influenced by the plasma conditions during sputtering. Radio frequency (RF) plasma during sputtering was analyzed using Langmuir Probe and Optical Emission Spectroscopy (OES). The plasma parameters such as ion density and electron temperature were determined and their dependence on properties of thin film deposited under similar plasma conditions were studied. Plasma parameters were determined for different RF powers keeping the distance from the target a constant.

Chapter 6 presents the influence of bias voltage on the properties of ITO thin films. ITO films were prepared at room temperature by RF bias sputtering on polyimide substrates. The influence of bias voltage on the structural and electrical properties was investigated. The films deposited at negative bias voltages showed a preferred orientation along [111] direction while positive bias voltages resulted in poorly crystalline films. The maximum grain size of about 28nm and a minimum resistivity of 2.24×10^{-2} Ωcm were obtained for the film deposited onto substrates biased at –20V. The plasma parameters during the deposition was analyzed using Langmuir probe technique and the observed plasma parameters were correlated with the film characteristics.

Chapter 7 presents the summary and conclusion.

Publications

1. Influence of target to substrate spacing on the properties of ITO thin films, Aldrin Antony, **Nisha M.**, Manoj R., M.K. Jayaraj, Appl. Surf. Sci. 225 (2004) 294
2. Effect of substrate temperature on the growth of ITO thin films, **M.Nisha**, S.Anusha, Aldrin Antony, R.Manoj , M.K.Jayaraj, Appl. Surf.Sci. 252 (2005)1430
3. Characterization of radio frequency plasma using Langmuir probe and optical emission spectroscopy, **M. Nisha**, K. J. Saji, R. S. Ajimsha, N. V. Joshy, and M. K. Jayaraj, J.Appl.Phys 99 (2006) 033304
4. Influence of RF power on the properties of sputtered ITO thin films, **M.Nisha**, M.K.Jayaraj (To be communicated)
5. Growth of ITO thin films under various processing conditions, **M.Nisha**, M.K.Jayaraj (to be communicated)
6. Bias sputtered ITO thin films on flexible substrates, **M.Nisha**, M.K.Jayaraj (to be communicated)

Conference Proceedings

1. Influence of substrate temperature on the properties of rf magnetron sputtered ITO thin films, Anusha S, **Nisha M**, Aldrin Antony, Manoj R and M.K. Jayaraj, DAE Solid State Physics Symposium, 2003
2. Effect of heat treatment on the properties of rf magnetron sputtered ITO thin films, **M.Nisha**, Aldrin Antony, Manoj.R and M.K.Jayaraj, Proc. DAE Solid State Physics Symposium, 45 (2002) p327
3. RF magnetron sputtered ITO thin films on flexible substrates, **M.Nisha**, M.K.Jayaraj (DAE SSPS –2004).

4. Studies On RF Plasma Using Optical Emission Spectroscopy Saji K.J., **Nisha M**., Ajimsha R.S., Joshy N.V., M.K.Jayaraj (Presented in Plasma 2004).
5. Influence of RF power on the properties of ITO thin films, Nisha M, M.K.Jayaraj (Presented in ICMAT 2005)
6. Influence of process parameters on the properties of ITO thin films, **Nisha M.,** M.K.Jayaraj (Presented in OMTAT -2005)
7. Electrical and optical properties of $ZnGa_2O_4$ thin films deposited by pulsed laser deposition, K.MiniKrishna, **M.Nisha**, R.Reshmi, R.Manoj, A.S.Asha, M.K.Jayaraj, Materials Forrum 29(2005)243
8. Electrical and optical properties of α-$AgGaO_2$ synthesized by hydrothermal reaction**,** K.A.Vanaja, **M.Nisha**, A.S.Asha, M.K.Jayaraj (DAE – SSPS 2004)
9. Transparent p-$AgCoO_2$/n-ZnO p-n Junction, K.A.Vanaja, **M.Nisha**, A.S. Asha, M.K.Jayaraj (Photonics 2004)
10. Zinc gallate phosphor for electroluminescent device applications G.Anoop, R.Manoj, **M.Nisha**, R.Reshmi,K.Minikrishna, M.K.Jayaraj(NCLA 2005)
11. Growth of Single Phase In_2S_3 Films by Chalcogenisation of Metallic Indium Films, Rahana Yoosuf, Aldrin Antony, Manoj R, Mini Krishna, **Nisha M** , M.K.Jayaraj, Proc. DAE Solid State Physics Symposium, 46 (2003) p771
12. RF Magnetron sputtered calcium doped copper yttrium oxide p-type transparent semiconductor, Manoj R., Sreejith S.Pillai, **Nisha M,** Vanaja K.A, M.K.Jayaraj, Proc. DAE Solid State Physics Symposium 46(2003)387
13. Structural and Electrical Properties of $CuY_{1-x}Ca_xO_2$ p-type Transparent Conducting Films, Manoj R, Vanaja K.A., **Nisha M**, M.K.Jayaraj (Presented in ICMAT 2005).

CHAPTER 1

Introduction to Transparent Conducting Oxides

Abstract

*Transparent electronics is becoming an important field in material science. The developments in the filed of transparent electronics calls for the need of understanding the basic properties of transparent conducting oxides. This chapter gives the description of the characteristic properties and applications of transparent conducting oxides. A brief discussion on the recent developments in transparent electronics is also presente*d.

1.1 Introduction

Rapid and significant advances have been taking place in the field of semiconductor physics during the past few decades. In the field of research and industry, semiconductors are the subject of great interest because of their numerous practical applications. Scientists are interested in developing those materials, which maintain their required properties under extreme environmental conditions. One of the most important fields of current interest in material science is the fundamental aspects and applications of semiconducting transparent thin films. Such materials are highly conducting and exhibit high transparency in the visible region of the electromagnetic spectrum. Because of this unique property, transparent conducting oxides (TCOs) are finding wide range of applications in research and industry. They are essential part of technologies that require large area electrical contact and optical access in the visible portion of the light spectrum.

A TCO is a wide band gap semiconductor that has relatively high concentration of free electrons in the conduction band. These arise either from defects in the material or from extrinsic dopants, the impurity levels of which lie near the conduction band edge. The high carrier concentration [1] causes absorption of electromagnetic radiations in both visible and IR portions of the spectrum. A TCO must necessarily represent a compromise between electrical conductivity and optical transmittance; a careful balance between these properties is required. Reduction of the resistivity involves either an increase in carrier concentration or in the mobility. But increase in the former will lead to an increase in the visible absorption while the increase in mobility has no adverse effect on the optical properties. So the search for new TCO materials must focus on achieving materials with higher electron motilities. The above target can be achieved by making material with longer electron relaxation times or by identifying materials with lower electron effective masses.

Most of the useful oxide-based materials are *n*-type conductors that ideally have a wide band gap (>3 eV), the ability to be doped to degeneracy, and a conduction band shape that ensures that the plasma absorption edge lies in the infrared range. The transparency of the TCO films in the visible region is a result of the wide band gap of the material and the n type conductivity is mainly due to the oxygen ion vacancies that contribute to the excess electrons in the metal atoms [2].

1.2 Historical Development of TCOs

The first report on TCO was published in 1907 by Badeker [3]. He reported that thin films of Cadmium metal deposited in a glow discharge chamber could be oxidized to become transparent while remaining electrically conducting. Since then, the commercial value of these thin films has been recognized, and the list of potential TCO materials has expanded to include Aluminium doped ZnO [4], SnO_2 [5], Fluorine doped In_2O_3 [6] etc. Most of the research to develop highly transparent and conducting thin films has focussed on n-type semiconductors consisting of metal oxides. Historically, TCO films composed of binary compounds which were developed by means of physical and chemical deposition methods [7, 8]. One of the advantage of using binary compound as TCO material is that their chemical composition in film deposition is relatively easier to control than that of ternary and multicomoponent oxides. Until now, undoped and impurity doped films such as SnO_2, In_2O_3, ZnO, CdO were developed. These materials have a free electron concentration of the order of 10^{20} cm $^{-3}$ provided by native donors such as oxygen vacancies and interstitial metal atoms. Since impurity doped materials can use both native and impurity donors, undoped binary materials have got limited range of applications. In addition to these binary compounds, ternary compounds such as Cd_2SnO_4, $CdSnO_3$ and $CdIn_2O_4$ were also developed prior to 1980[9,10].

In order to get TCO films suited for specialized applications, new TCO materials have been studied actively. TCO materials consisting of multicomponent oxides have been developed in 1990s. In these material systems, TCO materials consisting of ternary compounds such as Zn_2SnO_4[11],$MgIn_2O_4$[12] , $ZnSnO_3$[13], $GaInO_3$[14] as well as multicomponent oxides composed of combinations of these ternary compounds were developed. The advantage of the multicomponent oxide materials is the fact that their electrical, optical, chemical and physical properties can be controlled by altering their chemical compositions.

In 1999, Minami et al [15] reported $Zn_2In_2O_5$-$MgIn_2O_4$ multicomponent oxide as a new TCO material. Transparent conductors were prepared by magnetron sputtering of compounds such as $MgIn_2O_4$, $ZnSnO_3$, $GaInO_3$ $Zn_2In_2O_5$ and $In_4Sn_3O_{12}$.

1.3 Mechanism Behind Simultaneous Transparency and Conductivity

As far as the properties of a solid are concerned, one can see that optical transparency and electrical conductivity are antonyms to each other. This can be easily proved using the basic equations in electromagnetic theory [16,17] as described below.

For em waves passing through an uncharged semiconducting medium, the solution to Maxwell's equation gives the real and complex parts of the refractive index as

$$n^2 = \frac{\varepsilon}{2}\left[\left\{1+\left(\frac{2\sigma}{\upsilon}\right)^2\right\}^{1/2}+1\right] \quad \text{and}$$

$$k^2 = \frac{\varepsilon}{2}\left[\left\{1+\left(\frac{2\sigma}{\upsilon}\right)^2\right\}^{1/2} - 1\right]$$

where n is the refractive index of the medium, k is the extinction coefficient, ε is the dielectric constant, σ is the conductivity of the medium and ν is the frequency of the electromagnetic radiation. In the case of an insulator $\sigma \to 0$, $n \to \varepsilon^{1/2}$ and $k \to 0$. This implies that an insulator is transparent to electromagnetic waves.

For a perfect conductor, the solution to the Maxwell's equation yields, the reflected and transmitted component of the electric field vector as $E_R = -E_I$ and $E_T = 0$. This means that the wave is totally reflected with a 180^0 phase difference. Or in other words, a good conductor reflects the radiations incident on it, while a good insulator is transparent to the electromagnetic radiations.

1.4 Correlation of Electrical and Optical Properties

The optical phenomena in the IR range can be explained on the basis of Drude's theory for free electrons in metals [18-20]. When the free electrons interact with an em field, it may lead to polarizatrion of the field within the material. It affects the relative permittivity ε. For an electron moving in an electric field, the equation of motion can be written as,

$$m\left(\frac{d}{dt} + \frac{1}{\tau}\right)\delta v(t) = F \qquad (1.1)$$

where τ is the relaxation time .

The force on an electron in an alternating field is given by

$$F = -eE\, e^{-i\omega t} \qquad (1.2)$$

Let us assume a solution to (2) in the form $\delta v = \delta v\, e^{-i\omega t}$

Then (1.1) becomes, $m\left(-i\omega+\frac{1}{\tau}\right)\delta v=-eE$

or , $$\delta v=-\frac{e\tau/m}{1-i\omega\tau} \qquad (1.3)$$

The current density is j = nqδv = $\frac{ne^2\tau}{m(1-i\omega\tau)}E$, where n is the electron concentration and q is the charge on the electron.

The electrical conductivity is $\sigma(\omega)=\frac{ne^2\tau}{m(1-i\omega\tau)}=\sigma_0\frac{1+i\omega\tau}{1+(\omega\tau)^2}$ (1.4)

Here, $\sigma_0 = ne^2\tau / m$ is the dc conductivity.
At high frequencies, $\omega\tau >> 1$,we can write,

$$\sigma(\omega)=\sigma_0\left(\frac{1}{(\omega\tau)^2}+\frac{i}{\omega\tau}\right)=\frac{ne^2}{m\omega^2\tau}+i\frac{ne^2}{m\omega} \qquad (1.5)$$

In this equation the imaginary term is dominant and is independent of τ. Then we can express the result as a complex dielectric constant instead of expressing it as a complex conductivity.

The dielectric constant $\varepsilon = 1 + (4\pi P/E)$ where $P=-\frac{ne^2/m}{\omega^2+i\omega/\tau}E$.

Then,

$$\varepsilon(\omega)=1-\frac{4\pi ne^2/m}{\omega^2+i\omega/\tau}. \qquad (1.6)$$

This expression gives the dielectric constant of a free electron gas. For $\tau\rightarrow\infty$ the dielectric constant is positive and real if $\omega^2 > 4\pi ne^2/m$.

Electromagnetic wave can not propagate in a medium with negative dielectric constant because then wave vector is imaginary and the wave decays exponentially. Waves incident on such a medium are totally reflected. We can denote the cut off frequency as

$$\omega_p = \left(4\pi ne^2 / m\right)^{1/2} \tag{1.7}$$

which is also known as the plasma frequency. The material is transparent to the em radiation whose frequency is greater than the plasma frequency.

1.5 Properties of Transparent Conductors

1.5.1 Electrical properties

Numerous investigations have been made on the electrical properties of transparent conducting oxide films to understand the conduction phenomena involved [21-23]. Researchers have made a systematic study on the effect of various parameters such as nature and temperature of the substrate, film thickness, dopant and its concentration etc [24-26] on the electrical properties of TCO films in order to optimize the growth conditions.

The high conductivity of the TCO films results mainly from stoichiometric deviation. The conduction electrons in these films are supplied from donor sites associated with oxygen vacancies or excess metal ions [27]. These donor sites can be easily created by chemical reduction. Unintentional doping which happens mainly in the case of film deposition by spray pyrolysis, intentional doping and contamination by alkali ions from the glass substrate can affect electrical conductivity.

One of the major factor governing the conductivity of TCO films is the carrier mobility. The mobility of the carriers in the polycrystalline film is dependent on the mechanism by which carriers are scattered by lattice imperfections. The various scattering mechanisms involved in semiconducting thin films are acoustic deformation potential scattering, piezoelectric scattering, optical phonon scattering, neutral impurity scattering, ionized impurity scattering, electron-electron scattering and grain boundary scattering [28-30] .

In the case of a polycrystalline film, the conduction mechanism is dominated by the inherent inter-crystalline boundaries rather than the intra-crystalline characteristics. These boundaries generally contain fairly high densities of interface states which trap free carriers by virtue of the inherent disorders and the presence of trapped charges. The interface states results in a space charge region in the grain boundaries. Due to this space charge region, band bending occurs, resulting in potential barriers to charge transport.

1.5.2. Optical properties and plasma frequency

The optical properties of a transparent conducting film depend strongly on the deposition parameters, microstructure, level of impurities and growth techniques. Being transparent in the visible and NIR range and reflecting to IR radiations, they act as selective transmitting layer. The spectral dependence of a TCO is given in figure1.1.

The spectral dependence shows that for wavelengths longer than plasma wavelength (λ_p) the TCO reflects radiation while for shorter wavelengths upto λ_{gap} TCO is transparent. At frequencies higher than the plasma frequency, the electrons cannot respond, and the material behaves as a transparent dielectric. At frequencies below the plasma frequency, the TCO reflects and absorbs incident radiation.

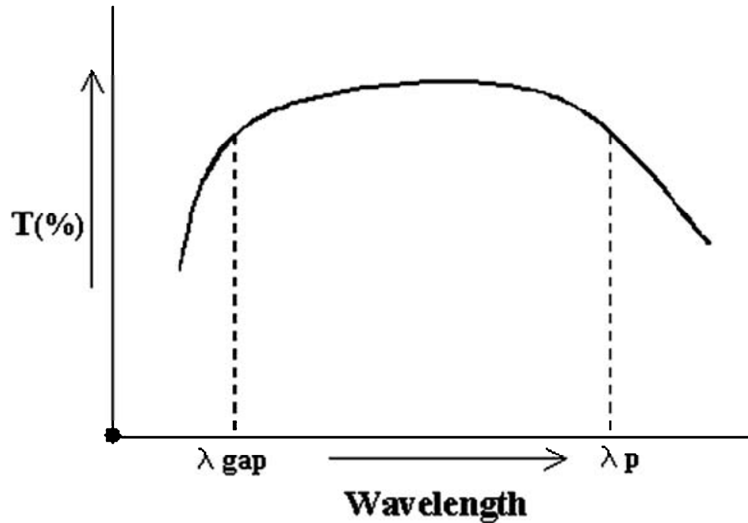

Figure 1.1. Spectral dependence of TCO

For most TCO materials, the plasma frequency falls in the near-infrared part of the spectrum, and the visible region is in the higher, transparent frequency range. The plasma frequency increases approximately with the square root of the conduction-electron concentration. The maximum obtainable electron concentration and the plasma frequency of TCOs generally increase in the same order as the resistivity [31].

1.5.3. Optical and Electrical Performance

TCOs can be judged on the basis of the two important qualities namely optical transmission and electrical conductivity. Since these two parameters are somewhat inversely related, a method of comparing the properties of these films by means of a figure of merit is essential. Figures of merit have allowed researchers to compare the various results in a reasonable and direct manner. Researchers have developed different methods for finding the figures of merit of the films.

One of the earliest equations defining a figure of merit was developed by Fraser and Cook [32] and is given by the relation $F_{FC} = \frac{T}{R_s}$ where T is the transmission and R_s is the sheet resistance of the thin film. This value was often multiplied by 1000 to allow comparisons of numbers greater than one. This definition depends on the film thickness.

Another way of defining the figure of merit F_H, developed by Haacke [33] is also related to the above definition. However, F_H puts more emphasis on the optical transparency because F_{FC} was too much in favor of sheet resistance, resulting in a maximum figure of merit at relatively large film thicknesses. The figure of merit was redefined as $F_H = \frac{T_a^x}{R_s}$ where x>1. Haacke selected the value of x = 10. The definition by Haacke is also thickness dependent. Iles and Soclof [34] defined the figure of merit that is independent of film thickness and is given by $F_{1s} = R_s[1-T] = \frac{\alpha}{\sigma}$. By this definition, a lower value of figure of merit indicates films of better quality.

Most of the variation in the figure of merit is due to variation in mobility, but the free-electron concentration does not affect the figure of merit. The electron mobility is determined by the electron-scattering mechanisms that operate in the material. First of all, some scattering mechanisms, such as scattering of electrons by phonons, are present in pure single crystals. Practical TCOs need much higher doping levels and for these high doping levels, scattering by the ionised dopant atoms become another important mechanism that alone limits the mobility. This maximum mobility is lowered still further by other scattering mechanisms such as grain-boundary scattering, present in polycrystalline thin films. The best TCO films, ZnO:F and Cd_2SnO_4, have been prepared with mobilities in the range of 50–60 $cm^2\ V^{-1}\ s^{-1}$.

1.5.4. Work Function

The work function of a TCO is defined as the minimum energy required to remove an electron from the conduction band to the vacuum. ITO has a work function of 4.8eV [35,36].

1.5.5. Thermal Stability of Transparent Conductors

TCOs will generally will have an increase in resistivity if heated to a high enough temperature for a long enough time. TCOs remains stable to temperatures slightly above the optimised deposition temperature. The high temperature stability of tin oxide films allows coated glass to be reheated in order to strengthen it by tempering. The thermal stability of tin oxide films is currently limited by the softening temperature of glass substrates than by any thermal decomposition of the SnO_2:F film.

1.5.6. Minimum Deposition Temperature

When TCOs are deposited onto a substrate, the temperature of the substrate generally must be maintained at a sufficiently high temperature in order to have the required properties in the TCO. The required temperatures are usually found to increase in the following order: Ag or ITO$<$ZnO$<SnO_2<Cd_2SnO_4$ [20]. Silver or ITO is preferred for deposition on thermally sensitive substrates, such as plastic, while cadmium stannate requires very refractory substrates to obtain its best properties.

1.5.7. Diffusion Barriers between Transparent Conductors and Sodium Containing Glass Substrates

When TCOs are deposited on sodium containing glass, such as soda-lime glass, sodium can diffuse into the TCO and increase its resistance. This effect is particularly noticeable for tin oxide, because sodium diffuses rapidly at the high substrate temperatures (often 550^0C) used for its deposition. It is common to deposit a barrier layer on the glass prior to the deposition of tin oxide. Silica or alumina is used commonly as the barrier layer between soda-lime glass and tin oxide.

1.5.8. Etching Patterns

Some applications of TCOs, such as displays, heaters, or antennas, parts of the TCO must be removed. Zinc oxide is the easiest material to etch, tin oxide is the most difficult, and indium oxide is intermediate in etching difficulty. Series-connected thin film solar cells need to remove TCOs along patterns of lines. This removal is usually carried out by laser ablation.

1.5.9. Chemical Durability

The ability of a TCO to withstand corrosive chemical environments is inversely related to its ease of etching. Tin oxide is the most resistant TCO, while zinc oxide is readily attacked by acids or bases.

1.5.10. Mechanical Hardness

The mechanical durability of TCOs is related to the hardness of the crystals from which they are formed. Titanium nitride and tin oxide are even harder than glass

and can be used in applications that are exposed to contact. zinc oxide is readily scratched, but can be handled with care. Thin silver films are so fragile that they cannot be touched and can be used only when coated with protective layers.

1.5.11. Production Costs

The costs of producing a transparent conducting material depend on the cost of the raw materials and the processing of it into a thin layer. The cost of the raw materials generally increases in this order: Cd <Zn<Ti< Sn< Ag< In. The costs of the deposition methods typically increase in the following order: Atmospheric pressure CVD<Vacuum Evaporation<Magnetron Sputtering<Low-Pressure CVD < Sol-gel <Pulsed Laser Deposition. The speed of the process is also very important in determining the cost.

1.5.12. Toxicity

Some of the elements used in TCOs are toxic. This increases the cost of processing them because of the need to protect workers and prevent the escape of toxic materials into the environment. Toxicity of the elements generally increases in as Zn<Sn<In<Ag<Cd. Cadmium compounds are carcinogens and thus are heavily regulated and even prohibited from some applications.

1.6 Types of Transparent Conducting Oxides

Reports show that the oxides of p-block heavy metal cations with ns^0 configuration can be changed to n-type conductors by electron doping. Most of the earlier research in the area of TCOs were focussed on n-type semiconductors consisting of metal oxides. Due to the lack of availability of p-type TCOs, the interest in semiconducting TCOs have been low [37]. Since p-n junction is an

essential structure in a wide variety of semiconductor devices, the realisation of transparent electronics calls for the development p-type TCO materials also.

The nonexistence of p-type transparent conducting oxides is thought to originate from a general characteristic in the electronic structure of oxides: the strong localization of the upper edge of the valence band to oxide ions. Therefore, any finding of a p-type conducting oxide must include modification of the energy band structure to reduce the localization behaviour, which in turn requires new insight into the relation between electronic structure and properties of oxide materials [38]. In the technological field, finding such a material may open the way to new applications such as ultraviolet-emitting diodes.

If the localization behaviour in the valence band of typical oxides is to be modified, the cationic species is required to have a closed shell whose energy is almost comparable to those of the 2*p* levels of oxygen anions. The closed shell valence state is required to avoid coloration due to intra-atomic excitations. The cations we selected are Cu^+, Ag^+ and Au^+, which have the electronic configuration $d^{10}s^0$. Within the group of cations having the same electronic configuration, the energy of the d^{10} closed shell electrons is highest for these three cations, and is expected to overlap with that of the 2*p* electrons on oxide ions.

The second condition to be considered in the selection of the candidate oxide is the crystal structure which enhances the covalency in the bonding between the cation and oxide ion. One of the possible structures is the delafossite structure (Fig 1.2). The chemical formula of a delafossite is AMO_2 in which A and M are monovalent cation and a trivalent anion respectively. Delafossites have a hexagonal, layered crystal structure with the layers of A cations and MO_2 stacked alternately perpendicular to the c axis. There is no oxygen within the A cation layers, and only two oxygen atoms are linearly coordinated to each a

cation in axial positions. The MO_2 layers consists of MO_6 octahedra, sharing edges. Each oxide ion is in pseudo-tetrahedral coordination.

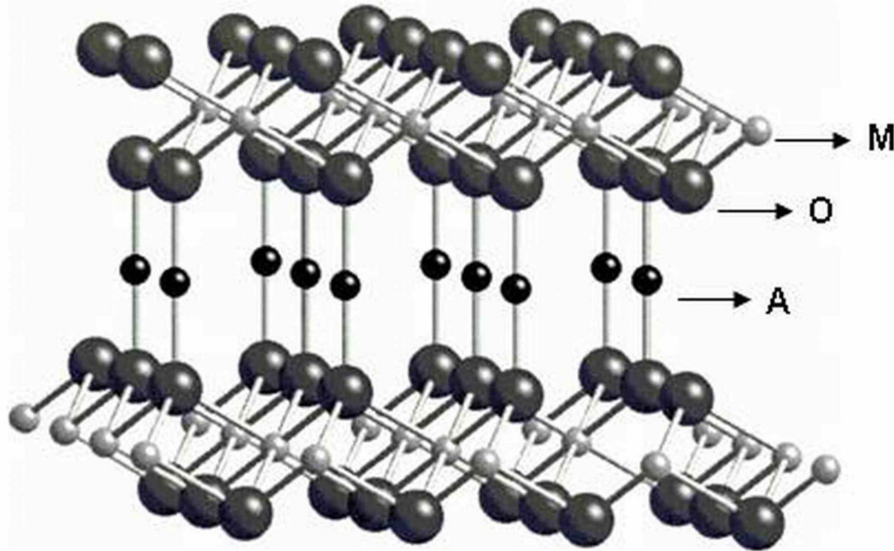

Figure 1.2. Delafossite structure

Recent interest has been directed to applications of p-type conductors, that exploit their transparency in the infra red spectral range where they could serve as RF shields for IR sensors. In this case optical transparency is less important while good conductivity is essential. For photovoltaic applications transparency is of paramount importance. Transparency and conductivity co-exist in materials but one has to trade transparency for conductivity and vice versa. Unless carrier mobility is increased, this trade off will be more severe in the case of p-type materials. Several strategies has been adopted to expand the possibilities in the delafossite material AMO_2, and several has been implemented in thin film form.

Transparent, p-type semiconducting crystalline thin films have recently gained tremendous interest in the field of active devices. All-transparent junctional

devices have begun a new generation in the optoelectronics technology called *Invisible Electronics*. In 1997, Kawazoe et al.[39] from Tokyo Institute of Technology, Japan, reported for the first time, p-type conductivity in a highly transparent thin film of copper aluminum oxide ($CuAlO_{2+x}$). This has opened up a new field in optoelectronics device technology, the so-called *Transparent Electronics* or *Invisible Electronics* , where a combination of the two types of TCOs in the form of a p-n junction could lead to a ‘‘functional’’ window, which transmits visible portion of solar radiation yet generates electricity by the absorption of the UV part. Until then non-stoichiometric and doped versions of various new types of p-type transparent conducting oxides with improved optical and electrical properties have been synthesized.

Now for diverse device applications, it is very important to prepare various new types of p-TCOs with superior optical and electrical characteristics, at least comparable to the existing, widely used n-TCOs, which have a transparency above 80% in the visible region and a conductivity of about 1000 S cm^{-1} or more. Intense works have been done for the last five years in this direction to fabricate new p-TCOs by various deposition techniques. Also quite a number of works have been carried out for proper understanding of the structural, optical and electrical characteristics of p-TCOs.

p-type transparent $CuAlO_2$ semiconductor films were made by the spin-on technique from nanocrystals [40]. The nanocrystals were synthesized by a hydrothermal metathesis reaction. Scanning electron microscopy, X-ray diffraction and energy dispersive X-ay spectrometry suggest that the films contain nanocrystalline phases of $CuAlO_2$. Both the Hall technique and Seebeck measurements reveal that the film is p-type and a very high room-temperature conductivity of 2.4 S cm^{-1} is achieved. This success in fabricating a high-conductivity transparent $CuAlO_2$ film indicates that nanotechnology will be helpful in enhancing the conductivity of p-type transparent semiconductors.

The sol-gel synthesis and pulsed laser deposition (PLD) of Cu_2SrO_2 opened up the possibility to make phase pure p-type TCOs by a variety of methods [41]. For Cu_2SrO_2 by the chemical solution route, samples were made by spray deposition on quartz substrates using an aqueous solution of copper formate and strontium acetate. Phase pure materials were obtained by an optimum two stage annealing sequence. This initial work led to the development of good quality homogeneous films by a related sol-gel approach. They have also used pulsed laser deposition (PLD) to deposit Cu_2SrO_2 and $CuInO_2$ thin films on quartz substrates and obtained improved conductivities in the $CuInO_2$ thin films.

p-type conduction in ZnO films with high hole concentration is being reported[42]. The films were grown on Si buffered with Si_3N_4 by radio-frequency (RF) magnetron sputtering along with nitrogen-implanted process. The role of nitrogen-implanted concentration in the electrical and photoluminescence, (PL) of ZnO films were investigated. The exact origin of the UV emission and local structural behaviors of p-type ZnO films grown on Si_3N_4/Si was also studied. The hole concentration, carrier mobility, and resistivity of p-type ZnO films were $5.0x10^{16}$– $7.3x10^{17}$ cm^{-3}, 2.51–6.02 cm^2 $V^{-1}s^{-1}$, and 10.11–15.3 Ωcm, respectively.

As-grown n-type ZnO films doped with phosphorus showing electron concentrations of 10^{16}–$10^{17}cm^{-3}$, have been converted to p-type ZnO by a thermal annealing process at a temperature above 800 °C under a N_2 ambient [43]. The electrical properties of the p-type ZnO showed a hole concentration of $1.0x10^{17}$– $1.7x10^{19}cm^{-3}$, a mobility of 0.53– 3.51 $cm^2V^{-1}s^{-1}$, and a low resistivity of 0.59 – 4.4 Ωcm. The phosphorus-doped ZnO thin films showed a strong photoluminescence peak at 3.35 eV at 10 K, which is closely related to neutral acceptor bound excitons of the p-type ZnO. This thermal activation process was

very reproducible and effective in producing phosphorus-doped p-type ZnO thin films, and the p-type ZnO was very stable.

ZnO:As films is reported to show good p-type conductivity with hole carrier concentrations up to the mid-10^{17} cm^{-3} range at room temperature using As as the dopant element[44]. The electrical and optical properties of p-type ZnO:As were explained very reasonably within the context of accepted semiconductor models. The experimental results were consistent with those calculated. It is demonstrated that ZnO:As films show electrical and optical behaviors that make them excellent candidates for a good p-type layer for ZnO-based devices.

First-principles band structure methods was employed to study the electronic and optical properties of p-type transparent oxides $A^{II}Cu_2O_2$, where A=Mg, Ca, Sr, and Ba, as well as their host material Cu_2O [45]. The trend of band gap variation of $A^{II}Cu_2O_2$ as a function of A^{II} is explained in terms of atomic energy levels and atomic sizes of the A^{II} elements. The calculated dipole matrix elements show that transitions between the valence band maximum(VBM) and other valence states are negligible within 4 eV below the VBM. This explains the transparencies in these p-type TCOs. They suggested that adding a small amount of Ca (~16%) into $SrCu_2O_2$ can increase the band gap and reduce the hole effective mass of $SrCu_2O_2$, thereby increasing the transparency and conductivity.

Most of the delafossite films reported in literature is based on monovalent copper. The corresponding silver compounds are harder to produce and require ion-exchange synthesis rather than a solid state reaction. Tate [46] et al reported the synthesis of silver based compound namely $AgCoO_2$ (powder) by a 4-day hydrothermal reaction in a parr bomb. The thin films were then prepared by the sputtering of a 2 inch diameter sputtering target. The films showed an optical band gap of 4.1eV and a conductivity of 0.2S/cm. Seebeck coefficient

measurement proved the p-type conductivity of the films. $AgGaO_2$ is also a p-type TCO.

1.7 Applications of TCOs

Because of the diversity of applications for TCOs, no one material can be said to be most suitable for all uses. Choice of transparent conductors depends on the material properties and application [47].

TCOs on window glass improve the energy efficiency of the window because free electrons reflect infrared radiation for wavelengths longer than the plasma wavelength. In cold climates, the plasma wavelength of about 2μm is desirable, so that most of the solar spectrum is transmitted to heat inside the building. Fluorine-doped tin oxide is the best material for this since it combines a suitable plasma wavelength with excellent durability and low cost. In hot climates, the plasma wavelength, about 1 μm is desirable, so that the near-infrared portion of incident sunlight can be reflected out of the building. Silver and titanium nitride is widely used for this application.

The front surfaces of solar cells are covered by transparent electrodes. Thermal stability and low cost are the primary factors in this choice. The high work function of SnO_2:F is also helpful in making low-resistance electrical contact to the p-type amorphous-silicon layer. Amorphous-silicon cells are grown on flexible steel or plastic substrates; in this case, the top TCO must be deposited at low temperature on thermally sensitive cells. ITO or ZnO is chosen for this purpose because both compounds can be deposited successfully at low temperatures.

Etchability is a very important consideration in forming patterns in the TCO electrode. The easier etchability of ITO has favoured its use over tin oxide,

which is more difficult to etch. The low deposition temperature of ITO is also a factor for colour displays in which the TCO is deposited over thermally sensitive organic dyes. Low resistance is another factor favouring ITO in very finely patterned displays, since the ITO layer can be made very thin, thus the etched topography remains fairly smooth.

Freezers in supermarkets pass electric current through TCOs on their display windows in order to prevent moisture in the air from condensing on them and obscuring the view. Low cost and durability are the main factors that make tin oxide a favourable choice for the application. ITO is used in modern cockpits because its lower resistance permits defrosting larger window areas with relatively low voltage (24 V). Some automobile windshields use silver or silver-copper alloy TCOs for electrical defrosting because the systems in automobiles require very low resistance, combined with the legal requirement of a minimum transmission of 70%.

Tin oxide coatings are placed on oven windows to improve their safety by lowering the outside temperature of the glass to safe levels. The tin oxide coating also improves the energy efficiency of the ovens. The main criteria for this choice of material are high temperature stability, chemical and mechanical durability, and low cost.

TCOs on glass can dissipate static charges that develop on xerographic copiers, television tubes, and CRT computer displays. Here the main concern is mechanical and chemical durability. Tin oxide is the material of choice for these applications .The durability and low cost of tin oxide make it a good choice for touch-sensitive control panels, such as those found on appliances, elevator controls and automated teller machine screens. TCO-coated glass can be used as part of invisible security circuits for windows or on glass over valuable works of art. Any TCO (except for coloured TiN) could be used. Silver or ZnO multi

layers provide the best UV protection. Some tin oxide coatings are used to take advantage of tin oxide's extraordinary durability. Tin oxide coatings are used on the windows of barcode readers to improve their abrasion resistance.

1.8 Latest Developments in Transparent Electronics

Thin-film transistors (TFTs) are the fundamental building blocks for state-of-the-art microelectronics, such as flat-panel displays and system-on-glass. Furthermore, the fabrication of low-temperature TFTs will allow flexible large-area electronic devices to be developed. These devices are flexible, lightweight, shock resistant and potentially affordable which are the properties that are necessary for large, economic, high-resolution displays, wearable computers and paper displays[48]. Further, when combined with 'transparent circuit technology' TFTs can integrate display functions even on the windscreens of cars.

Transparent electronic circuits are expected to serve as the basis for new optoelectronic devices. A key device for realizing transparent circuits is the transparent field-effect transistor (TFET). TFETs have been developed on the basis of compound wide–band gap semiconductors such as GaN (*2*) and SiC (*3*). These exhibit good performance [e.g., a field effect mobility of 140 $cm^2 V^{-1}s^{-1}$] and durability in high-temperature and high power operation. Oxide semiconductors present an alternative opportunity for discovering new transparent electronics applications with added functionality, because oxides display many properties in their magnetic and electronic behavior that originate from a variety of crystal structure and constituent elements. Crystalline thin-film transparent oxide semiconductor, $InGaO_3(ZnO)_5$ act as an electron channel and amorphous hafnium oxide as a gate insulator[49]. The device exhibits an on-to-off current ratio of $\sim 10^6$ and a field-effect mobility of ~80 ($cm^2V^{-1}S^{-1}$) at room temperature, with operation insensitive to visible light irradiation. The result

provides a step toward the realization of transparent electronics for next-generation optoelectronics.

Recently, researchers at Oregon State University have created the world's first completely transparent integrated circuit from inorganic compounds, another major step forward for the rapidly evolving field of transparent electronics. The circuit is a five-stage "ring oscillator," commonly used in electronics for testing and new technology demonstration. It marks a significant milestone on the path toward functioning transparent electronics applications, which many believe could be a large future industry. The new transparent integrated circuit is made from indium gallium oxide.

1.9 Conclusion

Development of transparent p and n type materials opens up exciting applications in the field of transparent electronics. Optimisation of various TCO materials for device applications have become the key part of research today. Fabrication of non-toxic TCOs by cost effective techniques is therefore very important in the present world.

References

1. T. J.Coutts, T.O.Mason, J. D.Perkins, D.S.Ginley, NREL/CP **520**(1999)
2. S.A.Knickerbocker, A.K.Kulkarni, J.Vac.Sci.Technol.A**13**(3)(1995)1048
3. Badeker, Ann.Phys(Leipzig) **22**(1907)749
4. A.J.Freeman, K.R.Poeppelmeir, T.O.Mason,R.P.H.Chang, T.J.Marks, M.R.S.Bulletin **25**(2000)45
5. M.M.B.Mohagheghi, M.S.Saremi, J.Phys D.Appl.Phys. **37**(2004)1248
6. Y.Shigesato, N.Shin, M. Kamei, P.K.Song, I.Yasui, Jpn.J.Appl.Phys. Part**1**, No.**11**(2000)6422
7. K.L.Chopra, S.Major, D.K.Pandya, Thin Solid Films **102**(1983)1
8. A.L.Dawar, J.C.Joshi, J.Mater.Sci.**19**(1984)1
9. T.J.Coutts, X.Wu, W.P.Mulligan, J.M.Webb , J.Electron.Mater. **25**(1996)935
10. T.Minami, MRS Bulletin (2000)38
11. H.Enoki, T.Nakayama,J.Echigoya, Phys.Stat.Sol.(a) **29**(1992)181
12. H.Un'no, N.Hikuma, T.Omata, N.Ueda, T.Hashimoto, H.Kawazoe, Jpn.J.Appl.Phys.Part2, Lett **32**(1992)l1260
13. T.Minami, H.Sonohara, S.Takata, H.Sato,Jpn.J.Appl.Phys., Part2 , Lett.**33**(1994)L1963
14. R.J.Cava, J.M.Phillips, J.Kwo, G.A.Thomas, R.B.van Dover, S.A.Carter, J.J.Karjewski, W.F.Peck,J.M.Marshall, D.H.Rapkine, Appl.Phys.Lett **64**,(1994)2071
15. T.Minami, S.Takata, T.Kakumu, H.Sonohara, Thin Solid Films **270**(1995)22
16. D.J.Griffiths, Introduction to Electrodynamics, 3rd Edn, Prentice Hall of India Pvt. Ltd. (2002)

17. E.C Jordan , K.G Balmain, Electromagnetic Waves and Radiating Systems, 2nd Edn, Prentice Hall (1968)
18. C.Kittel, Introduction to Solid State Physics, 7th Edn ,Wiley Eastern Ltd (1996)
19. Ali Omar, Elementary solid State Physics: Principles and Applications, Addison Wesely Publishing company Inc (1999)
20. H.L.Hartnagel, A.L.Dawar, A.K.Jain, C.Jagdish, Semiconducting Transparent Thin films, IOP Publishing Ltd, Bristol (1995)
21. J.C.C.Fan, J.B.Goodenough,J.Appl.Phys. **48**(1977)3524
22. I.Hamberg, C.G.Granqvist, K.F.Berggreen,B.E.Sernellius,L.Engstrom, Phys.Rev.B. **30**(1984)3240
23. O.N.Marysov,A.J.Freeman, Phys.Rev.B. **64**(2001)233111-1
24. H.Ohta, M.Orita, M.Hirano, H.Tanji, H.Kawazoe, H.Hosono, Appl.Phys. Lett. **70**(2000)2740
25. N.S.Murty, G.K.Bhagawat, S.R.Jawalekar, Thin Solid Films **92**(1982)347
26. Y.Shigesato, D.C.Paine, Appl.Phys.Lett. **62**(1993)1268
27. K.Sreenivas, T.Sudersana Rao, A.Mansingh, S.Chandra, J.Appl.Phys **57**(1985)384
28. J.Bardeen, W.Shockley, Phys.Rev. **80**(1950)72
29. A.R.Huston, J.Appl.Phys. **32**(1961)2287
30. H.Ehrenreich, J.Appl.Phys **32**(1961)2155
31. T.J.Coutts, D.L.Young, X.Li, MRS Bulletin (2000)58
32. D.B.Fraser, H.D.Cook, J.Electrochem. Soc. **119**(1972)1368
33. G.Haacke, J.Appl.Phys **47**(1976)4086
34. P.A.Hes,S.I.Soclof, Proceedings of the 12th IEEE Photovoltaic conference(1976)978
35. I.D.Parker, J.Appl.Phys. **75**(1994)1656
36. K.Sugiyama, H.Ishii, Y.ouchi, K.Seki, J.Appl.Phys. **87**(2000)295
37. H.Kawazoe, H.Yanagi, K.Ueda, H. Hosono, MRS Bulletin(2000)280

38. H.Yanagi, Transparent p/n type oxide semiconductors with delafossite structure: Chemical design and material exploration, PhD Thesis (2001) TIT, Japan.
39. H.Kawazoe, M.Yasukawa, H.Hyodo, M.Kurito, H.Yanagi, H.Hosono, Nature **389** (1997)939
40. S.Gao, Y.Zhao, P.Gou N.Chen, Y.Xie, Nanotechnology **14**(2003)538
41. B.Roy, A.Ode, D.Ready, D.Ginley, H.Hosono, NCPV and solar program review meeting **520-33586** (2003) 922
42. C.C.Lin, S.Y.Chen, S.Y.Cheng, H.Y.Lee, Appl.Phys.Lett. **84**(2004)5040
43. K.K.Kim, H.S.Kim, D.K.Hwang, J.H.Lim, S.J.Park, Appl.Phys.Lett **83**((2003)63
44. Y.R.Ryu, T.S.Lee, H.W.White, Appl.Phys.Lett. **83**(2000)87
45. D.C.Look, D.C.Reynolds, C.W.Litton, R.L.Jones, D.B.Eason,G.Cantwell, Appl.Phys.Lett **81**(2002)1803
46. J.Tate, M.K.Jayaraj, A.D.Draesek, T.Ulbrich, A.W.Sleight, K.A.Vanaja, R.Nagarajan, J.F.Wager, R.L.Hoffman, Thin Solid Films **411** (2002)119
47. R.G.Gordan, MRS Workshop (2000)
48. K.Nomura, H.Ohta, A.Takagi, T.Kamio, M.Hirano, H.Hosono, Nature **432** (2004)25
49. K.Nomura, H.Ohta, K.Ueda, T.Kamio, M.Hirano, H.Hosono, Science **300**(2003)23

CHAPTER 2

Indium Tin Oxide: An Overview of the Present Status

Abstract

Indium tin oxide is a potential candidate for transparent electronics. A great deal of research has been taking place to reveal the properties of this material. This chapter summarises the various properties of this material as far as the transparent conducting behaviour is concerned. The chapter also gives a detailed literature review on the material.

2.1 Introduction

The increasing interest in the interaction of light with electricity and electronically active materials, materials and techniques for producing transparent and electrically conducting films are particularly attractive. Transparent conductors have found major applications in a number of electronic and optoelectronic devices including resistors, transparent heating elements, antistatic and electromagnetic shield coatings, transparent electrode for solar cells, antireflection coatings, heat reflecting mirrors in glass windows and many other [1]. Tin doped indium oxide (indium tin oxide or ITO) is one of the most commonly used transparent conductive oxides. Since 1960s it is the most widely used TCO for Optoelectronic applications. At present and likely well into the future this material offers the best available performance in terms of conductivity and transmittivity. It is also a material with excellent environmental stability, reproducibility and good surface morphology. ITO can be deposited at room temperature and in general, its adhesion to most substrates is excellent. The ability to deposit high quality ITO films on temperature sensitive substrates is an important consideration in the selection of ITO over other TCOs [2].

Although partial transparency, with acceptable reduction in conductivity, can be obtained for very thin metallic films, high transparency and simultaneously high conductivity cannot be attained in intrinsic stoichiometric materials. The only way this can be achieved is by creating electron degeneracy in a wide bandgap (E_g > 3eV or more) material by introducing non-stoichiometry and/or appropriate dopants. These conditions can be conveniently met for in ITO as well as a number of other materials like zinc oxide, cadmium oxide etc.

ITO shows interesting and technologically important combination of properties viz high luminous transmittance, high IR reflectance, good electrical conductivity, excellent substrate adherence and chemical inertness. ITO is a key

part of solar cells, window coatings, energy efficient buildings, and flat panel displays. In solar cells, ITO can be the transparent, conducting top layer that lets light shine into the cell, and electricity flow out. Improving the ITO layer can improve the solar cell efficiency. A transparent conducting oxide is a material with high transparency in a derived part of the spectrum and high electrical conductivity. Beyond these key properties of TCOs, ITO has a number of other key characteristics. The structure can be amorphous, crystalline or mixed, depending on the deposition temperature and atmosphere. The electro-optical properties are a function of the crystallinity of the material. In general, ITO deposited at room temperature is amorphous, and ITO deposited at higher temperatures is crystalline. Depositing at high temperatures is more expensive than at room temperature, and this method may not be compatible with the underlying devices [3].

2.2 Crystal Structure of ITO

Indium oxide and ITO has cubic bixbyite structure which is also known as the c-type rare earth sesquioxide structure. It belongs to the space group Ia3, number 206. The bixbyite structure can be obtained by removing one forth of the anions from the fluorite structure and allowing for small shifts of the ions. 32 cations occupy the 8b and 24d positions (Figure 2.1). Each cation resides at the center of a distorted cube, with six corners occupied by oxygen anions. All 8b cations are coordinated to six oxygen anions at a distance of $2.18A^0$ and to 2 oxygen interstitial positions, which lie along a body diagonal of the cube. The 24d cations exhibit less symmetry as they are coordinated to six oxygen anions at three distances and to 2 oxygen interstitial sites along a face diagonal of the cube. The 48 oxygen anions are coordinated to four cations [4].

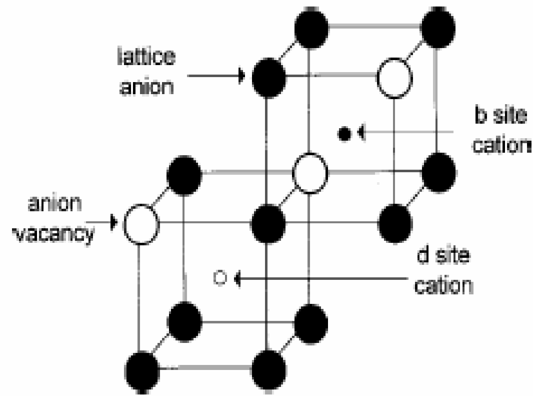

Figure 2.1.Cubic bixbyite structure showing the anion vacancy

Indium tin oxide is essentially formed by substitutional doping of In_2O_3 with tin, which replaces the In^{3+} atoms from the cubic bixbyite structure of indium oxide [5]. Tin thus forms an interstitial bond with oxygen and exists either as SnO or SnO_2 and accordingly it has a valency of +2 or +4 respectively. This valency state has a direct bearing on the ultimate conductivity of ITO. The lower valence state results in a net reduction in carrier concentration, since a hole is created which acts as a trap and reduces conductivity. On the other hand, prominence of the SnO_2 state means Sn^{4+} acts as an n-type donor releasing electrons to the conduction band. However, in ITO, both substitutional tin and oxygen vacancies contribute to the high conductivity and the material can be represented as $In_{2-x}Sn_xO_{3-2x}$.

2.3 Electronic Band Structure of ITO

The electronic band structure is the one of the most important factors for understanding the unique interplay between optical absorption and conductivity in TCO materials. Most of the important transparent oxide properties can be satisfactorily described on the microscopic level only on the basis of a sufficiently detailed and reliable model of the electronic band structure [6].

However, the electronic structure of ITO has not been investigated thoroughly. Several spectroscopic and optical measurements were undertaken to elucidate its electronic structure and electron scattering mechanisms.

Fan and Goodenough [5] proposed a schematic energy band model (Fig 2.2) for pure and doped In_2O_3 on the basis of electron spectroscopy for chemical analysis (ESCA) measurements. The energy band model developed by Fan and Good enough still represents an excellent and transparent starting description for describing the electronic structure of both the pure and doped materials.

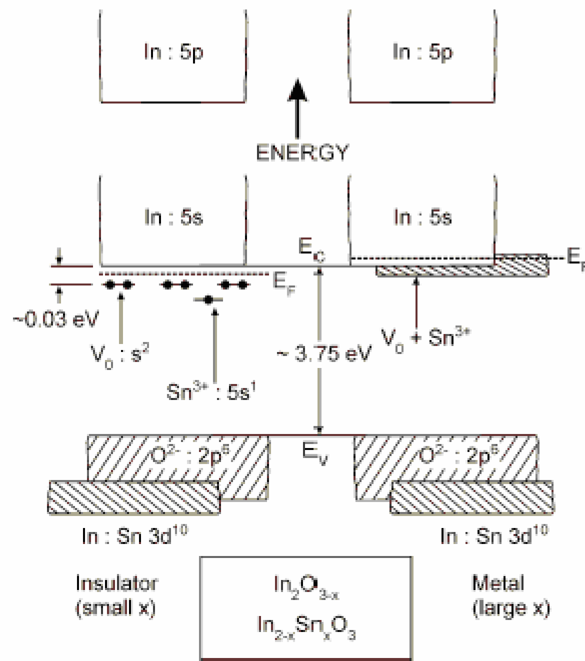

Figure 2.2. Schematic energy band model for pure and doped In_2O_3 based on ESCA measurement

In_2O_3 has a filled valence band (VB) that is primarily oxygen 2p in character. The (filled) In $3d^{10}$ core levels also lie well below the valence band edge, as depicted in figure 2.2. The direct semiconductor bandgap (E_g) is 3.75 eV. It has been proposed that the conduction band (CB) is mainly derived from the indium 5s electrons and for the undoped material the Fermi energy is located half way between the valence and conduction bands. With the substitution of In^{3+} by Sn^{4+} one electron donor or impurity states are formed below the (host) In 5s or 5sp conduction band. First-principle electronic structure calculations on In_2O_3 reveal that the unoccupied In 5sp orbital show wide spatial distribution, even extending over the third In shell.

Hamberg *et al* [7] have reported the results of the analysis of the optical and transport properties for a one dimensional model of the electronic structure, with effective masses taken from measurements (Fig 2.3).

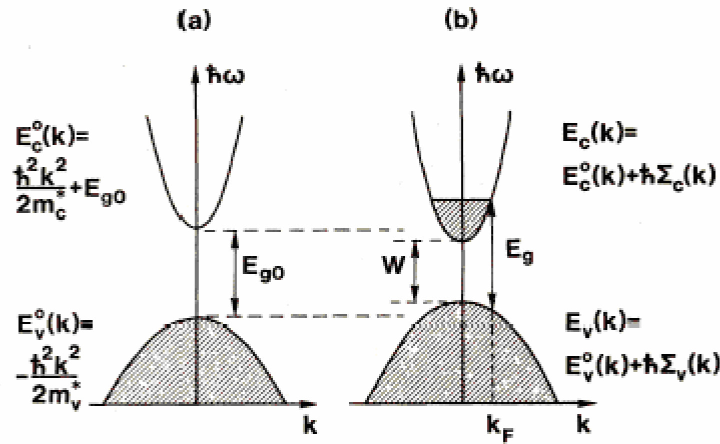

Figure2.3(a) Assumed band structure of undoped In_2O_3 in the vicinity of the top of the valence band and the bottom of the conduction band and (b)effect of tin doping in the band structure of In_2O_3

In this structure, the region around the bottom of the conduction band is thought to be parabolic with an effective mass (m_c^*) of 0.3m where m is the free electron mass. The valence band is also taken to be parabolic with an effective mass (m_v^*) of unknown magnitude. When tin doping is carried out, the valence band is shifted upwards and the conduction band is shifted downwards. This shift is happening because of three different effects. One of the reasons is that the shapes of the valence and the conduction bands may not be accounted for by the same effective masses as in the undoped material. Above the critical Mott density, the partial filling of the conduction band leads to a blocking of the lowest states and hence a widening of the optically observed bandgap (Burstein-Moss shift). Also, above the Mott critical density, the valence and conduction bands are shifted in energy as a result of electron –electron and electron-impurity scattering.

The only *ab initio* band structure calculations available for pure In_2O_3 were performed using the Linear Muffin-Tin Orbital method with the atomic sphere approximation (LMTO-ASA) [8]. The band structure calculations for pure and tin doped In_2O_3 has been done using the accurate and numerically efficient full potential linear muffin tin orbital (FLMTO) method . According to this model, the position, dispersion and character of the highly dispersed band at the bottom of the conduction band are the most important features of the host electronic band structure which provide necessary condition for transparent conducting behaviour with electron doping. The report also tells that this lowest band is split with Sn doping due to the strong hybridisation with dopant s-type and this splitting contributes to the decrease of plasma frequency and the mobility of the carriers.

Investigation of the electronic structure of ITO by using first principle calculation method, based on the density functional theory is also being reported [9]. The effect of substituting a tin atom for an indium one on the electronic structure of In_2O_3 was analysed using an augmented spherical wave (ASW)

method with an atomic sphere approximation (ASA). This method uses a minimum basis set and can be used to decompose the total density of states into a partial one. Therefore this method is effective for the analysis of large systems and is useful for obtaining the physical features of materials. The calculated partial density of states (PDOS) analysis showed that a tin atom substituted for an indium formed 3 impurity bands with s-like symmetry. The second one of the three bands overlapped the conduction band of In_2O_3 and the Fermi energy of ITO was captured in this impurity band. The analyses also showed that the substitution of a tin atom did not significantly destroy the shape of DOS around the bottom of the CB, which gave a physical foundation for the Burstein – Moss shift model. They have also discussed the carrier generation mechanism and past experimental results based on their calculation results.

2.4 Optical Properties of ITO

The window of transparency in ITO extends from the bandgap on the UV end to the plasma-absorption frequency at the IR end. In the ultraviolet region of the ITO, the absorption is strong due to excitations across the fundamental bandgap E_g. When the oxide is degeneratively doped, increasing carrier density leads to a widening of the bandgap due to the Burstein-Moss effect [10]. The IR end of the transparency window is defined by the plasma-absorption frequency, which also depends on the carrier density and the effective mass of the carrier.

The optical properties around E_g are complicated by the occurrence of logarithmic band edges, often referred to as 'Urbach tails', which give some weak absorption at the blue end of the luminous spectrum. Urbach tails are common features in semiconducting materials, and their origin has been the subject of much speculation. It appears that several physical mechanisms can contribute, and that one of them is associated with the existence of Sn^+ acting as an ionized impurity. The optical phenomena in the NIR region can be explained

on the basis of classical Drude theory [11]. According to the theory the transition from high transmittance to high reflection will occur at short wavelengths for films with higher carrier concentration.

The free electrons in the In_2O_3 lattice undergo scattering, whose strength limits conductivity as well as the infrared reflectivity of ITO. There are many types of scattering centers that have to be considered, including ionized and neutral impurities, phonons and dislocations. As a first theoretical representation, the Drude model can be used which yields a complex resistivity according to the equation

$$\rho^{Drude} = \frac{\gamma}{\varepsilon_0 \varpi_N{}^2} - \frac{\varpi}{\varepsilon_0 \varpi_N^2} \qquad (2.1)$$

where ħ γ is the relaxation energy that is taken as a constant,

ε_0 is the permittivity of free space,

ħ ω is photon energy and

ħ ω_N is approximately related to the longitudinal plasma energy ,ħ ω_p by the equation $\omega_p{}^2 =(\omega_N{}^2 / \varepsilon_{\alpha\,8}) - \gamma^2$ with ε_α =3.95.

This approach is hampered by the fact that γ is an empirical constant, so that quantitative predications of the effects of various scattering mechanisms cannot be made, further more, γ is taken to be frequency independent, which is an over simplification.

The screening of the ions increases with increasing wavelength and is essentially fully developed beyond the plasma energy at ħω_p, where free-electron like properties prevail unless n_e is too small. In the range between E_g and ħω_p, the ions are incompletely screened. And screening is due to neutral defects such as grain boundaries, impurity atoms, and vacancies can play a noticeable yet weak role. This range essentially corresponds to the luminous spectrum for the case of an ITO film.

The final part of the theoretical model for ITO is related to phonon effects. In_2O_3 transmission spectra show strong reflectance features at wavelengths between 20 and 30μm. The phonon effects can be modelled as a set of three damped Lorentz oscillators with energies in a range around $\hbar\omega_p$ [12]. The effects of bound electrons, free electrons and phonons can be combined into a quantitative theory for the dielectric function of ITO, from which the optical properties of thin films are readily computed. An increase of n_e is seen to give an onset of infrared reflectance and a concomitant lowering of transmittance, a band gap widening, and a swamping of the phonon effects.

2.5 Electrical Properties of ITO Thin Films

The values of electrical parameters of ITO thin films depend on the dopant concentration, deposition conditions and post-deposition process. The decrease in mobility with increase of dopant level is due to enhancement of scattering mechanisms such as ionized impurity scattering. The substrate temperature is found to significantly affect the electrical properties [13]. The resistivity initially decreases as the substrate temperature increases. This type of dependence of resistivity on substrate temperature may be due to the fact that crystallinity of the films improves with increase in substrate temperature, thereby increasing conductivity. At higher substrate temperatures the resistivity increases again. This increase in resistivity may be due to the oxidation of tin doped indium oxide films.

The high conductivity of the ITO films has been attributed to both substitutional tin and oxygen vacancies, created either during film growth or post-deposition annealing resulting in a material represented as $In_{2-x}Sn_xO_{3-2x}$ [14]. Increasing the oxygen partial pressure above a value which yields a near stoichiometric film composition would thus result in an accumulation of excess oxygen, mainly at

the grain boundaries acting as trapping centers for free carriers [15]. This means that the barrier scattering becomes the dominant process since the barrier height increases strongly. At the same time the density of free carriers is reduced as they are partly localized at the trapping sites [16]. This results in a decrease in the carrier mobility, and therefore a corresponding fall in the film conductivity is observed. Buchanan *et al* [17] have also suggested that the decrease in the conductivity in increased oxygen partial pressure is primarily due to a reduction in the carrier concentration caused by the occupation of oxygen vacancies rather than due to tin doping.

The conductivity of ITO films can be improved by increasing the electron mobility or carrier density. There is a trade off between these two parameters. Very high carrier density (~ $2x10^{21}$ cm^{-3}) causes strong optical absorption due to the plasma excitation of the carriers in the visible range [18]. Investigations on the kinetics of the crystallization of amorphous ITO and its relationship to the electrical behavior of the material during and after low temperature annealing showed that the resistivity of the material changes via two separate thermally activated processes that occur with different time constants but similar activation energies [19]. Upon heating, the as-deposited amorphous material begins to order locally via a process that obeys first order reaction rate kinetics. This change is associated with the relaxation of distorted bonds in the as-deposited amorphous material. One consequence of the local ordering that occurs during this relaxation process appears to be an increase in the ionized vacancy concentration and, consequently, the carrier density. The second stage of the transformation is crystallization via nucleation and growth with an Avrami–Johnson–Mehl growth mode parameter of 3–4, which is characteristic of two- to three-dimensional growth. This is consistent with the block-like microstructure observed by cross-sectional TEM in fully crystallized ITO. A more complete understanding of these processes may facilitate the development of conditions

for the deposition of low resistance, high optical transmissivity ITO using low kinetic energy processes and low substrate temperatures.

2.6 Work Function of ITO

In applications, where ITO is used as a hole injecting electrode in organic electroluminescent devices, the work function of ITO has a critical importance in device performance because it affects the energy barrier height at the heterojunction interface. A number of studies on surface treatments using mechanical polishing, UV-irradiation, wet chemical, and plasma etchant have been conducted to change the ITO work function [20-22]. Among such surface treatments, oxygen plasma treatment is known as the most effective technique in increasing the ITO work function [23]. It was proposed that the change of In, Sn, O and surface carbon account for the increase of the ITO work function by the oxygen plasma treatment.

The tunnelling characteristics of ITO/semiconductor heterojunctions that might introduce uncertainties due to interfacial layers was used to deduce the work function of ITO [24]. An absolute and direct measurement of ITO work function in ultra high vacuum can be done using an inelastic secondary electron cut off ultraviolet photoelectron spectroscopy (UPS) energy distribution curve (EDC). The advantage of this method is that it depends only on the photon energy of UV source which can be known very accurately. Ultrahigh vacuum exclude the possibility of surface contamination. The work function obtained by this method was 4.4 – 4.5 eV which is slightly lower than the commonly cited value. But the value did not change upon heating upto 300 ^{0}C in UHV or sputtering at 2keV for an extended period of time.

Studies on the effect of surface cleaning on the work function of ITO films using UV and X-ray photoemission spectroscopic studies [25] show that even after

ultrasonic cleaning in the organic solvent, considerable carbon contamination remained on the ITO surface and the work function is low(4.5eV). Ultraviolet and ozone treatment removed significant carbon contamination with an increase in work function up to 4.75eV, which improves the hole injection efficiency into the organic hole transport layer in organic electroluminescent devices. Ar^+ sputtering reduced the carbon contamination but it also affected the oxygen content on the ITO surface and led to a decrease in work function. The three major factors affecting the work function of ITO are Carbon containing contaminants, the O/In ratio and the In/Sn ratio.

The effects of O_2 inductively coupled plasma (ICP) treatment on the chemical composition and work function of ITO surface employing synchrotron radiation photoemission spectroscopy [26] showed that the O_2 ICP treatment resulted in the increase of the ITO work function by 0.8 eV. Incorporation of oxygen atoms near the ITO surface during the ICP treatment induced a peroxidic ITO surface, increasing the work function. The enhanced oxidation of a thin Ni over layer on the O_2-ICP-treated sample suggests that preventing the migration of oxygen atoms into the active region of organic light-emitting diodes is important for improving device lifetime.

Although many essential elements involved in low-cost production of polymer optoelectronics are available, reduction in cost is still inhibited by the complex fabrication of the electron injecting electrode. In a polymer light emitting device (*p*-LED), the cathode is typically formed by depositing a low work function metal onto polymer layer under high-vacuum conditions. Unfortunately, almost all low work function metals are highly reactive, and quickly oxidized in air. Consequently, they are difficult to handle in processing steps. In addition, such materials form very complex interfaces with organic materials [27,28]. Recent studies have shown that the barrier for charge injection can be effectively tuned by molecular adsorption. However, the efforts have been focused on the

reduction of the hole-injection barrier at the interface between indium tin oxide (ITO) and the active organic layer in *p*-LEDs. It has been demonstrated that either protonation of the ITO surface, or the adsorption of dipolar molecules strongly modifies this barrier. Reports show that a high work function electrode can be changed to a low work function electrode using molecular scale engineering [29]. In this technique, the strongly reducing Tetrakis (Dimethyl Amino) Ethylene (TDEA) molecules undergo a redox reaction with the ITO surface, leading to a reduction of the ITO work function, down to 3.7 eV. Low work function transparent ITO electrodes are easy to prepare and are stable in air and upon mild annealing. The characteristics of single-layer p-LEDs reveal that the electron-injection efficiency from TDAE-modified ITO electrodes is comparable to that of vapor-deposited Al electrodes.

2.7 Parameters Influencing the Properties of ITO Thin Films

The oxidation state and the impurity content affect the properties of ITO. The oxidising or reducing conditions during deposition modify the oxygen vacancy content, thus modifying the carrier density. For optical applications, the films must be etchable to enable device patterning via standard photolithography process [30]. The etching characteristics are highly dependent on the process parameter and process environment due to the different microstructure and crystallinity [31]. Either wet etching or dry etching can be employed to fabricate a pattern of ITO films. The dry etching has a lower etching rate and it is difficult to pump out the by-product. In contrast to dry etching, wet etching has relatively excellent throughput and is easy to transport the by-product away. A higher etching rate of ITO films is reported to be observed in acqua-regia than in hydrochloric acid. But the surface residual byproduct is more in acqua-regia than in HCl. The surface residual byproduct reduced the carrier mobility due to ionised impurity scattering. Also, due to faster etching rate, a serious undercut

occurred in ITO pattern after etching in acqua regia. A 9M HCl solution at room temperature is optimum for producing the ITO pattern on OLED.

A comprehensive picture of the defect structure of bulk and nano ITO is being carried out by employing synchrotron x-ray diffraction, neutron diffraction and extended x-ray absorption fine structure(EXAFS) experiments, with in situ electrical properties and using theoretical calculations [32]. Anomalous x-ray and time of flight (TOF) neutron diffraction were used as complementary techniques to determine Sn/In cation distribution a well as to examine carefully the behaviour of oxygen interstitial anion as a function of Sn doping level and oxygen partial pressure. The measurement of in situ conductivity and thermo power on the samples allowed a direct correlation between the defect structure and the electrical properties, while the theoretical calculations aid in the interpretation of experimental results and the development of improved defect models for ITO.

A real time evolution of ITO film structure and film properties during annealing in vacuum, the films deposited on unheated Si (100) substrates by reactive pulsed middle frequency magnetron sputtering yielded a crystallisation temperature of 250^0C. The resistivity of the films decreased with increase in annealing temperature, even in the amorphous state, due to the relaxation of distorted In-O bonds which leads to a free electron density enhancement by the creation of oxygen vacancies [33]. The rapid crystallisation was accompanied by film roughening and leads to a further decrease of the resistivity due to Sn donor concentration.

The presence of oxygen in the sputtering environment increases the crystallinity [34] of the films. The enhancement of crysatllinity is because of the fact that the scattering from the grain boundaries is less important for the films prepared under high oxygen concentration. This enhances the mobility of the carriers

thereby increasing the crystallinity. But at very high oxygen pressures, added oxygen can damage the film by introducing defects. Sn^{4+} ion pair attracts an additional oxygen atom, producing a neutral cluster $(SnO_2)_2$ in which the additional oxygen atoms play the role of electron traps which reduce the carrier mobility [35]. Introduction of oxygen during deposition favours the optical properties also. But the oxygen pressure has to fulfil the conflicting requirements of introducing enough oxygen vacancies without creating too large absorption. Too high oxygen pressure will result in a shift of the intrinsic absorption edge to longer wavelength.

The analysis on oxygen content by means of resonant backscattering of 3.045MeV, $^{4}He^{2+}$ ion beam [36] revealed an increase in carrier density with oxygen content averaged from surface to inside the film. This increase in carrier density is attributed to the crystallisation of the film. The study also suggested that a higher substrate temperature is necessary for the growth of stoichiometric films. When external heating is absent, continuous energetic ion bombardment acts as the source of energy for crystallisation. The crystallisation behaviour of ITO is influenced by the structure of the substrate [37]. Single crystal substrates affect the epitaxial growth of the films. Amorphous substrate retards the crystallisation at place adjacent to the amorphous substrate, but allows crystallisation at places away from the substrate.

A relation between the resistivity decrease and crystallisation behaviour has been investigated [38]. The films deposited at room temperature when heated to 533K in vacuum, a two step resistivity decrease was observed at 383K and 493K. The resistivity decrease at lower temperature is attributed to the increase in carrier density and mobility, while the decrease in resistivity at higher temperature is attributed to crystallisation from amorphous to crystalline state.

For device applications, the surface roughness of the films must be a minimum. The polishing process employed to smooth the surface is usually complicated, time consuming and low in production yield. So it is important to get a smooth surface in the as deposited films without sacrificing electrical conductivity. Reports [39] show that ITO films with domain structure exhibit rough surface while those with grain structure has flat surfaces. The surface roughness of domain structure is induced from the thickness variation between the domains. The smooth surface in grain structure is attributed to the preferential growth into [111] over the entire surface. Growth of ultra flat ITO films with excellent electrical conductivity using oxygen ambient in the growth phase up to 15nm and without oxygen during the rest of deposition is being reported [40]. The microstructure of the films depends on the growth conditions in the early phase of deposition while the electrical properties were influenced by the growth conditions of the bulk layer.

2.8 Deposition Methods for ITO Thin Films

The deposition of ITO in a manufacturing environment is typically by means of dc-magnetron sputtering. The choice of target—ceramic or metal—depends on the film quality sought and the process control available. The variables adjusted during process optimization include oxygen partial pressure, total gas pressure, residual water-vapor partial pressure, substrate temperature and target temperature (due to unintentional heating), sputter power, and target composition and configuration. The goals are the minimization of micro structural features and impurities that lead to reduced electron mobility, the maximization of activated substitutional Sn, and the creation of optimal oxygen sub stoichiometry. The oxygen stoichiometry is critical to the minimization of resistivity, since each doubly charged oxygen vacancy contributes two free electrons. In the crystalline form of indium oxide (bixbyite crystal structure), the presence of doubly charged vacancies (and substitutional Sn) creates an impurity

band that overlaps the conduction band, creating a degenerate semiconductor. An excess of charged defects, however, in the form of compositional impurities, singly charged Sn on an In site, or doubly charged oxygen vacancies, leads to charged impurity scattering and a decrease in electron mobility [41].

The initial growth mode in film deposition is considered very important [42] because the initial part of the growth may determine the bulk properties of the film. A solid film growth can take place through a 3-D nucleated growth mode (Volmer-Weber), a 2-D layer by layer growth mode (Frank-van de Merwe) and a mixed mode of 2D growth with a transition to 3D (Stranski-Krstinov). It has been reported that [43] the growth mode changed from 3D to 2D at the critical island growth step when the substrate temperature is increased beyond 150^0C. A similar transition was observed in pulsed laser deposited ITO films near the same temperature [44]. This transition in the growth mode is accompanied by a phase change from amorphous to polycrystalline.

The gaseous environment during deposition can have a significant effect on the quality of the ITO thin film. The oxygen flux rate during the sputtering process influences the surface morphology and grain size of the film. Oxygen incorporation during post-annealing in O_2, O_3 and air ambients play an important role in improving the optoelectronic properties of the e-beam evaporated films. In order to get maximum electrical conductivity and optical transmittance of ITO films, the gaseous atmosphere and the annealing temperature must be carefully chosen to optimize the incorporation of oxygen [45-47]. The presence of hydrogen is also reported to be beneficial to the electrical properties of the ITO films deposited by sputtering [48]. It has been found that the addition of hydrogen during sputtering increases the conductivity of the films. This is because of the fact that hydrogen reduces formation of oxide with a resulting increase in oxygen vacancy concentration.

2.8.1 Chemical vapour deposition (CVD)

Chemical vapour deposition (CVD) technique has not been fully exploited for the deposition of ITO thin films even though this process does not require high vacuum and it is easier to produce films over large areas. However, there are a few reports on the deposition of ITO thin films by CVD technique [49-51]. ITO thin films prepared by an atmospheric-pressure chemical vapor deposition method using indium acetylacetonate and tin (II) acetylacetonate, were polycrystalline [52] corresponding to a reaction temperature in the range of 350- 500^{0}C. For the 215nm-thick film deposited at 450 ^{0}C, the resistivity was $1.8X10^{-4}\Omega$cm, and the transmittance was more than 90% in the wave length range of above 400 nm. The atomic ratio Sn/In of the film was 0.031. The films deposited by CVD technique are always polycrystalline in nature and the preferred orientation of the films depends on the source materials used.

2.8.2 Vacuum evaporation

ITO thin films can be deposited by reactively evaporating either metallic alloy or an oxide mixture [53]. ITO thin films deposited by vacuum evaporation using oxide mixture are found to be oxygen deficient and an oxygen partial pressure of 10^{-4} Torr is required to get transparent films. The vacuum evaporation of ITO films from In_2O_3 and SnO_2 powders [54] from two independently controlled beryllia crucibles gave best results at a substrate temperature of 400^{0}C, oxygen partial pressure of $3x10^{-4}$ Torr and 5wt% of SnO_2. Reports on growth of ITO thin films from a single crucible with a pellet of ITO by vacuum evaporation suggest no trace of any oxide phase of tin even for heavily doped films [55]. Annealing of reactively evaporated ITO thin films in the temperature range 100^{0}C to 325^{0}C indicated an increase in bandgap of the thin films [56]. This study used a 90:10 In-Sn alloy source for evaporation. Annealing was carried out in the temperature range 100 to 325^{0}C under nitrogen atmosphere. A minimum

resistivity of 4.5×10^{-3} Ωcm and a maximum carrier concentration of $1.94 \times 10^{20} cm^{-3}$ were observed for the annealing temperature of $150^{0}C$.

2.8.3 Electron beam evaporation

Highly conducting and transparent ITO thin films were deposited at a relatively lower temperature using reactive e-beam evaporation [57]. The grain boundary scattering was negligibly small in those films and the average grain size increased with increase in substrate temperature. Also, tin doping in e-beam evaporated ITO thin films influenced the ionised impurity scattering.

The electrical and optical properties of the e beam evaporated ITO thin films depend strongly on the Sn^{4+} concentration [58]. ITO thin films were prepared by e-beam evaporation under various oxygen pressures and under ion beam irradiation. A 95:5 ITO target was used as source for evaporation and Si (100) was used as substrates . The substrate temperature during deposition was kept at $250^{0}C$. XPS was used to measure the composition and chemical states of these films. The films deposited under an oxygen atmosphere had a composition with lower Sn^{4+} concentration. Films deposited with ion beam irradiation had the lowest Sn^{4+} concentration. The study showed that an optimum amount of the concentration of the Sn^{4+} is needed for lower resistivity and a lower concentration of Sn^{4+} is favourable for higher transmission.

High quality, low resistivity, amorphous and polycrystalline, pure and Sn doped In_2O_3 films were prepared by high density plasma assisted electron beam evaporation [59]. Effect of tin doping on the electronic transport properties of the films was evaluated. Amorphous films with higher carrier density in the as-deposited state showed no effect of Sn doping on resistivity and mobility, when the Sn doping was in the range 0 to 5.3 wt%. But resistivity and mobility showed a dependence on Sn concentration after crystallisation. The analysis was

based on charged and neutral impurity scattering models and it suggested that increasing tin concentration leads to the formation of defect complexes which act as scattering centres but which do not contribute carriers to the material.

The deposition rate and annealing conditions strongly affect the optical properties of the ITO film deposited by e-beam evaporation [60]. Annealing the films under N_2/H_2 mixture is found to improve the transmittance of the films upto an annealing temperature of 300^0C and a drastic decrease in transmittivity was observed at 400^0C. However, air annealing at 400^0C improved the transmission of the darkened film because of the incorporation of oxygen into the ITO polycrystalline film.

The bombardment of e-beam evaporated thin-film ITO by energetic ions can result in an increase in neutral scattering centers and a decrease in carrier density, which increase the resistivity [61]. The creation of neutral scatter centers clearly has significance to thin-film ITO deposition technologies, such as sputtering, which may subject deposited films to energetic ion bombardment throughout growth. At the same time, however, high-dose ion implantation at room-temperature results in dynamic recovery and an improvement in the grain morphology of e-beam deposited thin-film ITO from irregular to equiaxed grain shapes. The implantation of either O^+ or H_2^+ does not result in the formation of vacancies that contribute additional carriers. Instead, the concentration of carriers due to ionized four-valent Sn atoms decreases by the implantation. The neutral scatter centers generated by the implantation appear to take the form of point defect complexes since transmission electron microscope studies failed to detect significant numbers of extended defects in the implanted films.

2.8.4 Sputtering

Sputtering technique can be employed to deposit highly transparent and conducting ITO films [62-64]. In-Sn alloy targets and In_2O_3-SnO_2 targets are being used for sputter deposition. When sputtering is done using a metal target, the deposition rate is reported to be a strong function of oxygen pressure and sputter power [65] and is a weak function of total sputtering pressure. For lower sputtering powers, the target surface is oxidised non-stoichometrically. The sputtered particles can oxidise further during their transport or film growth. With increase in sputter power, the number of sputtered species increases. The effect is a higher consumption of oxygen atoms needed to oxidise the target surface and the sputtered atoms. At higher powers, the number of oxygen atoms available to oxidise the target decreases and the surface of the target becomes more metallic. Use of oxide targets in the place of metallic targets helps in controlling the stoichiometry of the films more precisely.

Studies on ITO film texture development process during film deposition were carried out in an in-line magnetron sputter deposition system equipped with dc power supply [66]. The chamber was equipped with a load lock system and the base vacuum was 5×10^{-6} torr. The sputtering was carried out in pure Ar and Ar/O_2 gas mixture with varying sputtering parameters such as sputtering pressure, power density and oxygen flow rate and deposition temperature. The cross sectional TEM images showed that the films have columnar structure. ITO films deposited under conventional conditions evolved to (400) orientation with increasing film thickness while surplus amount of oxygen gas flow suppressed the growth of (400) oriented grains. Moderate ranges of pressure and power density and higher substrate temperature resulted in more (400) oriented film textures.

The deposition of ITO thin films from In-Sn alloy target by rf reactive magnetron sputtering at different substrate temperatures (Room temperature to 500^0C) showed that the films deposited at lower substrate temperatures had a very strong (222) diffraction peak. With increase in substrate temperature (400) diffraction peak emerged [67]. The appearance of (400) diffraction peak at higher substrate temperatures is attributed to the increase in energy of the sputtered particles reaching the substrate surface and also to oxygen deficiency.

Some of the approaches towards low temperature deposition are ion assisted deposition and ion beam sputtering. Ion beam sputtering has got the advantage that it can deposit dense and smooth films without radiation damage but with less contamination by operating at the lower pressure. Also ion beam sputtering system can exclude the substrate heating induced by high energy ion irradiation.

ITO thin films deposited at lower (0.32mbar) pressure are found to be crystalline and highly conducting [68]. Amorphous films produced at higher pressures get crystallised by annealing. A shift of the absorption and plasma resonance edges towards shorter wavelengths can be observed with increase in crystallinity. The deposition was carried out at room temperature at an RF power of 40W and a base pressure of 10^{-6} torr with argon pressures ranging from 10^{-2} to 10^{-3}torr. Increase in deposition pressure caused a decrease in deposition rate which is due to the decrease in mean free path of the gaseous species.

The characterisation of rf sputtered ITO films annealed in air from 100^0C to 500^0C for 15 minutes revealed a resistivity variation in the range $5x10^{-4}$ to $11.5x10^{-4}\Omega$cm [69].The rise in resistivity due to annealing is attributed to the filling up of oxygen vacancies and the fall in resistivity is attributed to the rearrangement and removal of defects as well as the improvement in the crystalline nature of the films. The texture and compactness of the ITO film is reported [70] to be highly influenced by the oxygen concentration (C_o) and the

deposition pressure (P_d) while the electrical properties are less affected by P_d than C_o. But the surface roughness was not found to change when the films growth orientation changed.

In order to study the characteristics of transparent electrode deposited on organic layer, Tanaka *et al* [71] fabricated an inversely stacked electroluminescent(EL) device. The top layer of ITO electrode was prepared by sputter deposition using a shield plate. The study showed that, by depositing ITO by two-stage sputter deposition method, low resistivity ITO can be fabricated without damaging the organic layer and improvement of life time compared to the conventional normally stacked EL device was made possible. The inverse stacking makes the fabrication of EL device by using a non transparent or flexible material as the substrate which opens up extended applications in future.

2.8.5 Pulsed laser deposition

Pulsed laser deposition (PLD) is one of the latest developing technologies offering a number of applications in optoelectronics. It has got the advantage of reproducing the source material to be ablated to form the thin film and reduction of film contamination. The main disadvantage is the inability to deposit films on large area substrates. ITO films deposited by pulsed laser deposition using 355nm Nd: YAG laser showed a transmission > 85% and a resistivity of 2×10^{-4} Ωcm [72]. The ablation efficiency was increased by heating the substrates to a temperature of 200^0C.

PLD coupled with laser irradiation of the growing films can be utilised for growing crystalline ITO films at room temperature [73]. Laser beam energy of $0.07 J/cm^2$ was used for irradiation and the laser-irradiated parts of the films were crystalline with (111) preferred orientation and non-irradiated part appeared to be amorphous. The authors suggest that the crystallization process at RT

occurred through a photochemical mechanism and not through thermal crystallisation. Laser irradiation affected the electrical properties of the films also. Laser irradiated parts of the films yielded a resistivity of $1.2x10^{-4}\Omega$cm. An increase in transmittance of the irradiated film was also observed.

The electro-optical properties of the films deposited by PLD from a 90:10 ITO target showed a strong dependence on the oxygen pressure during deposition [74]. The growth of the films under different oxygen pressures and substrate temperatures were evaluated. The deposition rate was found to decrease with increase of the oxygen pressure in the system. High quality films were obtained in the vicinity of $1x10^{-2}$ Torr oxygen pressure. The films deposited at room temperature were amorphous and had the lowest resistivity of $5.35x10^{-4}\Omega$cm.

The optimum target composition for getting high conductivity in ITO thin films using PLD technique is reported to be 5wt% SnO_2 + 95wt% In_2O_3 [75]. The deposition was carried out by varying a substrate temperature upto 300^0C in O_2 partial pressure ranging from 1 to 100 mTorr. Increase in substrate temperature created more tin donors and oxygen vacancies leading to an increase in conductivity. In the oxygen pressure range of 50 to 10 mTorr, more oxygen vacancies were there and it also increased the conductivity. Very low oxygen pressure created structural disorder and thus reduced the conductivity. Increase in thickness also lead to increased conductivity because of better crystallinity and larger grain size. The optimum condition with regard to both transparency and conductivity was 5wt% SnO_2, 250^0C substrate temperature, 190nm film thickness and 10mTorr oxygen pressure during the film growth. Under these conditions ITO films with T = 91% and resistivity of $4x10^{-4}\Omega$cm were obtained. Also the surface roughness of the films was one order of magnitude smaller than the commercial films grown by sputtering. These ITO films were then used as anode contact in OLEDs and the device performance was studied.

Yttria stabilized Zirconia (YSZ) can be used as the substrate for the epitaxial growth of ITO thin films [76]. The X-ray diffraction analysis indicated that the films exhibit a strong preferential alignment with (100)ITO║(100)YSZ. The oriented nature of the film reduced the grain boundary scattering and it caused a decrease in resistivity of the films. The surface roughness of ITO films on YSZ substrate was less than that on glass substrate. ITO thin films deposited on glass and YSZ substrates were used as anode contact in OLED and the device fabricated on ITO/YSZ showed higher external quantum efficiency compared with that based on ITO/glass.

The electrical conductivity of ITO thin films grown on YSZ substrates can be enhanced by [77] depositing ITO thin films on extremely flat YSZ single crystal using PLD at a substrate temperature of 600^0C. A base pressure of $2x10^{-6}$Pa and oxygen gas pressure of $1.2x10^{-3}$ Pa was used for the deposition. A lowest resistivity of $7.7x10^{-5}\Omega$cm, highest mobility of 44 $cm^2V^{-1}s^{-1}$ and the highest carrier density of $1.9x10^{21}cm^{-3}$ was obtained for the film containing 5wt% of SnO_2. The low resistivity originates from the specimens large electron mobility which resulted from the good crystal quality of the films. The transmissivity of the films exceeded 85% in the visible region of the electromagnetic spectrum.

2.9 Conclusion

The review on the various properties and deposition methods used for the growth of ITO thin films suggests the importance of the material for various optoelectronic applications. Being a degenerate and wide bandgap material, ITO is one of the best choices as the transparent electrode in solar cells and display devices. Even though ITO can be deposited using a wide variety of techniques as discussed in the previous section, sputtering turns out to be the best technique for the deposition of ITO thin films because it allows the deposition over large areas.

References

1. M.A.Martinez,J.herrero, M.T.Gutierrez, Thin Solid Films **269** (1995)80
2. T.Minami, MRS Bulletin **25** (2000) 8
3. Investigation of the Amorphous to Crystalline Transition in Indium Tin Oxide Films, Colleen Nehl,Office of Science, Energy Research Undergraduate, August 23, 2000
4. G.B.Gonzalez, J.B.Cohen, J.H.Hwang, T.O.Mason, J.P.Hodges, J.D.Jorgensen, J.Appl.Phys. **89** (2001)2550
5. J.C.C.Fan , J.B.Goodenough, J.Appl.Phys **48**(1977)3524
6. O.N.Mryasov, A.J.Freeman, Phys. Rev.B **64**(2001)233111-1
7. I.Hamberg,C.G.Granqvist,K.F.Berggreen,B.E.Sernelius,L.Engstrom, Phys.Rev.B **30** (1984)3240
8. H.Odaka, s.Iwata, N.Taga, S.Ohnishi, Y.Kaneta,Y.Shigesato, Jpn.J.Appl.Phys. **36**(1997)5551
9. H.Odaka, Y.Shigesato, T.Murakami, S.Iwata, Jpn.J.appl.Phys.**40**(2001)3231
10. I.Hamberg, C.G.Granqvist, K.F.Berggren, B.E.Sernelius, L.Engstrom, Phys.Rev.B. **30** (1984)3240
11. C.G.Granqvist, A.Hultakar, Thin Solid Films **411**(2002)1
12. I.Hamberg, C.G.Granqvist, J.Appl.Phys. **60** (1986) R123
13. S.I.Jun, T.E.Mc Knight, M.L.Simpson, P.D.Rack, Thin Solid Films **476**(2005)59
14. J.C.C.Fan and J.B.Goodenough, J.Appl.Phys. **48**(1977)3524
15. J. Szczyrbowski, A. Dietrich and H. Hoffmann, Phys Stat Sol (a).**78**(1983) 243
16. H.Haitjema, J.J.Ph.Elich , Thin Solid Films **205**(1991) 93
17. M. Buchanan, J.B. Webb and D. F. Williams, Thin Solid Films **80**(1981) 373
18. H.Ohta, M.Orita, M.Hirano, H.Tanji, H.Kawazoe, H.Hosono, Appl.Phys.Lett. **76**(2000)2740

19. D.C.Paine, T.Whitson, D.Janiac, R.Beresford, C.Ow.Yang, B.Lewis, J.Appl.Phys.**85**(1995)8445
20. C.C.Wu, C.I.Wu,J.C.Strum, A.Kahu, Appl.Phys.Lett. **70**(1997)1348
21. J.S.Kim , M.Granstrom, R.H.Friend,N.Johansson, W.R.Saleneck, R.Daik,W.J.Feast, F.Cacialli, J.Appl.Phys. **84**(1998)6859
22. M.G.Mason,L.S.Hung, C.W.Tang, S.T.Lee, K.W.Wong, M.Wang, J.Appl.Phys. **86**(1999)1688
23. Y.Park,V.Choong,Y.Gao,B.R.Hsieh,C.W.Tang, Appl.Phys.Lett.**68**(1996)2699
24. I.D.Parker, J.Appl.Phys.**75**(1994)1656
25. K.Sugiyama,H.Ishii, Y.Ouchi, K.Seki, J.Appl.Phys.**87**(2000)295
26. K. Lee, H.W.Jang, K.B.Kim, Y.H.Tak,J.L.Lee, J.Appl.Phys.**95**(2004)586
27. G.Greczynski, W.R.Saleneck, M.Fahlman, Appl.Surf.Sci. 175(2001)319
28. A.Rajagopal, N.Koch,J.Ghijsen, R.L.Johnson, K.Kaeriyama, G.Leising, J.J.Pireaux, J.Appl.Phys.**87**(2000)1331
29. W.Osikowicz, X.Crispin,C.Tengstedt, L.Lindell, T.Kugler, W.R.Saleneck, Appl.Phys.Lett. **85**(2004)1616
30. C.J.Huang, Y.K.Su, S.L.Wu, Mater.Chem and Phys. **84**(2004)146
31. T.J.Vink, W.Walrave, J.L.C.Daams, P.C.Baarslag and J.E.A.M.van den Meerakker, Thin Solid Films **266**(1995)152
32. G.B.Gonzalez, T.O.Mason, J.P.Quintana, O.Warschkow, D.E.Ellis, J.H.Hwang, J.P.Hodges, J.D. Jorgensen, J.Appl.Phys. **96**(2004)3912
33. A.Rogozin, N.Shevchenko, M.Vinnichenko, F.Prokert, V.Cantelli, A.Kolitsch, W.Moller, Appl.Phys.Lett. **85**(2004)212
34. W.F.Wu, B.S.Chiou, Semicond. Sci.Technol. **11**(1996)196
35. M.A.Martinez, J.Herrero, M.T.Gutierrez, Solar Energy Mater. **26**(1992)309
36. S Honda, A.Tsujimoto, M.Watamori, K.Oura, J.Vac.Sci.Technol.A **13**(1995)1100

37. J.O.Park, J.H.Lee, J.J.Kim, S.H.Cho, Y.K.Cho,Thin Solid Films **474**(2005)127
38. H.Morikawa and M.Fujita, Thin Solid Films **339**(1999)309
39. F.Niino, H.Hirasawa, K.Kondo, Thin Solid Films **411**(2002)28
40. Y.Han, D.Kim, J.S. Cho and S.K.Koh, Thin Solid Films **473**(2005)218
41. B.G.Lewis , D.C.Paine, MRS bulletin (2000)
42. Y.Han,D.Kim, J.S. Cho, Y.W.Whan Beag, S.K.Koh, V. S.Chernysh, J.Appl.Phys. **97** (2005)024910-1
43. V.Korobov, M.Leibovitch, Yoram Shapira, Appl.Phys.Lett. **65**(1994)2290
44. X.W.Sun, H.C.Huang, H.S.Kwok, Appl.Phys.Lett. **68** (1996)2663
45. Y.Hoshi, H.Kato, K.Funatsu, Thin Solid Films **445**(2003)245
46. M.A.M.paliza, R.F.Haglund, Jr., L.C.Feldman, Appl.Phys.Lett. **80**(2002)3757
47. J.P.Zheng, H.S.Kwok, Appl.phys.Lett. **63** (1993)1
48. K.Zhang, F.Zho,C.H.A.Huan, A.T.S Wee, Thin Solid Films **376** (2000) 255
49. T.Maruyama, K.Fukui, J.Appl.Phys.**70**(1991)3848
50. L.A.Ryabova,V.L.salun I.A.Serbinov, Thin Solid Films **92**(1982)327
51. T.Maruyama, K.Fukui, Thin Solid Films **203**(1991)297
52. Y.Shigesato, Y.Hayashi, T.Haranoh, Appl.Phys.Lett. **61**(1992)73
53. M.Mizuhashi, Thin Solid Films **70**(1980)91
54. S.A.Agnihotri, K.K.Saini,T.K.Saxena,K.C.Nagpal, S.Chandra, J.Phys.D.Appl.Phys. **18**(1985)2087
55. P.Thilakan, J.Kumar, Phys.Stat.Sol.(a)**160**(1997)97
56. P.Manivannan, A.Subrahmanyam, J.Phys.D.Appl.Phys **26**(1993)1510
57. M.Yamaguchi , A.I.Ektessabi , H.Nomura and N.Yasui, Thin Solid Films **447-448**(2004)115
58. Y.Shigesato, D.C.Paine, Appl.Phys.Lett. 62 (11)(1993)1268

59. R.X.Wang, C.D.Belings, S.Fung, A.B.Djurisic, C.C.Ling, C.Kwong, S.Li, J.Phys.D. Appl.Phys.**38**(2005)2000
60. Y.Shigesato, D.C.Paine, T.E.Haynes, J.Appl.Phys. **73**(1993)3805
61. D.B.Frasaer, H.D.Cook,J.Electrochem. Soc.**119**(1972)1368
62. K.Itoyama, Jpn.J.appl.Phys. **17**(1978)1191
63. M.K.Jachimowski, A.Brudnik, H.Czternastex, J.Phys.D.Appl.Phys. **18**(1985)L145
64. N.J.Arfsten, J.Non.Crystalline Sol. **63**(1984)243
65. Yeon sik Jung, Sung Soo Lee,J.Crystal Growth **259**(2003)343
66. Li-jian Meng, M.P.dos Santos, Thin Solid Films **322**(1998) 56
67. L.R.Cruz, C.Legnani,I.G.Matoso, C.L.Ferreira, H.R..Moutinho,MRS Bulletin **39**(2004)993
68. M.T. Bhatti, A.M Rana , A.F Khan, Materials Chem. and Phys. **84**(2004)126
69. I.Baia, B.Fernandes, P.Nunes, M.Quintela, R.Martins, Thin Solid Films, **383**(2001)244
70. K.Tanaka, M. Kasahara, H.Usui, Electronics and communications in Japan, **83**(2000)173
71. E.Holmelund, B.Thestrup,J.Schou,N.B.Larsen, M.M.Nielson, E.Johnson, S.Tougaard,Appl.Phys. A **74**(2002)147
72. F.O.Adurodija,H.Izumi,T.Ishihara,H.Yoshioka,M.Motoyama, K.Murai,Jpn J.Appl.Phys**39**(2000)L377
73. F.O.Adurodija, H.Izumi, T.Ishihara, K.Yamada, H.Matsui, M.Motoyama, Thin SolidFilms **350**(1999)79
74. H.Kim, C.M.Gilmore, A.Pique, J.S.Horwitz, H.Mattoussi, H.Murata, Z.H.Kafafi and D.B.Chrisey, J.Appl.Phys.**86**(1999)6451
75. H.Kim, J.S.Horwitz, WHKim, ZH.Kafafi, D.B.Chrisey J.Appl.Phys. **91**(2002)5371

CHAPTER 3

Deposition and Characterisation Techniques

Abstract

This chapter presents the various deposition techniques used for the growth of transparent conducting oxide thin films. The chapter also describes the various characterisatrion tools employed for analyzing the grown films.

3.1 Introduction

Transparent conducting oxide thin films exhibit high electrical conductivity, high optical transmittance in the visible region and high reflectance in the IR region. These unique properties make them suitable for a variety of applications. So various techniques for the growth of these films have been intensively investigated during the recent past. The same material deposited by two different techniques usually has different properties. So, growth techniques play a significant role in governing the properties of these films. This is due to the fact that electrical and optical properties of the films strongly depend on the structure, morphology and the nature of the impurities present [1]. Also, the films grown by any particular technique may often have different properties due to the involvement of various deposition parameters. The properties of the films, therefore, can be tailored by controlling the deposition parameters.

3.2 Thin Film Preparation Techniques

Generally any thin film deposition follows the sequential steps: a source material is converted into the vapour form (atomic/molecular/ionic species) from the condensed phase (solid or liquid), which is transported to the substrate and then it is allowed to condense on the substrate surface to form the solid film [2]. Depending on how the atoms/molecules/ions/clusters of species are created for the condensation process, the deposition techniques are broadly classified into two categories, viz. Physical methods and Chemical methods [3]. The general physical methods that have been used to grow the transparent conducting oxide films are vacuum evaporation and sputtering [4,5]. The vacuum evaporation techniques include, thermal evaporation by resistive heating and electron beam evaporation. All these physical methods of deposition of thin film were done in a high vacuum system in which a vacuum of 10^{-5} mbar was created using a

diffusion pump backed by a rotary pump. The chemical methods include chemical vapour deposition, spray pyrolysis and dip coating [6-8] .The following sections discuss the methodology and experimental set-ups used in various thin film deposition, especially techniques used for the growth of films used in the present investigation.

3.2.1 Vacuum Evaporation

It is the most widely used technique for the preparation of thin films for the deposition of metals, alloys, and also many compounds, as it is very simple and convenient. Here the only requirement is to have a vacuum environment in which sufficient amount of heat is given to the evaporants to attain the vapour pressure necessary for the evaporation. The evaporated material is allowed to condense on a substrate kept at a suitable temperature. A resistively heated tungsten or tantalum source is used to evaporate the charge. The important control parameters are the substrate temperature, evaporation rate, source to substrate distance and the oxygen partial pressure. Transparent conductors can be evaporated in three ways (i) by directly evaporating the metal oxides, (ii) reactive evaporation of the metal in the presence of oxygen and (iii) post oxidation of metal films. Always some deficiency of oxygen will be there when an oxide material is evaporated. To avoid this, the films must either be evaporated in the partial pressure of oxygen or some post deposition heat treatment in air must be done.

Reports on the growth of ITO thin films by evaporation involve reactive evaporation of either metallic alloy or an oxide mixture [9-12]. Films grown by vacuum evaporation using oxide mixtures are usually deficient in oxygen and an oxygen partial pressure of 10^{-4} Torr is necessary to have transparent thin films. X-ray diffraction studies of vacuum evaporated ITO films revealed no trace of any oxide phase of tin even for highly doped films [13]. The preferred

orientation observed in the vacuum evaporated films was (111). Thermal evaporation technique has been used for the deposition of metal electrodes in the present study.

3.2.2 Sputtering

Sputtering is one of the most versatile techniques used for the deposition of transparent conductors when device quality films are required. Sputtering process produces films with higher purity and better controlled composition, provides films with greater adhesion and homogeneity and permits better control of film thickness. The sputtering process involves the creation of gas plasma usually of an inert gas such as argon [14] by applying voltage between a cathode and anode. The cathode is used as a target holder and the anode is used as a substrate holder. Source material is subjected to intense bombardment by ions. By momentum transfer, particles are ejected from the surface of the cathode and they diffuse away from it, depositing a thin film onto a substrate. Sputtering is normally performed at a pressure of 10^{-2} – 10^{-3} Torr.

There are two modes of powering the sputtering system; dc and rf biasing. In dc sputtering system a direct voltage is applied between the cathode and the anode. This method is restricted for conducting targets only. RF sputtering is suitable for both conducting and non-conducting targets; a high frequency generator (13.56 MHz) is connected between the electrodes of the system.

In the process of sputtering, the material is knocked out of a surface by heavy argon ions and travel across the system to condense onto the substrate surface. For the sputtered material to arrive at the substrate surface with the high energy necessary to give a good coating, and for the process to be efficient, it is important for the material to travel without collision with the residual gas in the vacuum. However, the residual gas pressure needed to maintain a simple

electrical discharge, in order to provide the argon ions for bombardment, is too high to allow transfer of the sputtered material without many collisions. This give rise to a very slow deposition rate and poor quality coating. A magnetron uses a magnetic field to confine electrons close to the cathode, making it easier to sustain an electrical discharge at low pressure. Magnetron sputtering is particularly useful when high deposition rates and low substrate temperatures are required [15].

Both reactive and non-reactive forms of dc, RF and magnetron sputtering have been employed for the deposition of semiconducting transparent thin films. In reactive sputtering, the reactive gas is introduced into the sputtering chamber along with argon to deposit oxide films. The deposition rates and properties of the films strongly depend on the sputtering conditions such as the partial pressure of the reactive gas, the sputtering pressure, substrate temperature and target to substrate spacing.

In sputter deposition, the material arrives at the substrate mostly in atomic or molecular form. The atom diffuses around the substrate with a motion determined by its binding energy to the substrate, which is influenced by the nature and temperature of the substrate. The depressions on the substrate surface act as adsorption sites for the diffusing atoms. At each hop, the atom will either jump over the barrier into an adjacent site or will re-evaporate. After a certain time, the atom will either evaporate from the surface or will join another diffusing single atom to form a doublet. These doublets will be joined by other single atoms to form triplets, quadruplets and so on. This stage is known as the nucleation stage of thin film growth and it leads to the formation of quasi-stable islands. The islands will grow in size and it will lead to the coalescent stage. Coalescence proceeds until the film reaches continuity.

Sputtering may be carried out in a variety of systems, which may differ in sputtering configuration, geometry, target type etc. Experimental sputtering systems usually have small targets and low production rates, whereas commercial production systems have large targets and rapid substrate transport to maximize production rate. Irrespective of the sputtering system used, the basic sputtering process remains the same. Figure 3.1 shows a typical sputter deposition system.

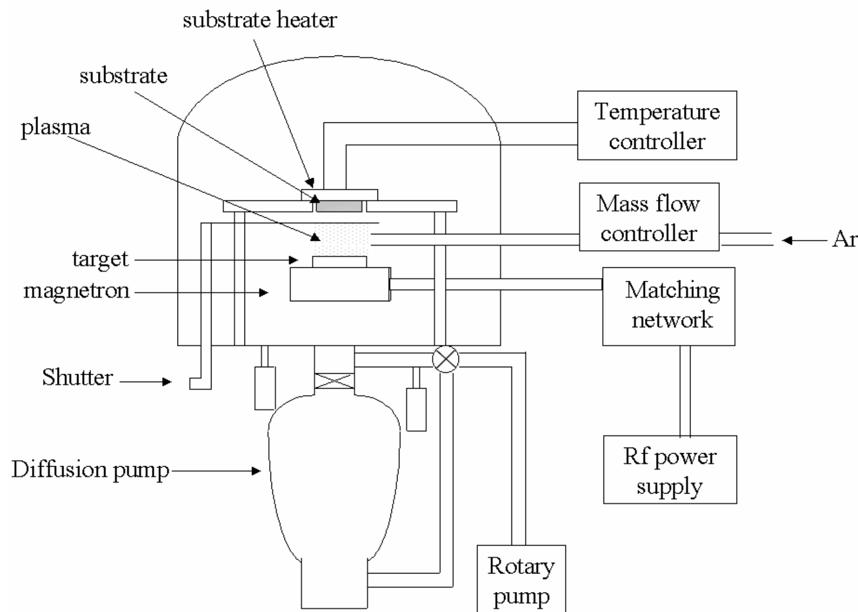

Figure 3.1 Schematic sketch of RF sputter deposition system

The process of RF sputter deposition is made possible due to the large difference in mass, and hence mobility, of electrons and inert gas ions. Because electrons are many times less massive than ions, electrons attain much greater velocities

and travel much further than ions during each cycle of the applied RF voltage waveform. Since electrons travel much further, they eventually accumulate on the target, substrate and chamber walls such that the plasma is the most positive potential in the system. These induced negative voltages or “sheath voltages”, cause acceleration of positive ions toward the negatively charged surfaces, which subsequently leads to sputtering events. The volume adjacent to a surface tends to be relatively free of electrons because of the negatively charged surface. This leads to a “dark space” because electrons are not available to excite gas atoms [8].

The target is selectively sputtered by controlling the relative surface areas of the target and the substrate holder. If space charge limited current is assumed, the ion current flux, J can be estimated by the Child- Langmuir equation [8],

$$J = \frac{KV^{3/2}}{D^2 m_{ion}} \qquad (3.1)$$

where D is the dark space thickness, V is the sheath voltage, m_{ion} is the ionic mass and K is the proportionality constant. Since the positive ion current must be equal at both the electrodes,

$$\frac{A_A V_A}{D_A^2} = \frac{A_B V_B}{D_B^2} \qquad (3.2)$$

where A_A and A_B are the surface areas of electrodes A and B respectively (Fig 3.2). It should be noted that this step differs from the assumption of treating the positive ion current densities equal.

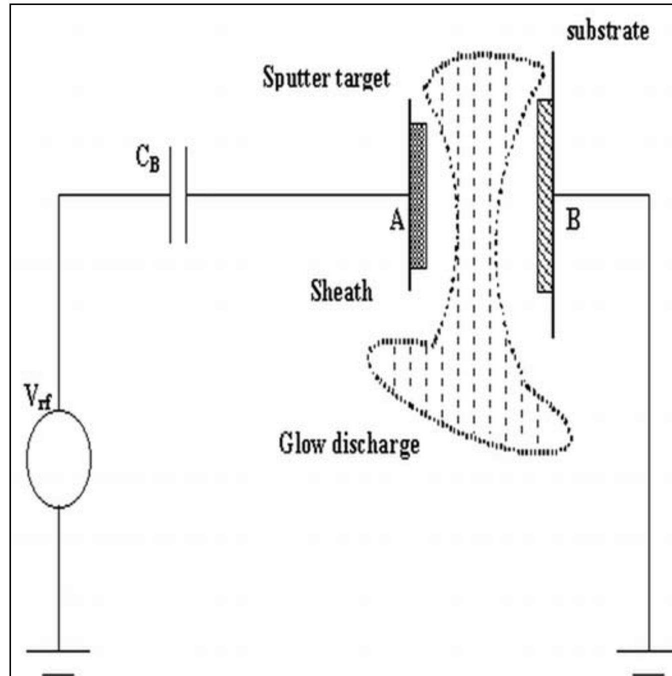

Figure 3.2 Deposition process during RF sputtering

If the positive ion current densities were equal, there would be a much greater positive ion current flowing during one half cycle of the applied voltage waveform than the other due to the much greater area of the grounded substrate electrode. Therefore, because this system is assumed to be in steady state, the total positive ion current per half cycle should be the relevant quantity.

The glow discharge itself is a region where large quantities of positive and negative charge exist and can be modelled as a wire. Since most of the voltage in the glow discharge is dropped across the dark space, and they have small conductivities, they can be modelled as capacitors such that the capacitances,

$$C \propto A/D \quad (3.3)$$

Furthermore, an AC voltage will divide across two series capacitors such that,

$$\frac{V_A}{V_B} = \frac{C_B}{C_A} \tag{3.4}$$

From equations (2.1), (2.2) and (2.3),

$$\frac{V_A}{V_B} = \left(\frac{A_B}{A_A}\right)^2 \tag{3.5}$$

This equation tells that smaller area will see larger sheath voltage, whereas larger area will see a smaller sheath voltage by a power of 2. The usefulness of this result is that $A_B > A_A$ must hold to selectively sputter the target. This is done in practice by grounding the substrate holder to the entire chamber resulting in a very large A_B. For this reason it is extremely important that the substrate holder and the system are well grounded to ensure that resputtering of the growing film does not occur.

We have used an in-house made magnetron for the rf sputtering of tin doped Indium oxide thin films. A magnet of 2000gauss was used to deflect the ions. A schematic diagram of the magnetron is shown in figure 3.3. The vacuum system consists of a six-inch diameter diffusion pump backed by a rotary pump (make – Indovision, Bangalore). The rf supply was connected to the magnetron through a capacitive matching network (make–Digilog Instruments, Bangalore). The flow of argon gas into the vacuum chamber was controlled using a mass flow controller (make Bronkhorst, Holland).

The reports on ITO films by sputtering of oxide target show that the use of oxide target helps in controlling the stoichiometry of the films [16,17]. Usually, oxygen added to the sputtering gas mixture improves the structural, electrical and optical properties of the films provided the oxygen partial pressure is low and is within a narrow range [18]. The films deposited at lower deposition rates show (400) peak while those deposited at higher deposition rates are reported to show (222) peak [19].

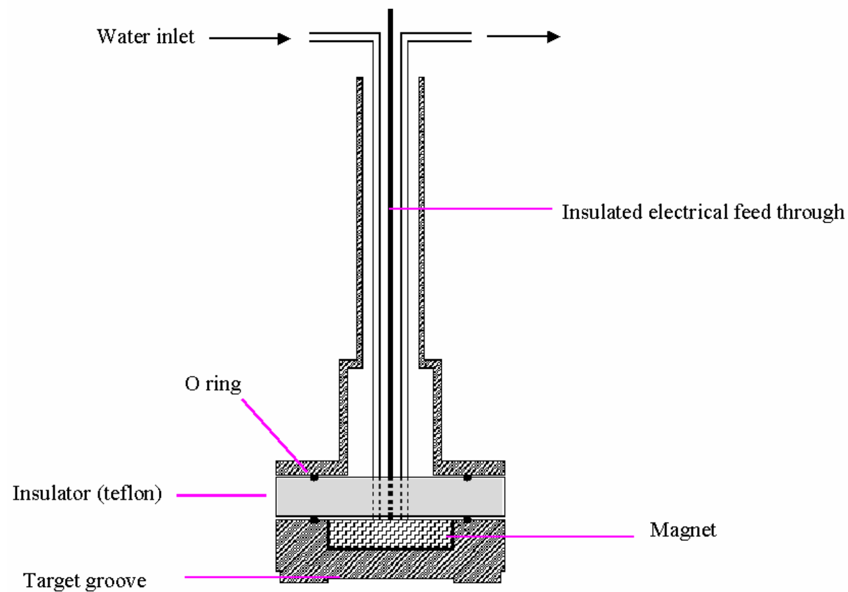

Figure 3.3 Schematic structure of the magnetron

3.2.3 Pulsed laser deposition

Pulsed laser deposition (PLD) is a relatively new technique used for depositing superconducting and transparent conducting oxide thin films. PLD provides several advantages compared to other deposition techniques in the growth of multicomponent oxide thin films [20]. For a multi component target, the composition of films grown by PLD reproduces that of the target. PLD film crystallize at lower substrate temperature relative to other physical vapour deposition techniques due to the high kinetic energy (>1 eV) of the ionised and ejected species in the laser produced plasma. Also the surface of the TCO film

grown by PLD is very smooth. ITO films grown by PLD, have already been used as the anode contact in organic light emitting diodes (OLEDs). The main issues confronting PLD technology is the small substrate coverage, low deposition rates and non-uniformity of film thickness.

3.2.4 Chemical vapour deposition

Chemical vapour deposition (CVD) is one of the most important methods used for producing semi conducting transparent thin films. The technique involves a reaction of one or more gaseous reacting species on a solid substrate. Here, metallic oxides are grown by the vaporization of a suitable organometallic compound. A vapor containing the condensate material is transported to a substrate surface, where it is decomposed by a heterogeneous process [21]. The decomposition condition should be such that the reaction occurs only at or near the substrate surface and not in the gaseous phase, to avoid the formation of powdery deposits, which may result in haziness in the films.

The quality of the films deposited by CVD depends on various parameters such as substrate temperature, gas flow rate and system geometry. All these parameters should be optimized and controlled in order to get best quality films. The main advantage of using the CVD process are simplicity, reproducibility and ease with which it can be adopted for large scale production without requiring vacuum as an essential requirement. The cost of production of thin films by this technique is very low. Films of high purity, stoichiometry and structural perfection can be obtained. The main disadvantage is that the morphology of the films deposited by CVD is strongly influenced by the nature of the chemical reaction and the activation mechanism.

The experimental set up for CVD consists of a quartz tube of diameter 18mm in which two separate temperature zones are maintained using resistance furnaces:

the evaporation zone (Temperature varies from 150 to 200^{0}C) and the reaction zone (Temperature varies from 350 to 450^{0}C). Vapors from the reactants are transported into the reaction zone by a carrier gas (N_2). The reactants used for the process were indium and tin acetyl acetonates mixed in the ratio 43:57 wt%. The films grown by this technique were found to be polycrystalline and showed (222) diffraction peak [22].

3.2.5 Spray pyrolysis

This is one of the relatively simple and cheap methods that can be easily adopted for the mass production of large area coatings for industrial applications. The method is based on the pyrolytic decomposition of a metallic compound dissolved in a liquid mixture when it is sprayed onto a preheated substrate [23]. The method depends on the surface hydrolysis of a metal chloride on a heated substrate surface in accordance with the reaction

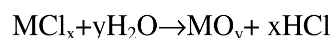

$$MCl_x + yH_2O \rightarrow MO_y + xHCl$$

in which M is any host metal such as Sn ,In or Zn of the oxide film.

The atomisation of the chemical solution into spray of fine droplets is accomplished by the spray nozzle with the help of a filtered carrier gas. The carrier gas and solution are fed into the spray nozzle at predetermined pressures and flow rates. The geometry of the gas and the liquid nozzles strongly determine the spray pattern, size distribution of droplets and spray rate which in turn determine the growth kinetics and hence the quality of the films grown. The other important parameters that affect the film quality are the nature and temperature of the substrate, the solution composition, the gas and solution flow rates and nozzle to substrate distance.

3.3 Characterization Tools

The optimisation of the preparation conditions is the main task in order to get device quality films. This is to be done on the basis of detailed structural, compositional, morphological, optical and electrical properties of the films obtained at different growth conditions. In the following sections the techniques used for the film characterizations are discussed briefly.

3.3.1 Thin film thickness

Thickness plays an important role in the film properties unlike a bulk material. Reproducible properties are achieved only when the film thickness and the deposition parameters are kept constant. Film thickness may be measured either by in-situ monitoring of the rate of deposition or after the film deposition. In the present work, the film thickness was determined by employing optical interference technique.

3.3.1a Optical interference method

Film thickness can be measured accurately from interference fringes using multiple beam interferometry. This technique was first used by Weiner [24] and later was modified by Tolansky [25]. Two reflecting surfaces are brought in close proximity such that a small wedge with a small air gap in between them is formed. If a monochromatic light falls at normal incidence on it, interference of light due to the multiple reflected beams results in a series of fringes (Fizeau). The distance between the fringes depends on the air gap as well as on the wavelength of the monochromatic light.

The film for thickness measurement is deposited on a flat surface so as to leave a sharp edge between the film and the uncoated region of the substrate. Over this film a highly reflecting coating of aluminium forms a sharp step on the film edge. Another optically flat glass slide known as the reference plate with a partially transparent aluminium film is then placed over the specimen with the metal coated surfaces in contact with each other so as to leave a small air gap at the step. A monochromatic parallel beam of light is then incident on this two plates assembly and reflected light is then observed through a microscope. A set of sharp fringes perpendicular to the step with equal displacements will be observed and the thickness (t) can be determined using the relation,

$$t = \frac{b\lambda}{2a} \qquad (3.7)$$

where b is the displacement of the fringes at the step and a is the distance between consecutive fringes. The sharpness of the fringes depends on the reflectivity of the metal coating, the spread of the incident beam, air gap etc.

3.3.2 Surface morphology

The uniformity and roughness of the thin film surface plays an important role in the optical properties of thin films. When the surface is rough, the films will be less transparent and the grain boundaries will affect the electrical properties of the thin films. The surface morphology of the films is studied using scanning electron microscopy (SEM).

Scanning electron microscopy (SEM) is one of the most widely used techniques for obtaining micro structural and surface features of thin films. An electron beam is focused onto the surface of the specimen and results in the ionization of the atoms in the specimen. This will cause the ejection of the secondary electrons from the surface, very close to the incident beam position. These secondary electrons can be attracted to a positively charged detector with high

efficiency. The secondary electron yield per primary electron is high and increases as the angle between electron beam and the surface normal increases [26]. The secondary electrons generated from the specimens are used for Z-modulation in a corresponding raster on an oscilloscope. In order to avoid charging problems a thin layer of gold is deposited on the specimen without altering the surface features. The secondary electron mode is generally preferred for topographical feature determination since these electrons generate only from about $10A^0$ or less from the film surface and hence the picture obtained is a faithful reproduction of the surface features.

The scanning electron microscopy can be effectively used for the surface analysis to know the details regarding the grain size, presence of minor or secondary phases, the orientation of the grains, uniformity, porosity of the sample etc. SEM gives a pictorial overview of the grains on the thin film surface.

3.3.3 Energy dispersive x-ray analysis (EDX)

EDX was used to estimate the composition of the thin film samples. x-rays are generated by the incident electrons within a volume similar to but rather larger than that for the backscattered electrons. Peak x-ray energies corresponding to the characteristics of the elements within that volume can be identified and the relative compositions of elements can be estimated. Thus the bulk composition of the sample and of the individual grains in a polycrystalline sample can be determined [26].

3.3.4 x-ray diffraction studies

Electrical and optical properties of the materials are influenced by the crystallographic nature of the films. x-ray diffraction (XRD) studies were carried out to study the crystallographic properties of the thin films prepared.

A given substance always produces a characteristic x-ray diffraction pattern whether that substance is present in the pure state or as one constituent of a mixture of substances. This fact is the basis for the diffraction method of chemical analysis. The particular advantage of x-ray diffraction analysis is that it discloses the presence of a substance and not in terms of its constituent chemical elements. Diffraction analysis is useful whenever it is necessary to know the state of chemical combination of the elements involved or the particular phase in which they are present. Compared with ordinary chemical analysis the diffraction method has the advantage that it is much faster, requires only very small sample and is non destructive [27,28].

The basic law involved in the diffraction method of structural analysis is the Bragg's law. When monochromatic x-rays impinge upon the atoms in a crystal lattice, each atom acts as a source of scattering. The crystal lattice acts as series of parallel reflecting planes. The intensity of the reflected beam at certain angles will be maximum when the path difference between two reflected waves from two different planes is an integral multiple of λ. This condition is called Bragg's law and is given by the relation,

$$2dSin\theta = n\lambda \qquad (3.8)$$

where n is the order of diffraction, λ is the wavelength of the x-rays, d is the spacing between consecutive parallel planes and θ is the glancing angle (or the complement of the angle of incidence)[29].

x-ray diffraction studies gives a whole range of information about the crystal structure, orientation, average crystalline size and stress in the films. Experimentally obtained diffraction patterns of the sample are compared with the standard Powder Diffraction Files published by the International Centre for Diffraction Data (ICDD).

The average grain size of the film can be calculated using the Scherrer's formula [27],

$$d = \frac{0.9\lambda}{\beta Cos\theta} \qquad (3.9)$$

where, λ is the wavelength of the x-ray and β is the full width at half maximum intensity in radians. The lattice parameter values for different crystallographic systems can be calculated from the following equations using the (hkl) parameters and the interplanar spacing d.

For cubic system,

$$\frac{1}{d^2} = \frac{h^2 + k^2 + l^2}{a^2} \qquad (3.10)$$

x-ray diffraction measurements of the different films were done using Rigaku automated x-ray diffractometer. The filtered copper Kα (λ=1.5418A^0) radiation was used for recording the diffraction pattern.

3.3.5 Optical characterisation

3.3.5a Determination of optical band gap

An important technique for measuring the band gap of a semiconductor is by studying the absorption of incident photons by the material. In this, photons of selected wavelength are directed at the sample and the relative transmission of the various photons is observed. Since photons with energies greater than the

band gap energy are absorbed while photons with energies less than band gap energy are transmitted, the experiment gives an accurate measure of band gap [30].

According to Bardeen et al. [31] for the parabolic band structure, the relation between the absorption coefficient (α) and the band gap of the material is given by,

$$\alpha = \frac{A}{h\nu}\,(h\nu - E_g)^{\,r} \qquad (3.11)$$

where, r =1/2 for allowed direct transitions, r =2 for allowed indirect transitions, r =3 for forbidden indirect transitions and r =3/2 for forbidden direct transitions. A is the parameter which depends on the transition probability. The absorption coefficient can be deduced from the absorption or transmission spectra using the relation,

$$I = I_0 e^{-\alpha t} \qquad (3.12)$$

where, I is the transmitted intensity and I_0 is the incident intensity of the light and t is the thickness of the film. In the case of direct transition, $(\alpha h\nu)^2$ will show a linear dependence on the photon energy (hν). A plot of $(\alpha h\nu)^2$ against hν will be a straight line and the intercept on energy axis at $(\alpha h\nu)^2$ equal to zero will give the band gap.

3.3.5b Determination of optical constants

The optical constants, the refractive index (n) and the extinction coefficient (k) of the films are calculated using the theory of Manificer et al. [32] for weakly absorbing films.

Since ITO is a very weakly absorbing film, the measurement of transmission of light through the film in the region of transparency is sufficient to determine the real and imaginary parts of the complex refractive index n* = n-ik. For such films the following method can be used for determining the optical constants.

If the incident light has unit amplitude then the amplitude of the transmitted wave is

$$A = \frac{t_1 t_2 \exp(-2\pi i n^* t/\lambda)}{1 + r_1 r_2 \exp(-4\pi i n^* t/\lambda)} \qquad (3.13)$$

Where t_1, t_2 , r_1 and r_2 are the transmission and reflection coefficients of the front and rear surfaces respectively and are given by

$$t_1 = \frac{2n_0}{n_0 + n} \quad , \quad t_2 = \frac{2n}{n + n_1} \qquad (3.14a) \ \& \ (3.14b)$$

$$r_1 = \frac{n_0 - n}{n_0 + n} \quad \text{and} \quad r_2 = \frac{n - n_1}{n + n_1} \qquad (3.14c) \ \& \ (3.14d)$$

n_0 , n and n_1 are the refractive indices of the substrate, film and the medium respectively.

Transmission coefficient of the layer is $T = \frac{n_1}{n_0} A^2$ (3.15)

If we consider the case of normal incidence and weak absorption (where $k^2 << (n - n_0)^2$ and $k^2 << (n-n_1)^2$).

Transmission coefficient is given by

$$T=\frac{16n_0n_1n^2\alpha_1}{c_1{}^2+c_2{}^2\alpha_1{}^2+2c_1c_2\alpha_1\cos(4\pi nt/\lambda)} \quad (3.16)$$

where $c_1 = (n+n_0)(n+n_1)$ (3.17)

$c_2 = (n-n_0)(n_1-n)$ (3.18)

and $\alpha_1 =(-4\pi\, kt/\lambda) = \exp(-\alpha t)$ (3.19)

Here α is the absorption coefficient of the thin film, t is the thickness, k is the extinction coefficient and λ is the wavelength of light.

The extreme values of T are

$$T_{max} = \frac{16n_0n_1n^2\alpha_1}{(c_1+c_2\alpha_1)^2} \quad (3.20) \text{ and}$$

$$T_{min} = \frac{16n_0n_1n^2\alpha_1}{(c_1-c_2\alpha_1)^2} \quad (3.21)$$

where $n =[N +(N^2 - n_0{}^2\, n_1{}^2)^{1/2}]^{1/2}$ (3.22) and

$$N = n_0{}^2+n_1{}^2+2\, n_0\, n_1 \frac{T_{max}-T_{min}}{T_{max}T_{min}}$$

Knowing T_{max}, T_{min}, n_0 and n_1 at the same wavelength refractive index(n) of the film can be calculated.

3.3.6 Electrical characterization

3.3.6a Resistivity by two probe method

The resistivity of the films is determined by the two-probe method with the electrodes in planar geometry. Evaporated indium layers or high conducting silver paste was used as the electrodes. The current voltage measurements were carried out using a Keithley`s source measure unit (Model SMU236). The resistivity (ρ) of the films is calculated applying ohm's law, by the relation ρ = RA/L where R is the resistance given by the slope of the current - voltage characteristic curves. A is the area of the film in planar geometry which is given by the product of the film thickness and the width of the film. L is the spacing between the electrodes

3.3.6b Hall measurement

The electrical resistivity of a semiconductor thin film can be written using Ohm's law,

$$\rho = \frac{1}{en\mu} \qquad (3.23)$$

where 'ρ' is the film resistivity, e is the electronic charge, n is the number of carriers corresponding to the carrier concentration and 'μ' is the carrier mobility. According to Ohm's law the carrier mobility affects resistivity. Low resistivity can be achieved by increasing the carrier concentration or mobility or both. Increasing carrier concentration is self-limiting because at some point the increased number of free carriers decreases the mobility of the film due to carrier scattering. Hence there is a trade off between the carrier density and carrier mobility for achieving low resistivity.

In the case of Indium tin oxide films, the resistivity (ρ), carrier concentration (n), carrier mobility (μ), and sheet resistance were measured using vander Pauw four point probe in geometry [33]. Samples used were 1cm x 1cm in size. The ohmic contacts were made using silver paste. The silver paste was applied at the corners of the sample symmetrically as shown in figure 3.4.

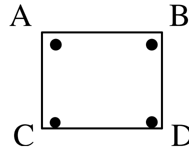

Figure 3.4 Symmetric contacts in vander Pauw geometry

Let R_1 be the potential difference between A and B per unit current through C and D or vice versa. Similarly R_2 the potential difference between B and C per unit current through D and A.
Then sheet resistance R_s can be calculated using the relation

$$R_s = \left(\frac{\pi}{\ln 2}\right)\left(\frac{R_1 + R_2}{2}\right) f\left(\frac{R_1}{R_2}\right) \qquad (3.24)$$

where $f\left(\frac{R_1}{R_2}\right)$ is the vander Pauw function and is given by the relation,

$$f\left(\frac{R_1}{R_2}\right) = 1 - 0.3466\left(\frac{R_1 - R_2}{R_1 + R_2}\right)^2 \qquad (3.25)$$

The Hall signal was measured between two ends while passing the current through the other two ends. Hall mobility is,

$$\mu = \Delta R \times \frac{10^8}{BR_s} \qquad (3.26)$$

where ΔR is the change in resistance due to magnetic field (B) which was applied to measure Hall voltage. Carrier concentration was determined using the equation 3.23. The hall coefficient R_H is given by,

$$R_H = \mu \, x \, \rho \qquad (3.27)$$

The type of carriers can be understood from the sign of the R_H. The negative values of R_H correspond to the electrons (n-type) carriers and positive values to holes (p-type).

3.4 Plasma Studies

3.4.1 Introduction

Plasma, the fourth state of matter, is a substance in which many of the atoms or molecules are effectively ionized, allowing charges to flow freely. Since more than 99% of the known universe is in the plasma state and has been so since the BigBang, plasma might be considered as the first state of matter. In earlier epochs of the universe, everything was plasma. In the present epoch, stars, nebulae, interstellar spaces etc are filled with plasma. The solar spectrum is also permeated with plasma in the form of solar wind, and the earth is completely surrounded by plasma trapped within its magnetic field. Terrestrial plasma occur in lightning, fluorescent lamps, a variety of laboratory equipments and industrial processes[34].

The distinction between the four states of matter can be expressed in terms of an ascending scale of energy as we pass from solid to liquid to gas and finally to plasma. The atomic theory has made us familiar with the concepts of basic particles like atoms, molecules and combinations of molecules etc; that they are common to the state of matter. The distinction among this states lies in the difference between the bond or the force joining these constituent particles. Thus a strong bonding characterize the solid state, liquid state by a weak bonding and gaseous state by lack of bonding between particles. In microscopic terms it is the kinetic energy of constituent particles that determines the matter state. Because this energy opposes the inter particle binding force and the resultant equilibrium determines its state.

In solid, particles are characterized to a rigid order. In liquid they are free to move around. In gas even though atoms are free to move randomly, the electrons in them performs a harmonic dance over their orbits according to the laws of quantum mechanics. But in plasma, the electrons are liberated from the atoms and acquire complete freedom of motion. In plasma, the ionization increases with increase of temperature. So in plasma, the particles exist in the form of +ve ions and –ve electrons. In hydrogen, at normal pressures ionization becomes complete at about 2×10^4 to 3×10^4 K. Fully ionized gas formed in this way is called as high temperature plasma. In this ionized gas there exists some cohesiveness, i.e., the formation of clusters within a very short time after the production of ions. Instead of remaining as singly ionized molecules they soon get attached to other molecules and form clusters; chiefly when polar molecules of other gases or vapors such as H_2O are present as impurity. This property is neither the usual characteristics of solids nor fluids. So plasma, in physics, is regarded as the 4th state of matter.

It was Irving Langmuir, who first used the term plasma to describe the oscillations that are observed in a low-pressure mercury discharge[35]. Later, a branch of physics that deals with properties of fully ionized gas was evolved. Developments in many branches of physics, from the time of Langmuir's work, have contributed directly and indirectly to the present state of plasma physics. After Langmuir, plasma research gradually spread in other directions. The development of radio broadcasting led to the discovery of earth's ionosphere, a layer of partially ionized gas in the upper atmosphere, which reflects radio waves. Unfortunately, the ionosphere also occasionally absorbs and distorts radio waves. Earth's magnetic field causes waves of different polarization to propagate at different velocities, which give rise to the 'ghost signals' i.e. signals which arrive at a little before or a little after the main signal. In order to understand some of the deficiencies in radio communication, Appleton and

Budden, systematically developed the theory of electromagnetic wave propagation through non-uniform magnetized plasma.

Later, astrophysicist recognized that much of the universe consists of plasma, and, thus a better understanding of astrophysical phenomena requires a better grasp of plasma physics. The pioneer in this field was Hannes Alfvein, who in 1940's developed the theory of magneto hydrodynamics (MHD) in which plasma is treated as a conducting fluid. MHD is a physical model describing the properties of electrically conducting fluids interacting with magnetic and electric fields. This theory has been both widely and successfully employed to investigate sunspots, solar flares, solar wind, star formation etc. Two topics of particular interest in MHD theory are magnetic reconnection and dynamo theory. Magnetic reconnection is a process by which magnetic field lines suddenly change their topology. It can give rise to the sudden conversion of a great deal of magnetic energy into thermal energy; as well as the acceleration of some charged particles to extremely high energies. This is thought to be the basic mechanism behind solar flares. Dynamo theory studies show the motion of an MHD fluid can give rise to the generation of a macroscopic magnetic field. This process is important because both terrestrial and solar magnetic fields would decay away comparatively rapidly (in astrophysical terms) were they not maintained by dynamo action. The earth's magnetic field is maintained by the motion of its molten core, which can be treated as an MHD fluid.

The creation of hydrogen bomb in 1952 generated a great deal of interest in controlled thermonuclear fusion as a possible power source for the future. In the initial years this research was carried out secretly in USA, Soviet Union and Britain. However in 1958 thermonuclear fusion research was declassified, leading to the publication of a number of immensely important and influential papers in the late 1950's and early 1960's. Theoretical plasma physics first emerged as a mathematically rigorous discipline in these years. Surprisingly,

fusion physicists are mostly concerned with understanding how thermonuclear plasma can be trapped, in most cases by a magnetic field, and investigating many plasma instabilities which may allow it to escape. The planned International Thermonuclear Experimental Reactor (ITER) is hoped to be the final step before practical fusion energy becomes a reality.

In 1958, James A Allen discovered Van Allen radiation belts surrounding the earth. Radiation belts are plasma regions in the earth's magnetosphere in which charged particles are trapped by magnetic mirror effect. It is discovered by using data transmitted by the U S explorer satellite, marked the start of the systematic exploration of earth's magnetosphere via satellite, and opened up the field of space plasma physics.

The development of high-powered lasers in 1960s opened up the field of laser plasma physics. When a high-powered laser beam strikes a solid target material is immediately ablated, and a plasma forms at the boundary between the beam and the target. Laser plasmas tend to have fairly extreme properties (e.g. densities characteristic of solids) not found in more conventional plasmas. A major application of laser plasma physics is the approach to fusion energy known as inertial confinement fusion. In this approach highly focused laser beams are used to implode a small solid target until the densities and temperatures characteristics of nuclear fusion (i.e., the center of a hydrogen bomb) are achieved. Another interacting application of laser plasma physics is the use of extremely strong electric fields generated when a high intensity laser pulse passes through plasma to accelerate particles. High-energy physicist hopes to use plasma acceleration techniques to dramatically reduce the size and cost of particle accelerators.

3.4.2 Different types of plasma

Generally plasma is classified into four types depending upon temperature and density. There are various types of plasma ranging from very high density ($n \sim 10^{36}/m^3$, inside a white dwarf) to a very low density ($n \sim 10^6/m^3$, in interstellar spaces).

3.4.2a Weakly ionized plasma

It is not necessary for every particle to be ionized to be involved in plasma phenomena. In Langmuir's experiment he named plasma for that part of the discharge remote from boundaries. Physical significance of this is that particles inside plasma region are not influenced by the boundary potential of discharge. In weakly ionized plasma, only a small fraction of the atoms are ionized.

3.4.2b Strongly ionized plasma

As the temperature increases, the kinetic energy of the particles increases and degree of ionization also increases. So the collision behaviour of plasma particle increases and all collisions becomes coulombic interaction. In fully ionized plasma, all atoms are stripped of electrons nearly all the time and all particles are subjected to coulombic interaction.

3.4.2c Hot plasma

In hot plasma, the temperature is that much high so that particles acquires very large kinetic energy and passes each other very quickly without much interference. Such plasma offers almost no resistance to electric current. In hot plasma temperature is of the order of 10^6 ^oK and can be confined in a magnetic field.

3.4.2d Cold plasma

Cold plasma is one with low conductivity. Due to higher interaction there is a charge leakage and the temperature is of the order of 10 or 100 thousand degrees.

3.5 Plasma Diagnostics

Plasma diagnostics plays an important role in all plasma experiments and at the present time represents a rapidly expanding field of research. Plasma is a gas ionized sufficiently so that the charge separation, which can take place in it, is small compared to its microscopic charge density. On a macroscopic scale, therefore, plasma is approximately neutral, although its principal constituents are charged ions and electrons. In order to produce and maintain such a medium, significant amount of energy is required to dissociate and ionize the initially neutral gas to give the electrons and ions with sufficient kinetic energy to prevent immediate reattachment and recombination during the period of the experiment. Most methods for transferring this energy to plasma makes use of developing plasma as a variable electric component. Thus the time dependence of circuit current and voltage parameters gives basic and important information about over-all plasma conditions.

Information about fundamental plasma parameters, like electron temperature, electron density etc., are essential in order to evaluate the energy transport into the plasma. There are several diagnostic techniques employed for the determination of electron density and temperature which includes, plasma spectroscopy, Langmuir probe, Microwave and laser interferometry and Thomson scattering [36]. In the present investigation, Langmuir probe and Optical Emission Spectroscopy were used as the diagnostic tools.

3.5.1 Langmuir Probe

Langmuir probe is one of the simplest techniques for obtaining information about the ions in the plasma. It consists of an electrode of known area inserted in the plasma and connected electrically to a variable-voltage power supply (Fig3.5). This power supply is in turn grounded to a reference electrode inserted in the plasma. The reference electrode in the case of a single Langmuir Probe is much larger than the probe itself and typically consists of the chamber walls or any other convenient conducting surface in contact with the plasma. This apparently simple experimental technique is associated with rather complicated theories that are needed to explain the current-voltage behaviour of these probes in the plasma [37].

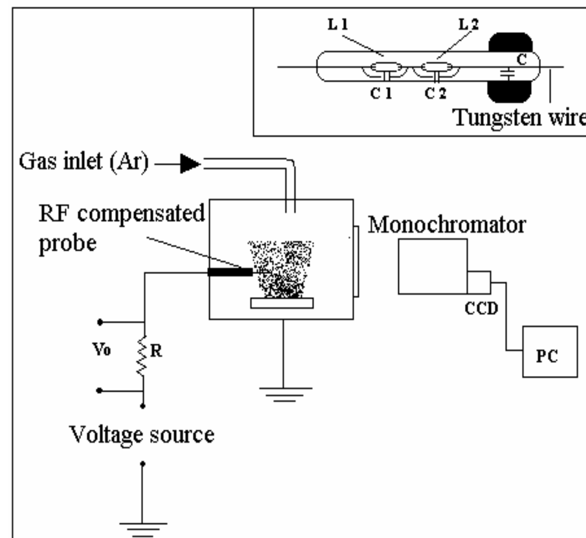

Figure 3.5 Langmuir probe and circuit to measure current – voltage characteristics

3.5.1a Theory of Langmuir Probes

The probe current is dependent on the potential imposed on the probe. A typical current-voltage plot is shown in figure 3.6. This characteristic is normally determined by the plasma properties in the immediate vicinity of the probe[39]. The general shape of the *I-V* characteristic can be divided into three regions. When the probe is biased positively with respect to the local plasma potential the flux of particles reaching the probe will consist of carriers of negative charge (normally electrons). This region is called the electron-accelerating region and is labelled III in figure 3.6. These electrons will be collected from a region called the sheath, which is the region close to the probe surface where the potential exerted by the probe is not shielded by the plasma. When the probe is biased at a potential slightly smaller than the plasma potential only particles with enough energy to overcome the potential barrier will be collected. This region (region II in figure 3.6) is called the electron retarding region. The region I is accessed when the probe is biased increasingly negative relative to the plasma potential. In this region (region I in figure 3.6) only positive ions will reach the probe. This region is called the ion saturation region. The governing theories applicable to these three regions in the *I-V* plot are discussed in the remainder of this section.

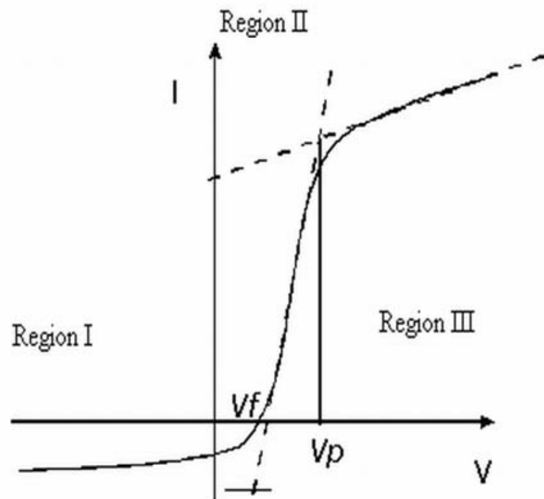

Figure 3.6 Typical current voltage plot, representing the plasma potential (V_p) and floating potential (V_f)

In the electron-retarding region (region II), the probe actually acts as an energy selector, collecting only those electrons which have large enough kinetic energies to overcome the potential barrier. If the electron distribution is in local thermal equilibrium, the electron energy distribution function can be assumed to be Maxwellian and the current drawn in this regime follows the relation:

$$I_e = n_e e A_p \left(\frac{kT_e}{2\pi m_e} \right)^{\frac{1}{2}} \exp\left(\frac{e(V - V_p)}{kT_e} \right), \tag{3.22}$$

where V_p is the plasma potential, V is applied potential, I_e is the electron current, n_e the electron number density, e the electron charge, A_p the probe area, k the

Boltzmann constant, T_e the electron temperature and m_e the electron mass. The gradient of a plot of $\ln[I_e]$ versus the applied voltage V, yields the electron temperature and, given knowledge of the electron current at the plasma potential, substitution of T_e in equation (3.22) yields to the electron number density.

The electron acceleration region (region III) is governed by the orbital motion theory, and an expression for the electron current in this region can be derived as follows: consider a point charge at a bias potential V, a placed at a distance r_0 from an electron with charge e , where the potential is V_p. Assume that the electron has a forward trajectory, with velocity v_0 and impact parameter p as defined in figure 3.7.

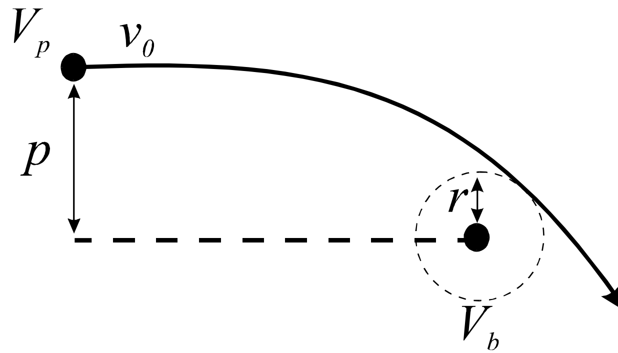

Figure 3.7 Schematic of the input for the orbital motion theory.

The total kinetic energy T of the particle at any time during its trajectory is given by:

$$T = \frac{1}{2} m \left[v^2 + r^2 \left(\frac{d\psi}{dt} \right)^2 \right] \qquad (3.23)$$

where the two terms on the right hand side of expression (3.23) are, respectively, the translational and the rotational parts of the total kinetic energy. Given that (conservation of angular momentum):

$$\frac{d\psi}{dt} = \frac{pv_0}{r^2} \tag{3.24}$$

we can rewrite the expression (3.23) as

$$T = \frac{1}{2}mv^2 + T_0 \frac{p^2}{r^2} \tag{3.25}$$

Given equation (3.25) we can rewrite the total energy of the system as:

$$E_T = \frac{1}{2}mv_0^2 - eV_p = \frac{1}{2}mv^2 + T_0 \frac{p^2}{r^2} - eV \tag{3.26}$$

At the point of closest distance to the probe (r_c), the translational kinetic energy is totally converted into centrifugal energy (v = 0), thus the total energy expression (3.26) can be rewritten as:

$$\frac{1}{2}mv_0^2 - eV_p = T_0 \frac{p^2}{r_c^2} - eV_c \tag{3.27}$$

Rearranging expression (3.27) gives:

$$p = r_c \left[1 - \frac{e\left(V_c - V_p\right)}{T_0} \right]^{1/2} \tag{3.28}$$

Taking r_c as the probe radius a, any particle with $p < a[1+(V_c-V_p)/T_0]^{1/2} = p_a$ will be collected. The expression for the current collected by a cylindrical probe given a Maxwellian electron velocity distribution can also be derived . It takes the form:

$$I_e = n_e e A_p \left(\frac{kT_e}{2\pi m_e} \right)^{\frac{1}{2}} \frac{2}{\sqrt{\pi}} \left(1 - \frac{e(V - V_p)}{kT_e} \right)^{\frac{1}{2}} \tag{3.29}$$

Plotting the square of the electron current against the probe voltage yields a straight line, the gradient of which provides a measure of $(n_e)^2$.

The ion saturation current region (I) is a more difficult region to describe. The amount of ion current is governed by the Bohm criterion, since the ion temperature is much lower than the electron temperature in the plasmas under consideration. The Bohm criterion states that the ion velocity must acquire a positive (towards the probe) velocity at the plasma sheet edge even when the ions have very low temperatures. This velocity is provided by the existence of a "pre-sheet" potential drop that occurs at long distances in the plasma. The ion current is thus dependent on the electron temperature and is given by:

$$I_i = 0.6 n_{i\infty} e S \sqrt{\frac{T_e}{m_i}} \tag{3.30}$$

where $n_{i,\infty}$ is the unperturbed (by the electric field of the probe) ion density and S is the surface area of the probe.

Since the ion current is dependent on the electron temperature there is no easy way to deconvolute the total signal into the ion density and the electron temperature without independent measurement of one of the parameters.

The above expressions are strictly only valid in collisionless sheath conditions (i.e. when the mean free path $\lambda >$ sheath dimensions). Higher order corrections have to be included in the expressions in situations where collisions occur within the plasma sheath.

3.5.1b Specifics of the Langmuir probe

The Langmuir probe assembly consists of a Tungsten wire, 200 μm in diameter and 5 mm in length, supported by a glass sleeve (Fig 3.6). The wire can be biased at voltages in the range of -50 to 50 V, relative to the target and the vacuum chamber. Great care was taken to prevent the probe feed wires being exposed to the plasma since this will contribute to the measured probe current. To ensure a clean probe surface, the probe wire is replaced frequently. The output of the Langmuir probes was measured with a multimeter.

3.5.1c Practical complications

Real probe measurement is much more complex, for a variety of reasons. The effective current-collecting area of the probe is not its geometric surface area, but rather the area of the interface between the plasma and sheath around the probe; and the thickness of the sheath. For a given plasma, it is a function of the probe potential. The probe should be small, so that the probe current does not constitute a significant drain on the plasma. With a cylindrical probe, the varying sheath thickness is an even larger effect [38]. Two more complications are associated with additional charge generation. Secondary electrons may be generated at the probe due the direct impact of ions, electrons and photons. The

heating effects caused by such impact, give rise to additional current flow and electron impact ionisation may occur in the sheath, which enhances current flow.

.

3.5.2 Optical Emission Spectroscopy (OES)

OES examines the light given off by the species in the plasma that have been raised to excited states by impact [39]. Excited species radiates characteristic set of wavelengths that can be used as fingerprints. This unique fingerprint is determined by the fundamental atomic energy levels that are different for each element. OES is an attractive option for plasma process control because it is fast, non-intrusive, monitors multiple elements simultaneously and provides information regarding deposition conditions in the plasma. However, it is just beginning to be used to control deposition processes. This is because the dependence between OES signals and film properties can frequently be a complex function of electron and gas densities, emitting species concentration, electron impact excitation cross section, electron energy distribution function and the probability of inelastic collision between plasma species. The OES system in the present work consist of a spectrometer, monochromator, a CCD detector and a personal computer .

3.5.2a Charge Coupled Device

Charge Coupled Devices (CCD) are multichannel silicon array detectors designed using standard MOS architecture. These are array devices in which individual pixel elements are defined by three electrode gates of varied applied potential (3-phase devices). The electrodes are made from vertically stacked, conductively doped polysilicon and overlay the photosensitive semiconducting silicon. The electrodes are separated from the silicon surface by a thin layer of insulating silicon dioxide. When appropriate voltages are applied to the different electrodes, the electrostatic potentials in the silicon are changed to produce

zones of negative potentials surrounding a potential well. Photoelectrons generated by the incident light are then collected and stored in these localized potential wells (Fig 3.8). CCDs detect and measure light in a three step process [40].

1) **Absorption of incident photon energy followed by the creation of electron-hole pairs proportional to the number of absorbed photons**. The amount of electron-hole pairs generated in each discrete pixel directly depends on the incident light intensity. However the number of the generated electron-hole pairs is a non-linear function of the incident wavelength. As shown in the figure, the charge resulting from the generated electron-hole pairs in a given pixel is collected in the potential well of that pixel.

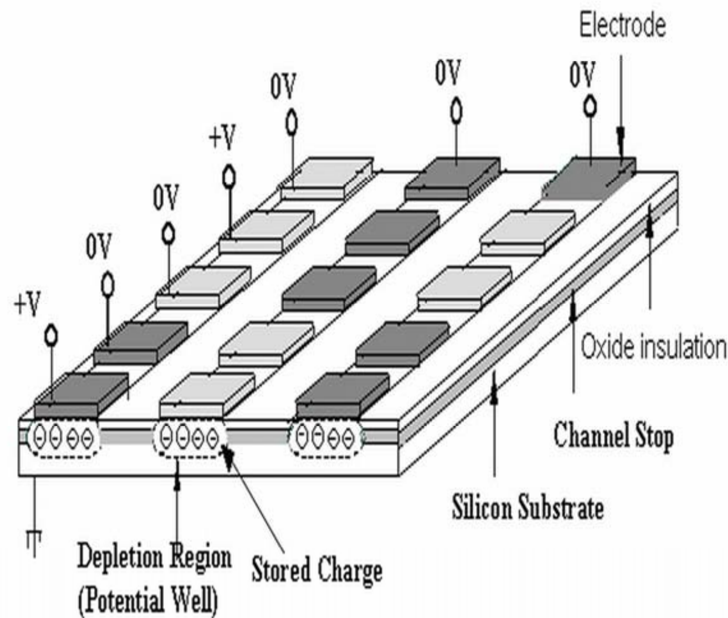

Figure 3.8 Schematic of a CCD detector

2) **Transfer of the resulting charge packets within the array from one pixel to the next:**. At the end of an exposure, the charge integrated in each pixel is transferred from one pixel to the next in a column until it finally reaches the readout registers located along one edge of the chip. This charge transfer is accomplished by sequentially changing the applied potential to the different electrodes as shown in figure 3.9. During this process of parallel charge transfer, the charge accumulated in one row of pixel is simultaneously transferred to the corresponding pixel in the next row.

3) **Conversion of charge to voltage and subsequent amplification**. After the parallel charge transfer process, the charge from each row of pixels is accumulated in the readout registers, located at the edge of the chip. The charge from the individual readout registers is then shifted to an output sense node by an analogous serial charge transfer process. Here the charge is converted to an appropriate voltage. The potential level in this "floating diffusion" sense node varies depending on the amount of charge present at the node. The sense node is followed by a charge-to-voltage amplifier, which preserves the linear relationship between the generated charge and the voltage output.

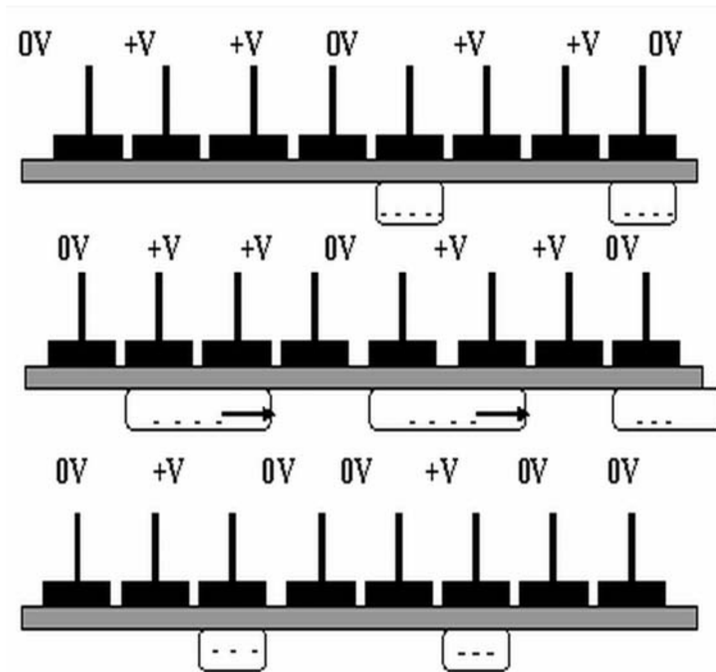

Figure 3.9 Charge transfer process within a CCD detector

The CCD used in the present investigation for the spectral studies was Spectrum One CCD 3000, 1024×256 pixels (ISA Jobin Yvon – Spex).

3.5.2b Spectrometer

Spectrometer used for analysis was Triax 320 (Fig 3.10). The TRIAX 320 is a 1/3 meter instrument offering superb scanning and imaging performance. The large f/4.1 aperture ensures better light gathering. For multichannel detection, the corrected optics and large focal plane offer excellent spectral resolution and spatial separation with wide single exposure wavelength coverage [40].

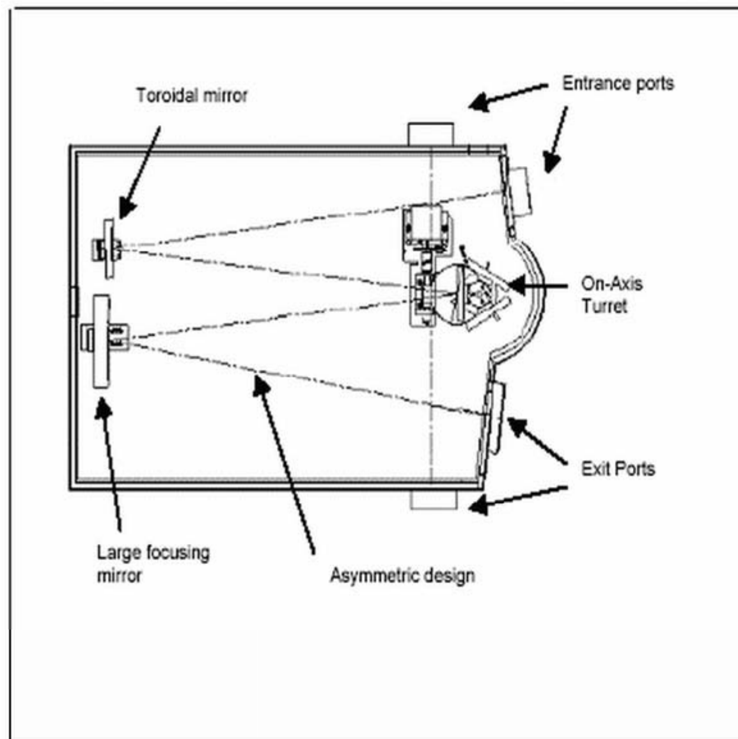

Figure 3.10 Triax-320 top view

Specifications of Triax 320

Focal Length f	: 0.32 meters
Entrance Aperture Ratio	: f/4.1
Grating	: 1200 grooves/mm
Grating size	: 68 × 68 mm
Blazed at	: 500 nm
Image magnification at the exit	: 1.00
Spectral dispersion	: 2.64 nm
Spectral resolution	: 0.06 nm
Wavelength positioning accuracy	: +/- 0.3 nm

3.5.2c Monochromator Calibration

To ensure the accuracy of results, it is important to consider the influence of natural broadening. We have used a mercury lamp to measure the resolution of spectrometer. Spectrum of the mercury lamp in the wavelength range 570 – 580 nm was recorded (Fig 3.11). The peaks were identified and compared with standard wavelength [41].

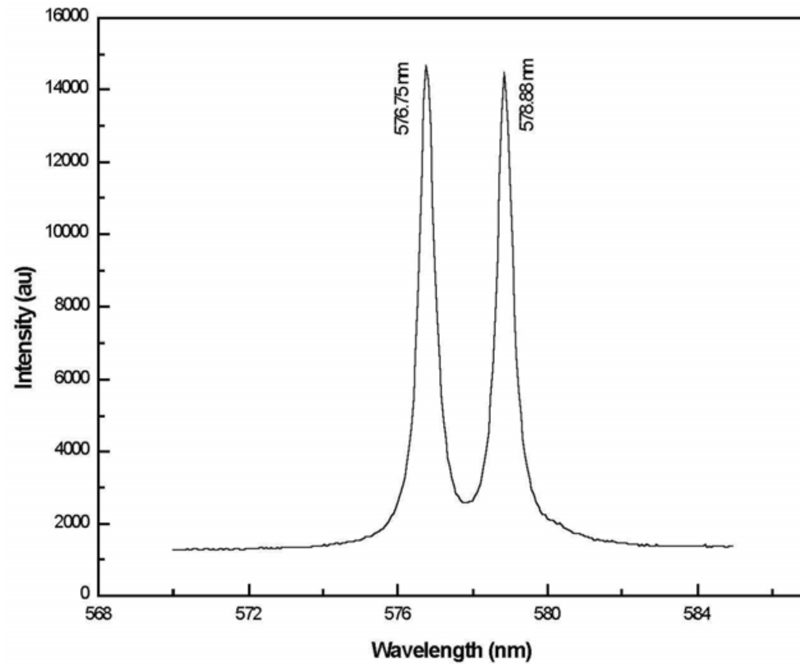

Figure 3.11 Emission spectra of Hg

The resolution of the spectrometer is given by the equation

$$\Delta\lambda = \frac{FWHM}{a} \times \Delta A \qquad (3.31)$$

where ΔA (the difference between the standard wavelength) = 579.065 – 576.965 = 2.1 mm. Here the FWHM is the full width at half maximum of Hg line (I), which is about 0.4901 nm and *a* is the distance between the two peaks of the Hg lines recorded using the spectrometer (Figure 3.12), which is , *a* = 578.876 – 576.754 = 2.122 nm. Thus the spectrometer has a resolution of $\Delta\lambda = 0.485$ nm.

3.5.2d OES Recording

The plasma plume is focused to the entrance slit of a monochromatic by means of a convex lens (focal length 17 cm) so as to have one to one correspondence with the sampled area of the plasma and the image. The f-number of the lens is made equal to the f-number of monochromator for better optical coupling. Optical emission from the plasma plume is recorded by means of a scanning monochromator equipped with grating and a CCD array detector. The CCD and spectrometer were interfaced to a PC equipped with Spectra Max for Windows for data acquisition and processing (Fig 3.12). Wavelength dispersed optical spectra within the range 300 – 950 nm have been recorded.

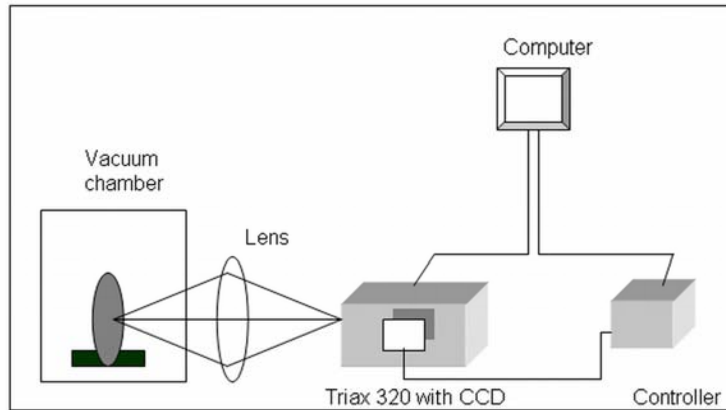

Figure 3.12 Experimental set up for recording the OES.

References

1. H.L.Hartnagal, A.L.Dawar,A.K.Jain, C.Jagdish, Semiconducting Transparent Thin Films, IOP Publishing Ltd, Bristol (1995)
2. A.Goswami, Thin film fundamentals, New age international (P) Ltd, New Delhi(1996)
3. R.W.Berry, P.M.Hall, M.T.Harris, Thin Film Technology, D.Van Nostrand company Inc (1968)
4. L.Holland, Vacuum Deposition of Thin films, John Wiley & Sons Inc., New York (1956)
5. Brian Chapman, Glow discharge processes- Sputtering and Plasma Etching, John Wiley & sons, New York (1980)
6. J.M.Blocher, Thin Solid Films **77**(1981)51
7. W.Siefert, Thin Solid Films **121**(1984)275
8. S.Seki, Y.Sawada, T.Nishide, Thin Solid Films **388** (2001)21
9. M.Mizuhashi, Thin Solid Films **70**(1980)91
10. K.D.J.Christian, S.R.Shatynski, Thin Solid Films **108**(1983)319
11. Y.Shigesato,Y.Hayashi,T.Haranoh, Appl.Phys.Lett. **61**(12992)73
12. H.U.Habermeier, Thin Solid Films **80**(1981)157
13. S.A.Agnihotri, K.K.Saini, T.K.Saxena, K.C.Nagpal, S.Chandra, J.Phys.D.Appl.Phys **18**(1985)2087
14. B.Chapman and S.Mangano, Thin-film deposition processes and techniques
15. F.L.Akkad, A.Punnose, J.Prabu, J.Appl.Phys A **71**(2000) 157
16. Y.Shigesato, Y.Hayashi, A.Masui, T.Haranoh, Jpn.J.Appl.Phys. **30**(1991)814
17. R.Latz, K.Michael, M.Scherer, Jpn.J.Appl.Phys. **30**(1991)L149
18. S.Honda, A.Tsujimoto, M.Watamori, K.Oura, J.Vac.Sci. Technol.A**13**(3)(1995)1100
19. K.Itoyama, Jpn.J.Appl.Phys. **17**(1978)1191

20. D.B.Chrisey, G.K.Hubbler, Pulsed Laser Deposition of Thin Films, John Wiley & Sons Inc, New York (1994)
21. T.Maruyama, K.Fukui, Thin Solid Films **203**(1991)297
22. L.A.Ryabova, V.S.Salun, I.A.Serbinov, Thin Solid Films **92**(1982)327
23. J.C.Manifacier, L.Szepessy, J.P.Bresse, M.Perotin, R.Stuck, Mater. Res.Bull.**14**(1979)163
24. O.Weiner, Wied.Ann. **31**(1887) 629
25. S. Tolansky, Multiple Beam Interferometry of Surfaces and Thin films, Oxford University Press, Fair Lawn, NJ (1948)
26. D.J.O'Connor, B.A. Sexton, R.St.C.Smart (Eds), Surface Analysis Methods in Material Science, Springer-Verlag, Berlin-Heidelberg 1992
27. B.D. Cullity and S.R. Stock, Elements of X ray diffraction, Third edition, New Jersey, Prentice Hall (2001)
28. M.J.Buerger, X-ray Crystallography, John Wiley & Sons, NewYork (1962)
29. C.Kittel, Introduction to Solid State Physics, Seventh edn, Wiley Eastern Limited, (1996)
30. B.G.Streetman , Solid state electronic devices, 4th edn, Prentice hall of India private Ltd,New Delhi (1995)
31. J.Bardeen, F.J.Blatt and L.H. Hall, in: Proceedings of Photoconductivity Conf. (1954,Atlantic City), (Eds) R.Breckenridze, B.Russel and T.Hahn, J.Wiley and Chapman and Hall, New York, (1956)
32. J.C.Manifacier,J.Gasiot, J.P.Fillard, J.Phys.E.Scien.Instrum. **9**(1976)1002
33. Manual, Model H50 MMR Technologies Inc, California
34. H.R.Griem, Plasma spectroscopy, Mc.Graw Hill, New York (1964)
35. R.H.Huddlestone, S.L.Leonard, Plasma diagnostic techniques, Academic press, London (1965)
36. S.S.Harilal, C.V.Bindhu, R.C.Issac, V.P.N.Nampoori, C.P.G.Vallabhan, J.Appl.Phys. **82**(1997)2140

37. F.Claeyssens, PhD Thesis , University of Bristol (2001)
38. B.Chapman, Glow discharge processes: sputtering and plama etching, John Wiley & sons, New York (1964)
39. I.L.Eisgruber, J.R.Engel, R.E.Hollingsworth, P.K.Bhat, R.Wendt, J.Vac.Sci.Technol.A. **17**(1999)190
40. Spectrum one, CCD manual, ISA Jobin Yvon Spex
41. Triax 320, Spectrometer manual, ISA Jobin Yvon Spex

CHAPTER 4

Influence of Annealing and Substrate Temperature on the Properties of ITO Thin Films

Abstract

Indium tin oxide thin films were deposited by RF magnetron sputtering of ITO target. The influence of annealing temperature and substrate temperature on the properties of the films were investigated. The as deposited films showed (222) and (440) peaks of Indium oxide, and an enhancement in the (222) peak intensity were observed with increase in annealing temperature. The films deposited onto preheated substrates showed (400) diffraction peak along with (222) peak. The structural characteristics also showed a dependence on the oxygen partial pressure during sputtering. Oxygen deficient films showed (400) plane texturing while oxygen-incorporated films were preferentially oriented in the [111] direction. An annealing temperature of 250^0C resulted in films with maximum bandgap and minimum resistivity whereas a substrate temperature of 150^0C was sufficient to get films with low resistivity and high bandgap.

4.1 Introduction

Growth techniques and the sputtering environment play an important role in governing the properties of Indium tin oxide (ITO) thin films. This is because of the fact that the optical and electrical properties of the films strongly depend on the structure, morphology and nature of the impurities present, which depend on the method of preparation. Among the various deposition techniques mentioned in the previous chapter, sputtering helps one to grow high quality films onto large area substrates. The sputtering conditions namely post deposition heat treatment and substrate temperature affects the properties of the deposited films.

4.2 Experimental

Indium tin oxide thin films were deposited by RF magnetron sputtering of ITO target containing 95wt% of In_2O_3 and 5wt% of SnO_2. The target used for sputtering was prepared from In_2O_3 (99.99% pure) and SnO_2 (99.999%pure) powders. The powders were mixed in a mechanical shaker for one hour pressed into a pellet of two-inch diameter and then sintered at 1300^0C for 6 hours in air. Figure 4.1 shows the XRD pattern of the In_2O_3 powder and ITO target.

The sputtering was carried out in a vacuum chamber in which high vacuum (< $2x10^{-5}$mbar) was created by means of an oil diffusion pump backed by a rotary pump. RF power was delivered to the target material by an RF generator (13.56MHz) through an impedance matching network. Glass slides of dimension 2.5 cm x 1 cm was used as the substrates. The substrates were kept above the target at a distance of 4cm, which was found to be the optimum for the growth of good quality crystalline films [1].

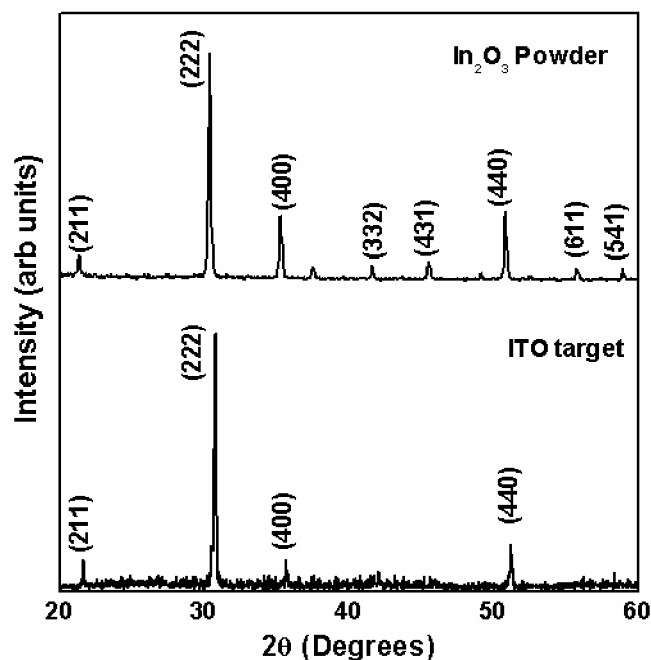

Figure 4.1. XRD pattern of In_2O_3 powder and ITO target

The influence of substrate temperature on the properties of ITO thin films was analyzed by depositing the films onto preheated substrates at an RF power of 30W. For this, the substrate was heated to the required temperature initially. After attaining the required substrate temperature high purity argon was allowed to flow into the chamber and it was so adjusted by a mass flow controller that the argon pressure is 0.01 mbar. The films were deposited at an RF power of 30W. The target was pre-sputtered for 10 minutes before each deposition in order to remove any contaminants and to eliminate any differential sputtering effects. By keeping all other parameters the same, the sputtering was carried out for various substrate temperatures ranging from room temperature to 300^0C. For films deposited at room temperature, the temperature of the substrate increased

from 20^0C to 50^0C during deposition. But when the deposition was carried out onto preheated substrates, the temperature of the substrate was maintained at the specified value by controlling power into the heating coil. The deposition rate was found to increase when the substrate temperature was increased from room temperature to 100^0C. With further increase in substrate temperature upto 150^0C the deposition rate decreased sharply and thereafter it remained almost a constant. The sputtering time was adjusted such that all the resulting films used in this study were of thickness 220nm.

In order to study the influence of annealing temperature on the properties of ITO thin films, the films were deposited onto unheated substrates at an RF power of 20W. Base vacuum in the chamber was $< 2x10^{-5}$ m bar and the argon pressure was maintained at 0.01 mbar during deposition. The thickness of the films was 280nm. The as deposited films were then annealed at various temperatures from 100^0C to 300^0C for 1 hour under high vacuum.

4.3. Results and discussion

4.3.1 Influence of annealing temperature

Figure 4.2 shows the XRD pattern of the ITO films deposited at a target to substrate spacing (T-S spacing) of 4cm as a function of annealing temperature. From the XRD pattern it can be seen that the as deposited films are polycrystalline even though the crystallization temperature of ITO is 150^0C [2]. All of them showed a peak at $2\theta = 30^0$ which correspond to (222) plane and at $2\theta = 51^0$ which corresponds to (440) plane of In_2O_3 [3]. The crystalline nature of the films even at lower processing temperatures is because of the greater kinetic energy of the sputtered particles reaching the substrate surface.

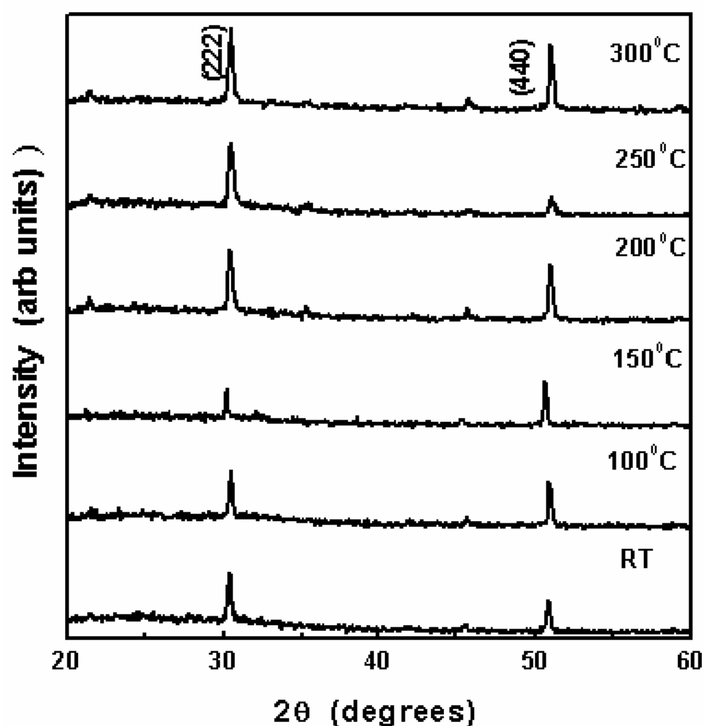

Figure 4.2.XRD Pattern of ITO thin films deposited at room temperature and annealed at various temperatures.

Generally, sputtered particles have kinetic energies of several electron volts. This kinetic energy enhances the surface migration of sputtered particles arriving at the substrate surface and the crystallinity of the films is greatly affected by them. Thus it is possible to deposit polycrystalline films even at room temperature by sputtering [4,5]. The intensity ratio I(222)/I(440) increased with increase in annealing temperature upto 250^0C and then decreased (Fig 4.3). A sharp rise in the intensity ratio is observed corresponding to an annealing temperature of 250^0C. The enhancement of the (222) peak intensity with annealing temperature is reported [6].

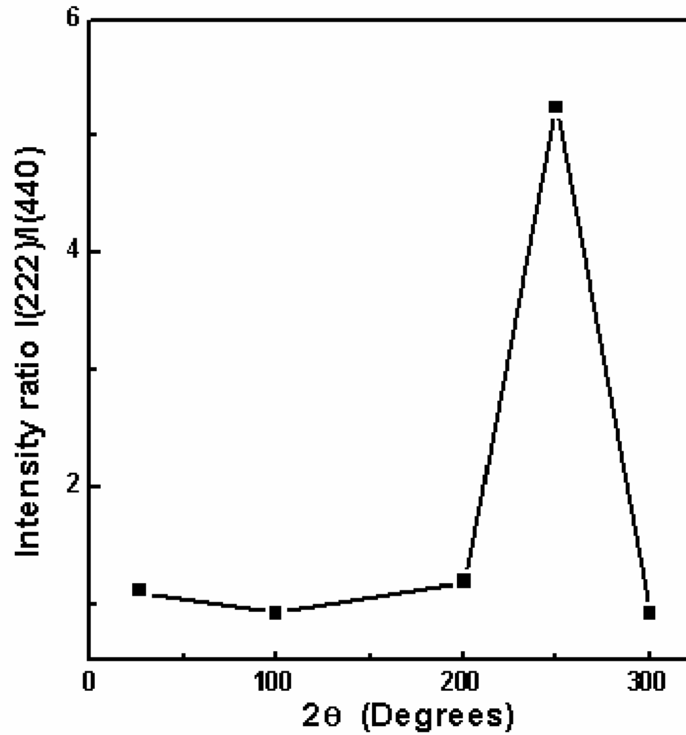

Figure 4.3. Variation of intensity ratio of XRD peaks I(222)/I(440) with annealing temperature

The annealed films exhibited high transmission in the visible region with long tail in the IR region (Fig 4.4). It was seen that the reflecting edge shift towards the lower wavelength region, on annealing the film at high temperature in vacuum. The shift in reflecting edge is due to increase in carrier concentration introduced by the oxygen deficiency created during annealing [7].

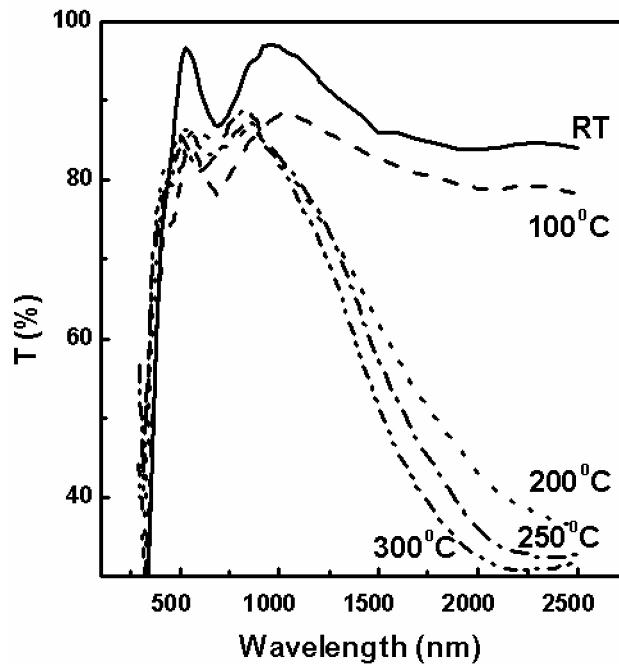

Figure 4.4. Transmission spectra of ITO thin films deposited at room temperature and annealed at various temperatures

The bandgap of the ITO films were calculated from the transmission spectra. By assuming a parabolic band structure for the material, the absorption coefficient and bandgap can be related by the expression $\alpha h\nu = A(h\nu - E_g)^{1/N}$ where E_g is the band gap energy and α is the absorption coefficient corresponding to frequency ν[8]. The absorption coefficient α was determined from the relation, $I = I_0 \exp(-\alpha t)$ where t is the thickness of the sample, I is the transmitted intensity at a particular wavelength and I_0 is the maximum transmitted intensity which is taken to be 100%. This relation gives $\alpha = (1/t)\ln(I_0/I)$. The constant N depends on the nature of electronic transition. In the case of ITO films N is equal to 2, for direct allowed transition [9]. The bandgap of ITO films were determined from the plot

of $(\alpha h\nu)^2$ vs $h\nu$ by extrapolating the linear portion of the curve to the energy axis where $\alpha h\nu$ is equal to zero.

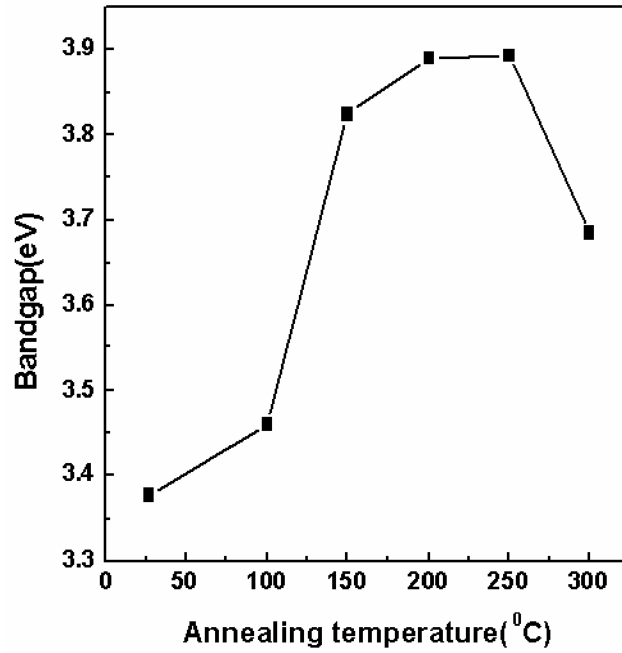

Figure 4.5. Variation of bandgap of ITO thin films as a function of annealing temperature.

In the present study, the band gap of ITO thin films increased with increase in annealing temperature, showed a maximum value at 250^{0}C (3.89eV) and then decreased. The variation of band gap with annealing temperature is shown in figure 4.5. The increase in band gap can be explained on the basis of Burstein-Moss effect [10]. Assuming that the conduction band and valence band are parabolic in nature and that B-M shift is the predominant effect, we can write $E_g=E_{g0}+\Delta E_g^{B\text{-}M}$ where E_{g0} is the intrinsic bandgap and $\Delta E_g^{B\text{-}M}$ is the B-M shift

due to filling of low lying levels in the conduction band [20]. An expression for B-M shift is given by $\Delta E_g^{B\text{-}M} = (h^2/8\pi^2 m_{vc}^*)(3\pi^2 n)^{2/3}$ where n is the carrier concentration and m_{vc}^* is the reduced effective mass of the carriers.From this expression it is clear that B-M shift is directly proportional to $n^{2/3}$. Increase in carrier concentration with increase in annealing temperature resulted in band gap widening. However, at very high carrier concentrations it is seen that there is bandgap narrowing due to electron-electron scattering and electron –impurity scattering.

The resistivity and sheet resistance of the ITO films were found to decrease with increase of annealing temperature (Fig 4.6).

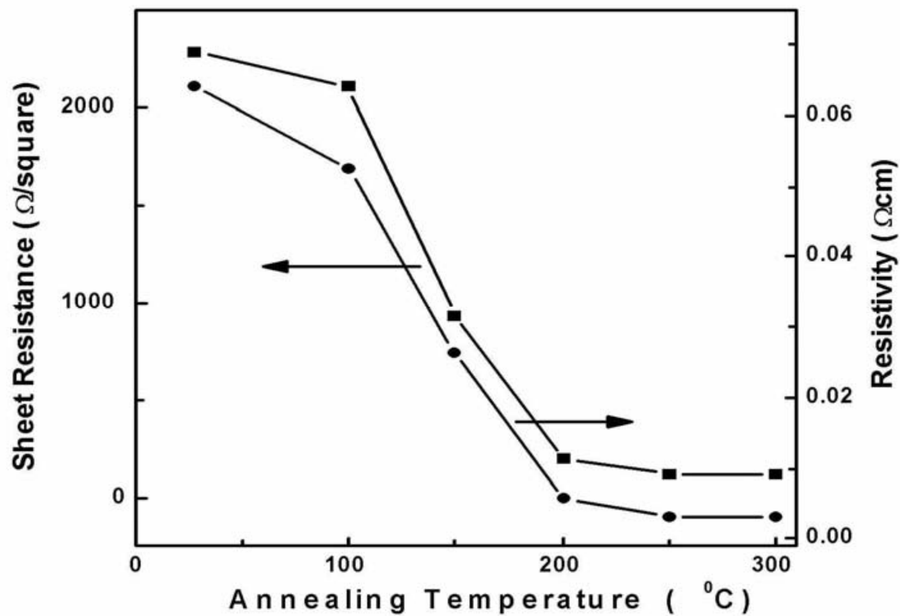

Figure 4.6. Variation of resistivity and sheet resistance of ITO thin films with annealing temperature

The lowest resistivity of 3.07×10^{-3} Ω cm and sheet resistance of 110square/ohms was obtained for the film annealed at 250^0C. The mobility of the ITO films

increased with the increase of annealing temperature whereas carrier concentration was maximum for ITO films annealed at 250^0C (Fig 4.7).

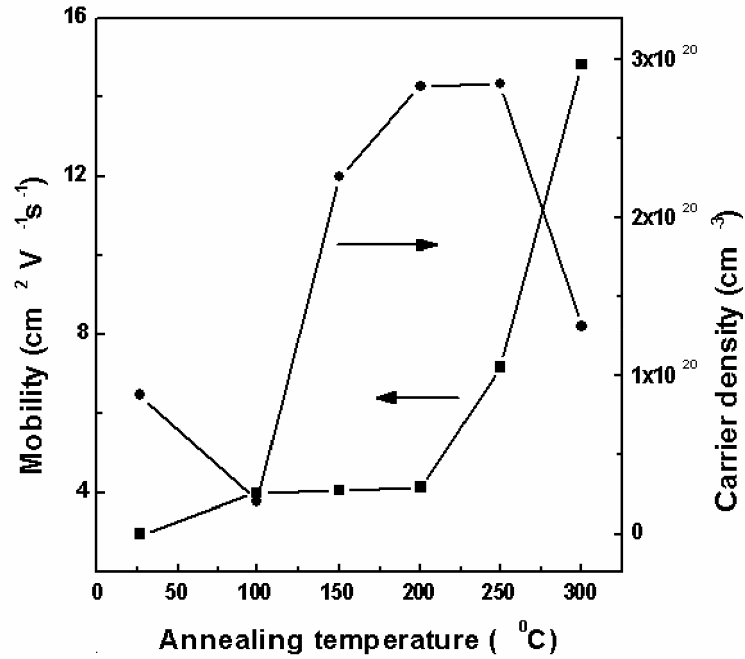

Figure 4.7 Variation of mobility and carrier density of ITO thin films with annealing temperature

In ITO, oxygen deficiency is one of the reasons for high conductivity. Oxygen deficiencies induce free electrons as conduction carriers [11-13]. Vacuum annealing creates oxygen deficiency and this reduces the resistivity of the ITO films. The increase in carrier concentration, mobility and crystallinity of the films is also responsible for the decrease in resistivity. The films annealed at 250^0C showed a preferred orientation in the (222) plane and showed the minimum resistivity. ITO may be having a minimum resistivity in the <111> orientation and this might be the reason for the observed minimum value of

resistivity at 250^{0}C. Table 4.1 summarises the important properties of ITO thin films as a function of annealing temperature.

Table 4.1 Properties of ITO thin films as a function of annealing temperature

Annealing temperature (^{0}C)	Grain size (nm)	Bandgap (eV)	Resistivity (Ωcm)	Mobility ($cm^2V^{-1}s^{-1}$)	Carrier density ($x10^{19} cm^{-3}$)	Sheet resistance (Ω/□)
RT	19.4	3.38	0.0641	2.99	3.26	2290
100	15.8	3.46	0.0526	4.0	2.64	2110
150	16.8	3.82	0.0263	4.1	22.5	230
200	17.5	3.89	0.00573	4.12	28.2	192
250	16.0	3.89	0.00307	7.15	28.4	110
300	14.4	3.69	0.0032	14.8	13.1	115

4.3.2 Influence of substrate temperature

Figure 4.8 shows the x-ray diffraction (XRD) pattern of the ITO thin films deposited at various substrate temperatures. All the films are polycrystalline and crystallized in the cubic bixbyite structure of indium oxide. The growth of the films showed preferred orientation depending on the substrate temperature. The films deposited onto unheated substrates showed reflection corresponding to (222) and (440) planes [3]. A substrate temperature of 100^{0}C resulted in films with a prominent (400) peak indicating a preferred orientation along [100] direction. The films grown at all other substrate temperatures do not show any preferential orientation as seen from the XRD pattern. It was also observed that all the films deposited onto heated substrates showed (400) plane texturing. With an increase in substrate temperature above 100^{0}C, a decrease in intensity of (400) peak and an increase in intensity of (222) peak was observed (Fig 4.9).

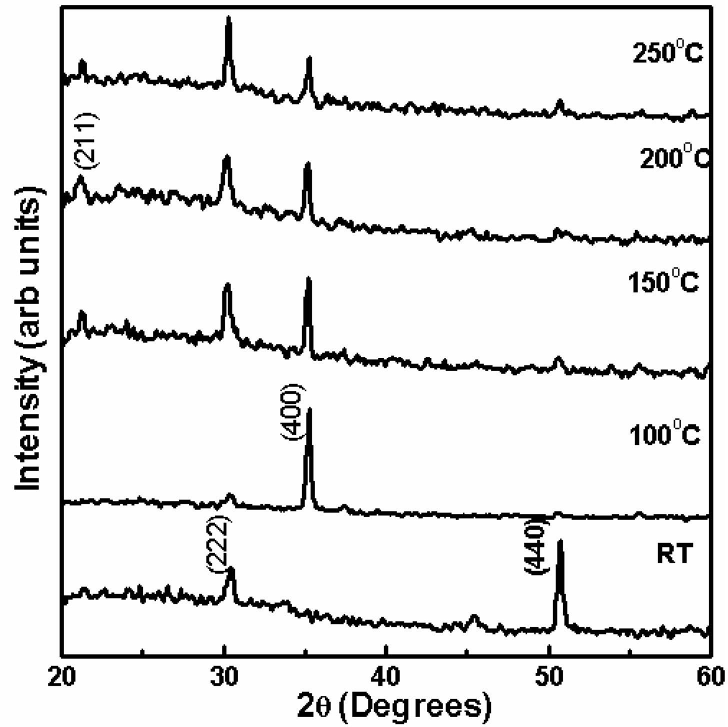

Figure 4.8 XRD pattern of ITO thin films deposited at various substrate temperatures

The appearance of (400) diffraction peak in the XRD pattern is related to the deposition conditions. Energy of the sputtered particles reaching the substrate surface should attain a certain value in order to form thin film with (100) orientation [14]. Sputtering at higher substrate temperature satisfies this criterion and it result in the (100) orientation.

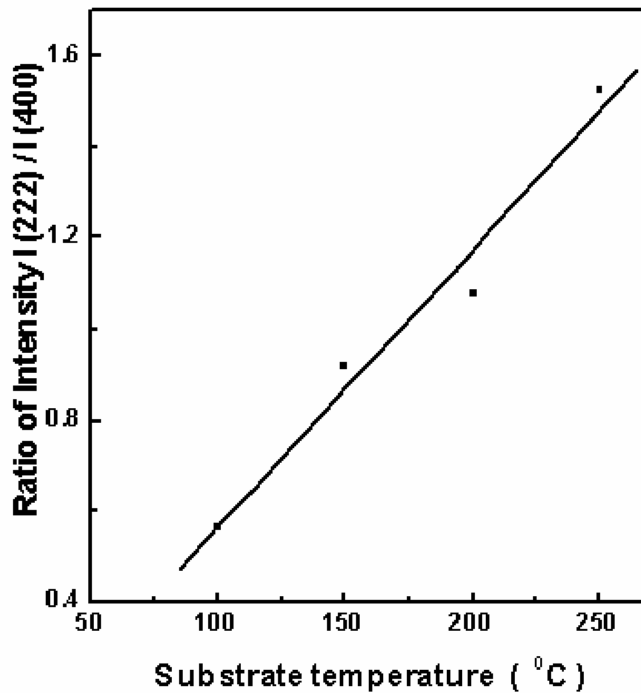

Figure 4.9 Variation of the ratio of peak intensity of (222) and (400) planes with substrate temperature.

The influence of oxygen incorporation on the structural properties of the films were studied by depositing the films at various oxygen partial pressures. The deposition was carried at a substrate temperature of 150^{0}C and an RF power of 30W. XRD patterns (Fig 4.10) of the films deposited at oxygen pressure of 4 x10^{-5}mbar showed a (222) peak, while films prepared at 5x10^{-5}mbar showed of (400) peak along with (222) peak. The increase in the oxygen flow cause an increase in the (400) peak intensity and a decrease in (222) peak intensity. The grain alignment of the films deposited at low oxygen flow rate can be related to the oxygen vacancy, diffusion rate and tin substitution over the indium sites. At low oxygen flow rate, the films consisted of more oxygen vacancies, which provide sites for ions to migrate. Both the nucleation and growth may control the

preferred alignment of the grains [15]. Or, in other words, in the absence of oxygen, the grains orient randomly. Oxygen incorporation leads to grains in the films orient in the (111) direction. According to Kim et al (100) orientation is related to oxygen deficiency [16]. The change in orientation of the films from (100) to (111) texture results from the incorporation of oxygen into the films.

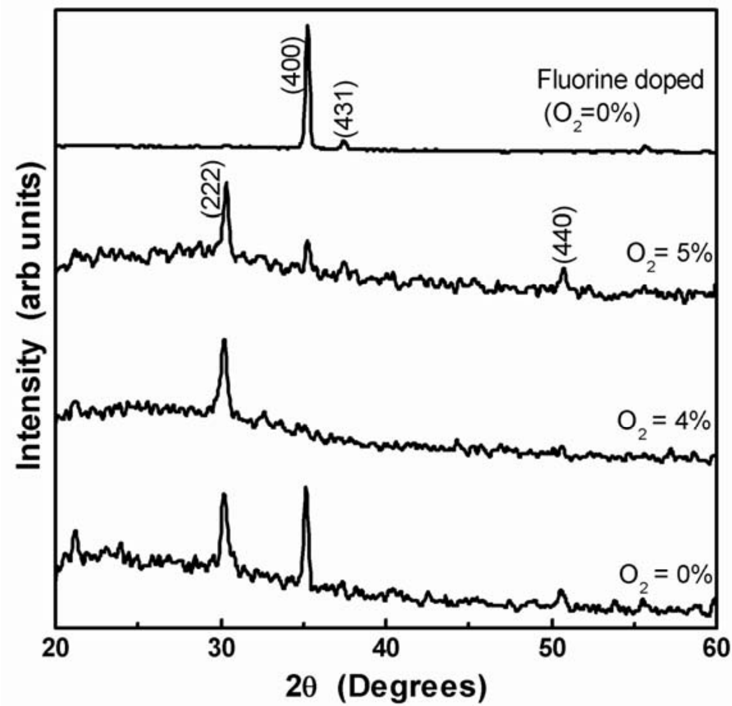

Figure 4.10. XRD pattern of fluorine doped ITO thin films and those deposited at various oxygen pressures. Substrate temperature = 150^0C and RF power = 30W

Fluorine doping in ITO thin films enhanced the crystallinity (Fig 4.10). Doping was carried out by placing indium fluoride (InF_3) pellets on the erosion area of the target. The deposition was carried out at an RF power of 30W and a substrate temperature of 150^0C. Incorporation of fluorine resulted in films with (100) preferred orientation. This may be due to the substitutional incorporation of

fluorine in the place of oxygen which arises because their radii are comparable [17]. The resulting oxygen deficiency leads to (100) oriented films. Figure 4.11 shows the influence of sputtering duration on the structural properties of fluorine doped ITO films. With increase in duration of sputtering, the film gets preferentially oriented in the (400) direction. A decrease in the value of FWHM was also observed (Fig 4.12).

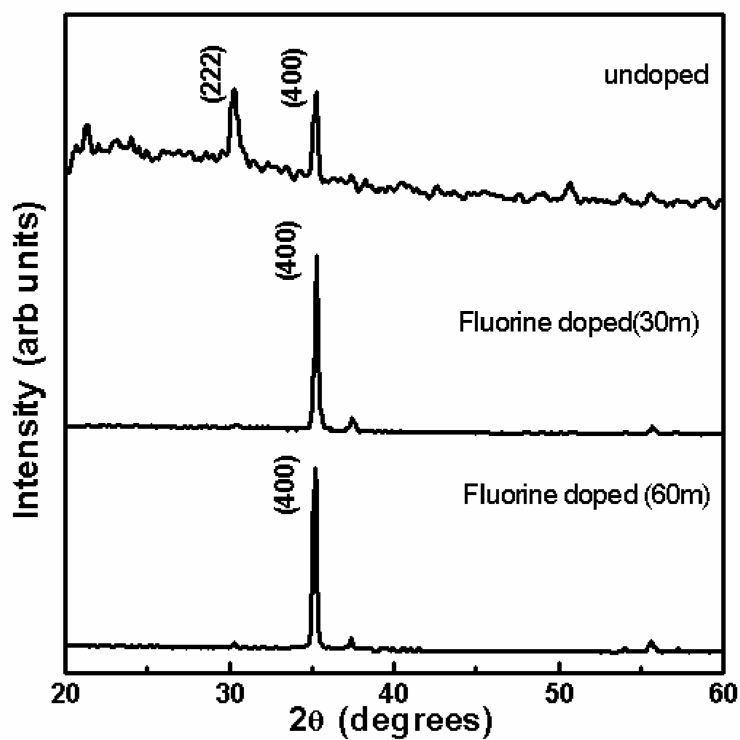

Figure 4.11. XRD pattern of fluorine doped ITO films as a function of deposition time

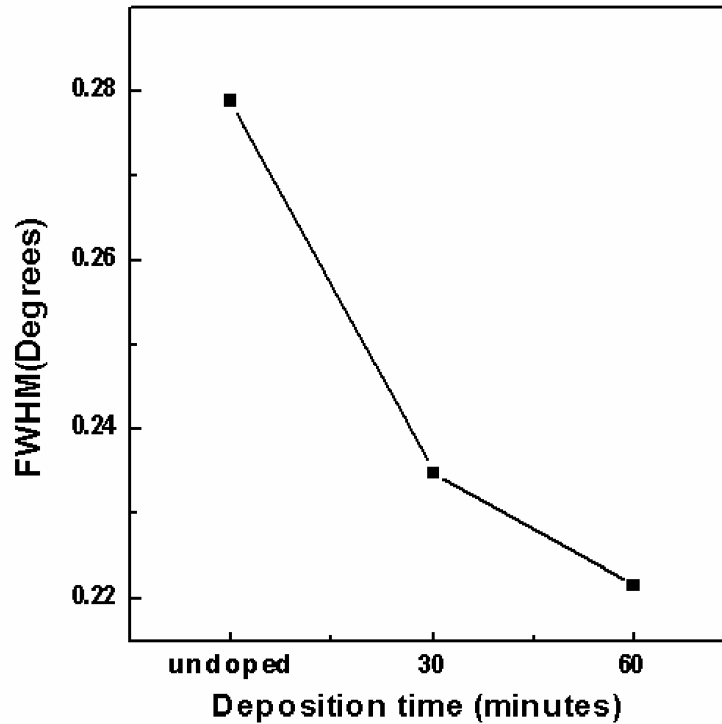

Figure 4.12.Variation of FWHM of (400) diffraction peak of ITO:F films with duration of sputtering

The lattice parameter of the films were calculated [18,19] using the equation

$$\frac{n^2}{d^2} = \frac{h^2 + k^2 + l^2}{a^2} \qquad (4.1)$$

An increase in lattice parameter of ITO thin films with substrate temperature was observed (Fig 4.13). The increase in lattice parameter is attributed to the increase in repulsive forces arising from the extra positive charge of the tin cations. Tin is incorporated into In_2O_3 lattice as Sn^{4+}. In the oxidised state, the interstitial oxygen anion charge compensates the material [20]. As those oxygen

anions are removed, which is the case with higher substrate temperatures, the repulsive forces increase, leading to an enlargement of the unit cell.

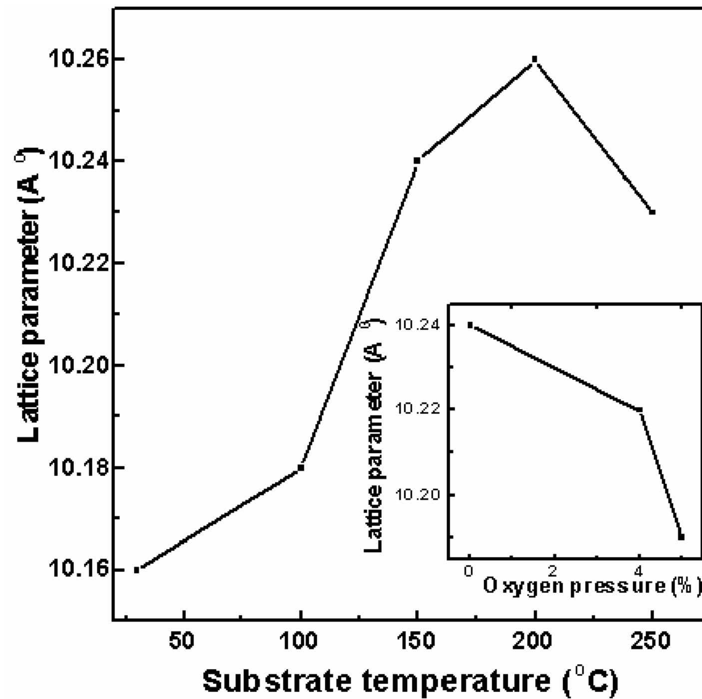

Figure 4.13 Variation of lattice parameter of ITO thin films with substrate temperature. Inset shows the variation of lattice parameter with oxygen concentration of ITO thin films deposited at a substrate temperature of 150^0C

In the present investigation, increase in substrate temperature resulted in oxygen deficient films. This was confirmed by the carrier density measurements, which will be discussed along with the electrical properties of the films. Similar effect was observed in thin films prepared at various oxygen concentrations (inset of Figure 4.13). The lattice constant decreased with increase in oxygen concentration.

The scanning electron microscopic (SEM) pictures of the films prepared under various deposition conditions, viz room temperature, 150^0C using pure argon, 150^0C using Argon/oxygen mixture and fluorine doped films is shown in figure 4.14. SEM pictures show that the films are having a smooth surface.

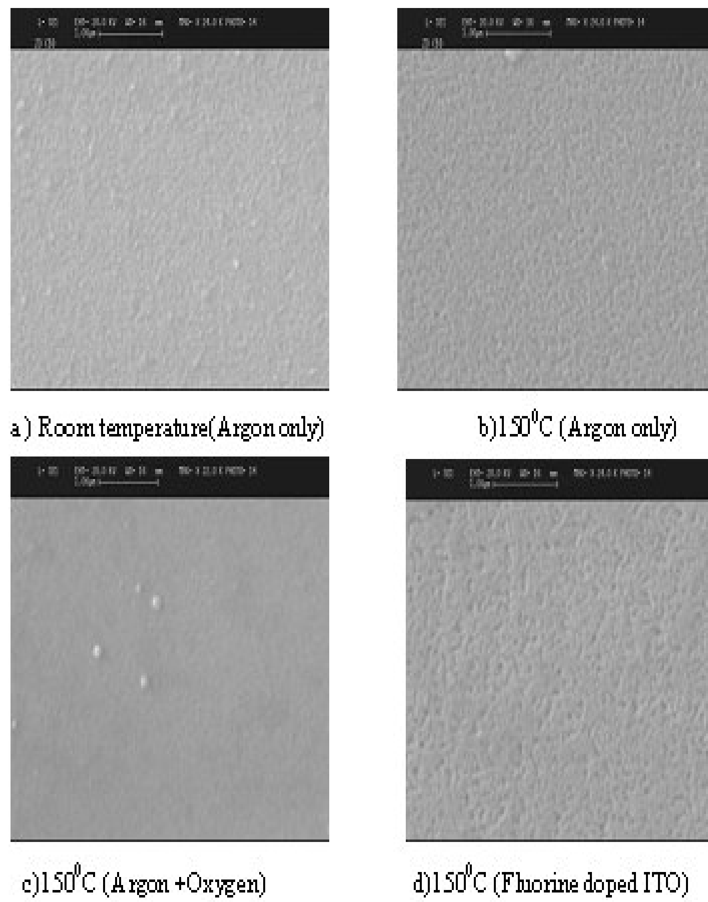

Figure 4.14. SEM picture of ITO thin films deposited under various conditions

The transmission spectra (Fig 4.15) of the films deposited at various substrate temperatures shows that the films are highly transparent in the visible region of the electromagnetic spectrum. The average transmission in the visible range was greater than 80%. The transmission in the higher wavelength region decreased with increase in substrate temperature. This is because, at high deposition temperature carrier concentration increases because of oxygen deficiency. Higher carrier concentration results in higher reflection in long wavelength region. Inset of figure 4.15 shows the absorption and cut off for glass substrate.

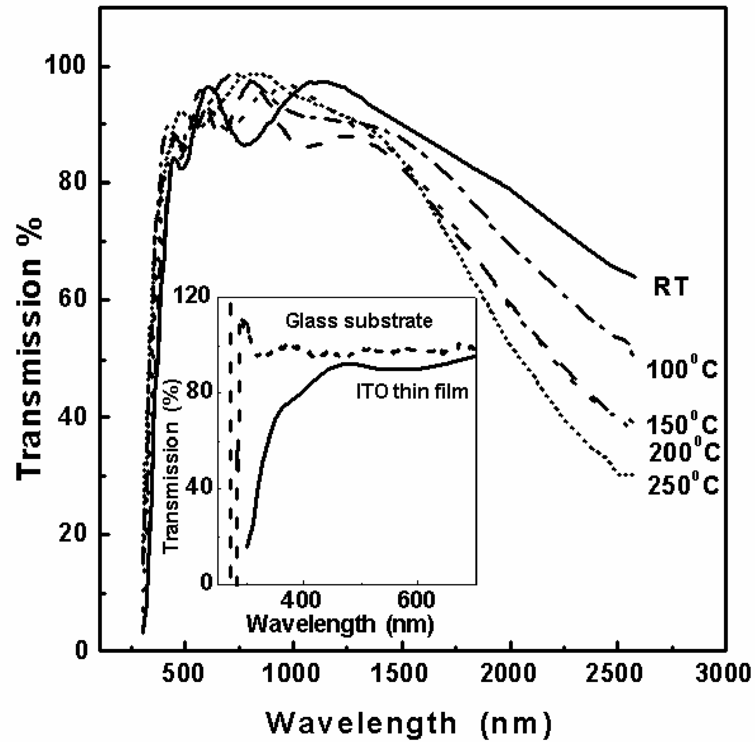

Figure 4.15. Transmission spectra of ITO thin films deposited at various substrate temperatures. Inset shows the transmission and cut off for glass substrate.

The optical bandgap of the films were determined by extrapolating the linear portion of the hν vs $(\alpha h\nu)^2$ curve to $(\alpha h\nu) = 0$ (Inset of Figure 4.16). In the present study it has been found that bandgap of ITO films increased with increase in substrate temperature (Fig 4.16). The increase in bandgap may be due to an increase in carrier concentration with substrate temperature as a result of which the absorption edge shifts towards the near UV range [21]. The increase in bandgap with carrier concentration is due to Burstein-Moss effect, which is already discussed in this chapter.

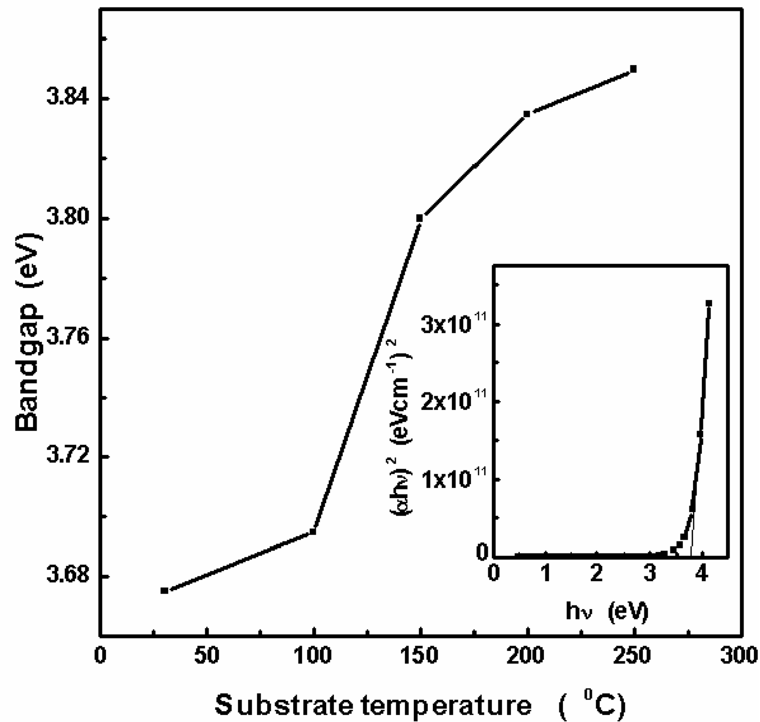

Figure 4.16. Variation of bandgap of ITO thin films with substrate temperature. Inset shows a typical plot of hν vs $(\alpha h\nu)^2$ for ITO film deposited at a substrate temperature 150^0C

The refractive index and extinction coefficient of the films were evaluated using a method deviced by Manifacier et al[22].The refractive index of the films varied from 1.6 to 2 while extinction coefficient varied from 0.6 to 1 in the visible range of the electromagnetic spectrum. Figure 4.17 shows a typical plot of n and k against the wavelength of ITO thin films.

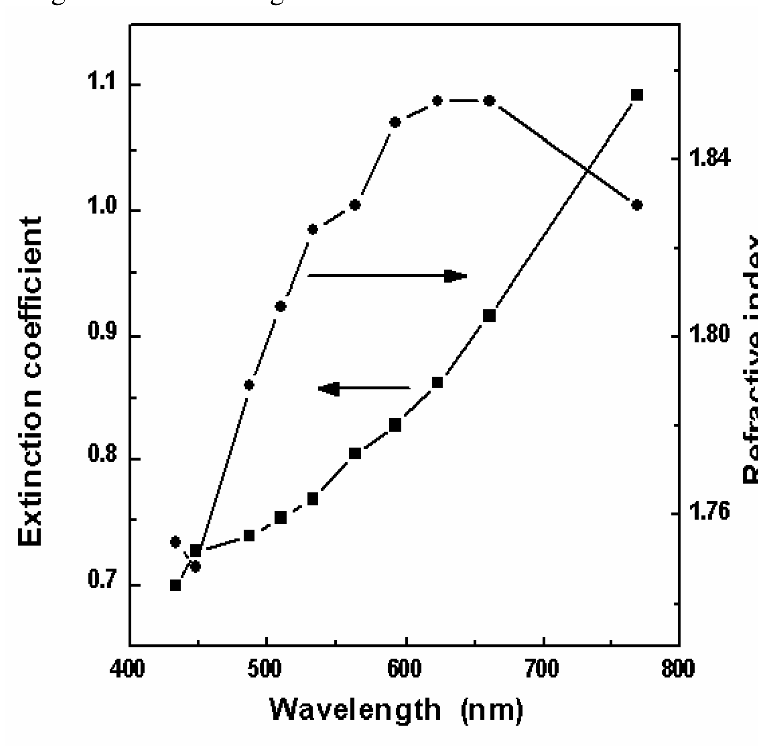

Figure 4.17. Refractive index and extinction coefficient of ITO thin films in the visible range of the electromagnetic spectrum(deposition temperature = 150^0C)

The resistivity (ρ) of a semiconducting thin film is given by the expression $\rho = 1/ne\mu$ where e is the electronic charge, μ is the carrier mobility and n is the carrier density. Lowest resistivity can be achieved by increasing the carrier density or carrier mobility or both. But increasing the carrier density is self limiting because at some point, the increased number of free carriers decrease the

mobility of the carriers due to carrier-carrier scattering. This means that there is a trade off between carrier density and carrier mobility for achieving low resistivity [23].

The electrical properties of the ITO thin film depends on the film composition and deposition parameters such as substrate temperature, oxygen pressure etc. In the present study it was found that the resistivity and sheet resistance decreased with increase in substrate temperature and became a minimum at a temperature of 150^0C and then increased on further increase of substrate temperature (Fig 4.18). The carrier mobility and carrier density also increased with increase of substrate temperature and shows a maximum value around 150^0C (Fig 4.19).

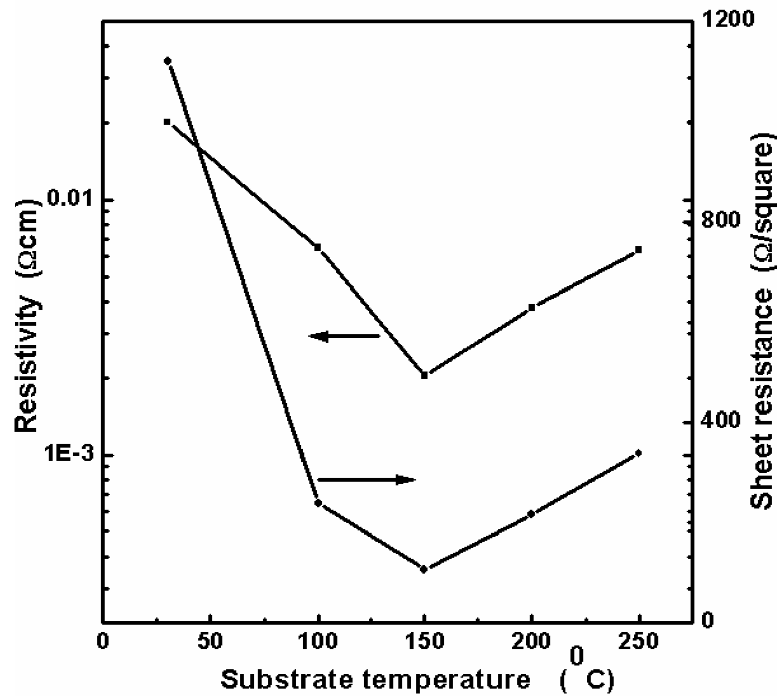

Figure 4.18 Variation of resistivity and sheet resistance of ITO thin films with substrate temperature

The increase in mobility may be due to better crystallinity of the film, which increases with the increase in substrate temperature. The increase in carrier concentration can be explained on the basis of diffusion of tin atoms from the interstitial locations and grain boundaries into the indium cation sites [21]. Since tin is tetravalent and indium is trivalent, tin atom act as donor in ITO thin films. Hence the increase in tin diffusion with substrate temperature results in higher electron concentration.

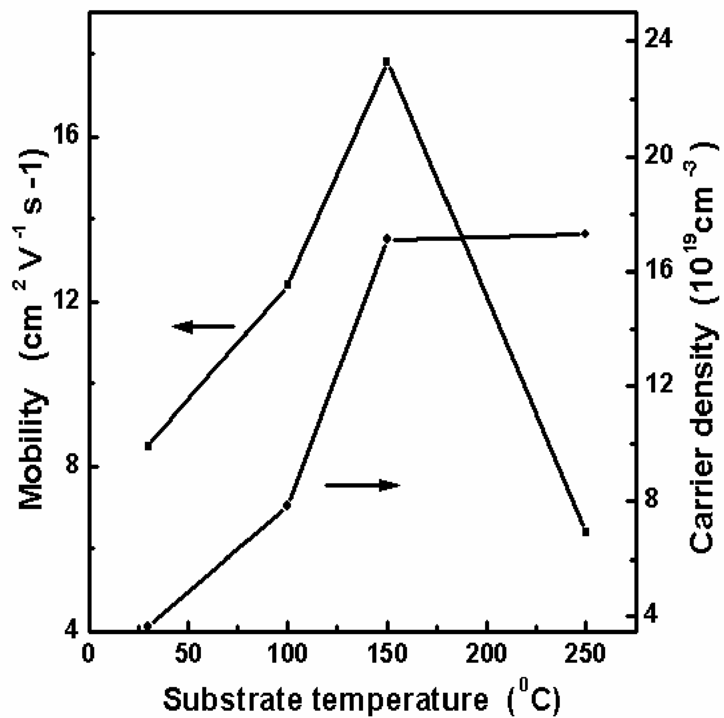

Figure 4.19 Variation mobility and carrier density of ITO thin films with substrate temperature

The decrease in resistivity with increase in substrate temperature can be explained by the fact that the crystallite grain size increases significantly with the increase in deposition temperature, thus reducing grain boundary scattering and increasing conductivity. The decrease in resistivity was also associated with the observed increase in carrier mobility. For the film grown at higher substrate temperatures >200^0C the resistivity was found to increase again. This increase may be due to the contamination of the films by alkali ions from glass substrates [24]. Table 4.2 summarises the important properties of ITO thin films as a function of substrate temperature.

Table 4.2 Properties of ITO thin films as a function of substrate temperature.

Substrate temperature (^{0}C)	Grain size (nm)	Band gap (eV)	Resistivity (Ωcm)	Mobility ($cm^2V^{-1}s^{-1}$)	Carrier density ($x10^{19}cm^{-3}$)
RT	16.8	3.68	.0201	8.46	3.67
100	25.68	3.7	.0065	12.4	7.82
150	26.08	3.8	.0021	17.8	17.1
200	25.2	3.84	.0038	17.6	9.39
250	30.0	3.85	.0064	6.39	17.3

The figure of merit (Φ) proposed by Haake[25] for transparent conductors for photovoltaic applications is given by $\Phi = T_a^{10} / R_s$ where T_a is the average transmittance in the visible range and R_s is the sheet resistance of the film. The highest value of figure of merit was observed for the film deposited at a substrate temperature of 150^0C (Fig 4.20a). In the case of annealed films the highest figure of merit was obtained for an annealing temperature of 250^0C (Fig 4.20b). The figure of merit for commercial ITO thin film was $5.9x10^{-2}$□/Ω.

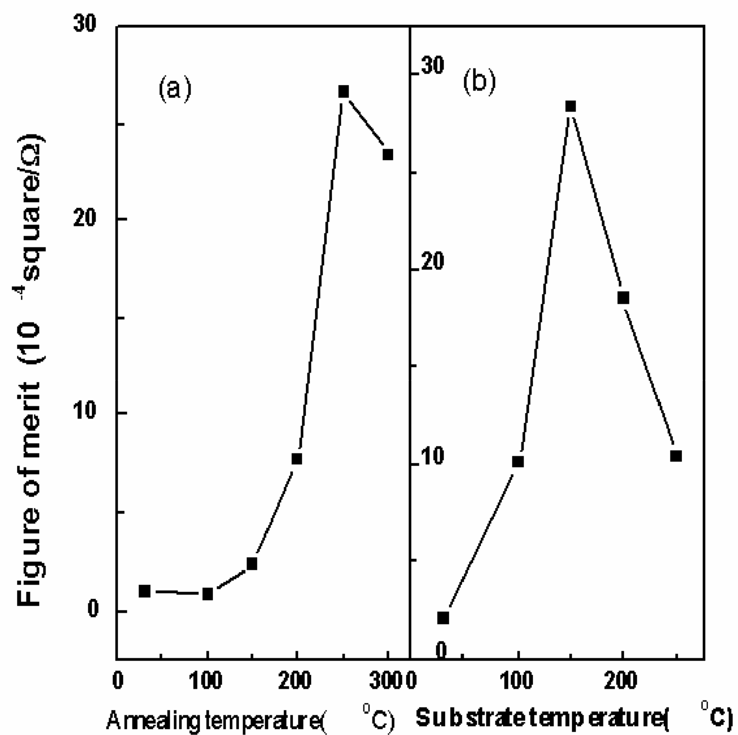

Figure 4.20 Variation of figure of merit of ITO thin films with (a) annealing temperature and (b) substrate temperature

The electrical properties of ITO thin films were also investigated as function of oxygen pressure and fluorine incorporation (Table 4.3). No improvement in conductivity was observed for the films deposited under oxygen atmosphere. This may be due to the reduction in the number of oxygen vacancies which results from the presence of oxygen in the sputtering gas. A similar result was observed in the case of fluorine doped ITO thin films also.

Table 4.3 Electrical properties of fluorine doped ITO thin films and ITO thin films deposited under various oxygen pressures.

% of oxygen	Resistivity (Ωcm)	Sheet resistance(square/Ω)
0	$2.1x10^{-3}$	106
0.4	$9.5x10^{-3}$	1330
0.5	$6.9x10^{-3}$	626
ITO:F	$4.47x10^{-3}$	320

4.4 Comparison of post annealing and substrate temperature on the properties of ITO thin films

Based on the detailed description on the influence of pre and post deposition heat treatments on ITO thin films, the following conclusions can be made.

- Post deposition heat treatment results in films showing (222) and (440) diffraction peaks. With increase in annealing temperature up to 250^0C, an enhancement of the (222) peak intensity can be observed. The film annealed at 250^0C was preferentially oriented in the (222) plane parallel to the substrate surface. The films deposited onto preheated substrates showed (222) and (400) diffraction peak. The film deposited at a substrate temperature of 100^0C was preferentially oriented in the (400) plane. With increase in substrate temperature beyond 100^0C intensity of (222) peak was found to increase gradually. The appearance of the (400) diffraction peak is a consequence of the greater amount of kinetic energy of the sputtered particles reaching the substrate surface.
- The optical transmission in the visible range of the electromagnetic spectrum was greater than 85% for both annealed films and films deposited onto preheated substrates. In the higher wavelength range a reduction in transmission was observed due to free carrier absorption.

- An increase in optical band gap was observed with increase in annealing temperature as well as substrate temperature. This is due to Burstein – Moss effect.
- Desirable properties such as minimum resistivity, minimum sheet resistance , maximum mobility and maximum carrier density were observed corresponding to a temperature of 250^0C in the case of post deposition heat treatment and at 150^0C in the case of films deposited onto pre heated substrates.
- The figure of merit, a quantitative measure of the quality of the TCO, was also found to be maximum corresponding to an annealing temperature of 250^0C in the case of post annealed films while a substrate temperature of 150^0C results in higher figure of merit..

4.5 Conclusion

Indium tin oxide thin films were deposited onto glass substrates by RF magnetron sputtering of ITO target and the influence of annealing temperature and substrate temperature on the properties of the films were investigated. In the case of annealing, a temperature of 250^0C was found to be optimum for getting films of better quality whereas a substrate temperature of 150^0C was sufficient for getting high quality films.

References

1. Aldrin Antony, Nisha M., Manoj R., M.K.Jayaraj, Appl.Surf.Sci **225**(2004)294
2. P.K.Song, Y.Shigesato, I.Yasui,, C.O.Yang, D.C.Paine, Jpn.J.Appl.Phys. **37**(1998)1870
3. JCPDS card No. 6-416
4. P.K.Song, Y.Shigesato, M.Kamei, I.Yasui, Jpn.J.Appl.Phys. **38**(1999)2921
5. M.Girtan, G.I.Rusu, G.G.Rusu, Mater.Sci.Eng.B **76**(2000)156
6. M.Higuchi, S.Uekusa, R.Nanako, K.Yokogawa, Jpn.J.Appl.Phys. **33**(1994)302
7. C.H.L. Weijtens, P.A.C Vanloon, Thin Solid Films **196**(1991)
8. J.Tauc, R.Grigorovici, A.Vancu, Phys.Stat.Sol(a)**15**(1966)627
9. H.L.Hartnagel, A.L.Dawar, A.K.Jain, C.Jagdish, Semiconducting Transparent Thin Films, IOP Publishing Ltd (1995)
10. E.Burstein,Phys. Rev.**93**(1954)632
11. F.O.Adurodija, H.Izumi, T.Ishihara, H.Yohioka, M.Motoyama, Solar energy Mater. Solar cells **71**(2002)1
12. R.B.H.Tahar, T.Ban, Y.Ohya, Y.Takahashi, J.Appl.Phys. **83**(1998)2631
13. Z.M.Jarzebski, Phys.Stat.Sol(a) **71**(1982)13
14. L.J.Meng, M.P.dos Santos, Thin Solid Films **322**(1998)56
15. Y.C.Park, Y.S. Kim, H.K. Seo, S.G.Ansari, H.S.Shin, Surf.Coat.Technol **161**(2002)62
16. D.Kim, Y.Han, J.S. Cho, S.K. Koh, Thin Solid Films **377**(2000)81
17. M.Nisha, S.Anusha, Aldrin Antony, R.Manoj, M.K.Jayaraj, Appl.Surf.Sci.**252** (2005)1430
18. B.D. Cullity and S.R. Stock, Elements of X ray diffraction, Third edition, New Jersey, Prentice Hall (2001)

19. Charles Kittel, Introduction to Solid State Physics, Seventh edn Wiley Eastern Limited, (1996)
20. G.G.Gonzalez, J.B.Cohen, J.H.Hwang, T.O.Mason, J.Appl.Phys. **87**(2001)2550
21. C.G.Granqvist, A.Hultakar, Thin Solid Films **411**(2002)1
22. J.C.Manifacier, J.Gasiot, J.P.Fillard, J.Phys.E.Scientific Instruments **9**(1976)1002
23. H.Kim, J.S.Horwitz, G.P.Kushto, S.B.Qadri, Z.H.Kafafi, D.B.Chrisey, Appl.Phys.Lett **78**(2001)1050
24. H.Kim, J.S.Horwitz, W.H.Kim, Z.H.Kafafi, D.B.Chrisey, J.Appl.Phys. **91**(2000)5371
25. G. Haake, Appl. Phys. **47** (1976)4086

CHAPTER 5

Influence of RF Power on the Properties of ITO Thin Films

Abstract

Highly transparent and conducting ITO thin films were deposited at room temperature by RF magnetron sputtering of ITO target (95wt%In_2O_3 and 5wt% SnO_2) in pure argon atmosphere. Thin films were deposited on glass substrate without any intentional heating at various RF powers ranging from 20W to 50W and the influence of RF power on the structural, electrical and optical properties of the films were investigated. The influence of fluorine doping on the properties of ITO thin films was also investigated as a function of RF power. Enhancement of crystallinity and conductivity was observed with increase in RF power. Film deposited on glass substrates at an RF power of 50W was oriented in the (100) direction and it showed a minimum resistivity of $1.27 \times 10^{-3} \Omega cm$. It has been observed that the film properties are greatly influenced by the plasma conditions during sputtering. Radio frequency (RF) plasma during sputtering was analyzed using Langmuir Probe and Optical Emission Spectroscopy (OES). The plasma parameters such as ion density and electron temperature were determined and their dependence on properties of thin film deposited under similar plasma conditions were studied. Plasma parameters were determined for different RF powers keeping the distance from the target a constant.

5.1 Introduction

The properties of Indium tin oxide thin films can be optimized by carefully selecting the process parameters during deposition. In the case of sputtered films, RF power is one of the process parameters that can be controlled during the film growth. This chapter presents the dependence of RF power on the ITO film properties.

5.2 Experimental

5.2.1 Thin film deposition

ITO films were deposited on to glass substrates at room temperature by rf magnetron sputtering of an ITO target (2 inch diameter) containing 95wt% of In_2O_3 and 5 wt% of SnO_2. The base pressure in the chamber was $2x10^{-5}$ m bar. Sputtering was carried out in argon atmosphere at a pressure of 0.01 m bar. Glass slides of dimension 2.5 cm x 1 cm were used as the substrates. The substrates were kept at a distance of 4cm above the target. Highly transparent and conducting films were obtained when deposition was carried out at that distance[1]. A 13.56 MHz RF power supply was used to provide the RF field. The RF power was varied in the range 20W to 50W.

Even though the substrates were not heated intentionally during sputtering, an increase in substrate temperature was observed during sputtering. The increase in substrate temperature can be attributed to the plasma surface interactions which causes the transfer of energy to the substrate. Energy transfer from plasma to solid surface occurs through optical radiations and fluxes of neutral particles and ions. Optical radiation has components in the IR, visible and UV regions. When these radiations are absorbed by a solid surface, the radiations transforms into heat. But the energy of optical radiations is very low. At lower sputtering pressures, ion collisions become prominent [2]. During the ion bombardment, the dissipation of kinetic and vibrational energy fractions of ions causes heating

of the substrate surface. Figure 5.1 shows the variation in substrate temperature measured at the end of sputtering as a function of RF power. The deposition rate was found to increase with increase in RF power, became maximum at 45W and then decreased slightly (Fig 5.1). The sputtering time was so adjusted that the thickness of all the films studied were 250nm.

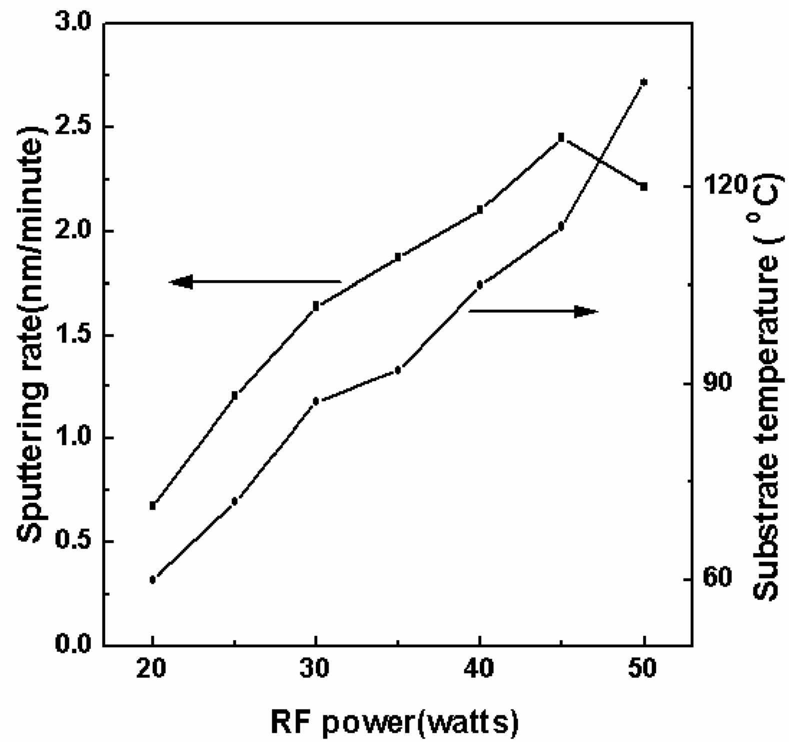

Figure 5.1. Variation of sputtering rate and substrate temperature with RF power

5.2.2 Plasma diagnostics

Langmuir probe is one of the simplest techniques for obtaining information about the ions in plasma. An RF compensated probe was used for plasma diagnostics. The Langmuir probe assembly consists of a tungsten wire, 0.5 mm in diameter and 5 mm in length, supported by a glass sleeve (Fig 5.2) along with the RF compensating circuit. Probe current is measured for bias voltages in the range of –60V to + 60 V. The probe voltage – current (V – I) characteristics are plotted for different RF powers (20W to 50W). Great care was taken to prevent the probe feed wires being exposed to the plasma since this will contribute to the measured probe current. To ensure a clean probe surface, the probe wire was replaced frequently.

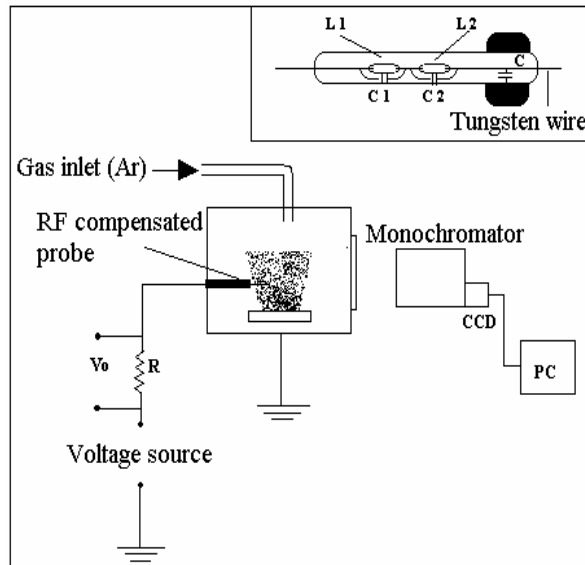

Figure 5.2. Experimental set up for Langmuir probe and optical emission spectral studies.

To investigate the ionic species present in the RF plasma in detail optical emission spectra (OES) of plasma plume generated during the RF sputtering of ITO target was recorded using a 0.32m monochromator and charge coupled device (CCD) detector. OES examines the light given off by species in the plasma that have been raised to excited states by electron impact. Excited species radiate at wavelengths corresponding to the quantum mechanically allowed transitions between electron energy levels. It is an attractive option for process control because it is fast, non intrusive, can monitor multiple elements simultaneously and provides information about deposition conditions in the plasma [3]. In the present investigation, the OES studies were made through the side window of the chamber (Fig 5.2). The spectral studies were carried out for different RF powers keeping the distance from the target at 4cm.

5.3 Structural characterization

The x-ray diffraction (XRD) pattern of the ITO thin films grown by sputtering at various RF powers is shown in figure5.3. All the films are polycrystalline and showed diffraction peaks of In_2O_3 [4]. The crystallinity of ITO thin films is strongly dominated by the kinetic energy of indium atoms reaching the substrate surface. The average kinetic energy of the sputtered particles is about 1 to 3 eV, which is high enough to enable the sputtered particles to migrate and to find the most suitable site to form the crystalline structure when they arrive at the substrate surface [5]. All the peaks detected were of In_2O_3 [4]. The films grown at lower RF power showed x-ray diffraction peak at $2\theta = 30.6^0$ which correspond to reflection from (222) plane indicating an orientation along the [111] direction and at $2\theta = 50.5^0$ corresponding to reflection from (440) plane indicating the orientation along [110] direction. The intensity of (440) peak increased with increase in RF power up to 35W. As the power is increased beyond 35W a new peak emerges at $2\theta = 35^0$ which correspond to (400) plane of In_2O_3 indicating a preferred orientation along the [100] direction. The increase

in RF power enhances the energy of the sputtered particles. The crystallites in the thin films deposited at higher RF powers will then try to orient in the [100] direction.

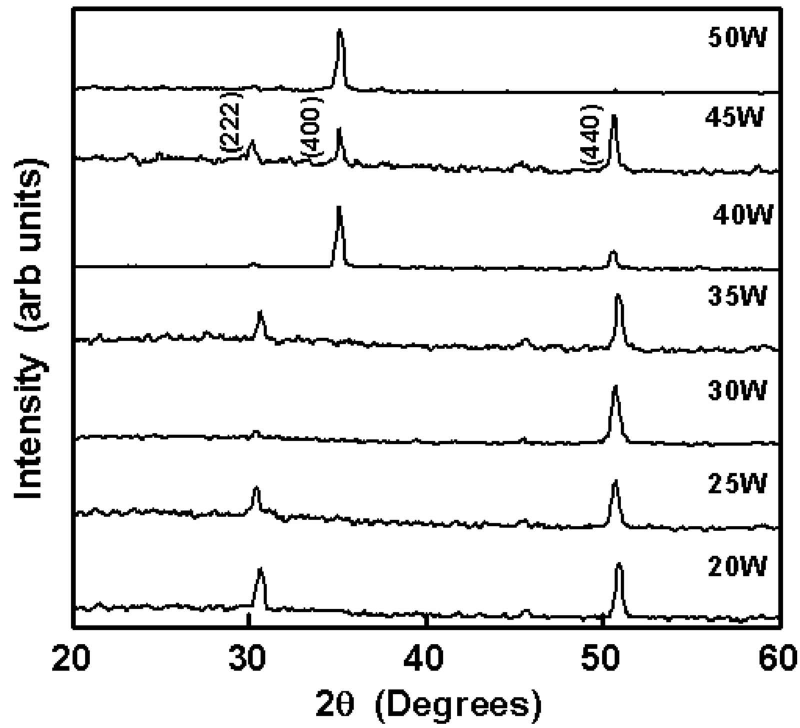

Figure 5.3. XRD pattern of ITO thin films deposited at various RF powers.

The change in preferred orientation of growth of ITO film with deposition conditions is already being reported. Some reports show that the orientation of the films change from (400) to (222) when the oxygen pressure is increased during sputtering [6,7]. Increase in substrate temperature is also reported to favor (400) orientation [8]. Though there have been controversial reports on the effect

of pressure on the film orientation, (400) peak intensity mainly decreased as the sputtering pressure is increased[9,10]. From a thermodynamic point of view, the preferred orientation of thin films is known to be the planes of lowest surface energy [11]. Also from the viewpoint of kinetics, only grains with the highest growth rate eventually survive [12]. In the case of ITO, (222) plane is known to be the most densly packed plane[13]. As a result it is the plane with highest energy and (400) plane has the lowest energy. The degree of orientation of the (400) plane is expected to be dependent on the mobility of the adatoms on the substrate[14].

The adatom mobility is found to be proportional to the diffusivity of adatoms on the substrate which is given by the expression,

$$D_s = \frac{1}{2} a_0^2 \upsilon \exp\left(\frac{-E_s}{kT}\right) \qquad (5.1)$$

where a_0 is the atomic dimension, ν is the vibrational frequency of adatoms and E_s is the activation energy for surface diffusion [15].

The mean square distance traveled by the adatoms in a time t is given by the expression

$$\langle X^2 \rangle = 2D_s t \qquad (5.2)$$

If the adatoms have a sufficient amount of energy, then they would form nucleation centers that have thermodynamically favorable (400) orientations. The average energy of adatoms is determined by the kinetic energy of the sputtered atoms just before arriving the substrate surface and Ar^+ bombardment energy. Ar^+ ions that are incident on the substrate surface can supply considerable energy to the adatoms[16].

In the present study, the grains showed (222) and (440) orientations at lower RF powers and the orientation changed to (400) as the power was increased. At low

sputtering power, the energy of Ar^+ ions, which collide with the target surface, is low and hence the average energy of the sputtered particles is also low. Therefore the supplied energy by ion bombardment is low and consequently the adatom mobility is very low at very low sputtering power. This favors the grain orientation along (222) and (440) planes. Increase in RF power caused increase in energy of the Ar^+ ions, which in turn increases the adatom mobility. This favors the grain orientation along (400) plane. The (400) orientation is also reported to be prominent in films that are oxygen deficient [17,18]. In the present investigation, the increase in RF power resulted in an increase in oxygen vacancy which is shown by the carrier density measurements.

The full width at half maximum (FWHM) for the (440) diffraction peak was analysed as a function of RF power. A decrease in FWHM with RF power (Fig 5.4) indicates the enhancement of crystallinity. The lattice constant ' a' can be determined using equation (4.1). The calculated value of 'a' for the ITO film is slightly greater than that of indium oxide ($10.117A^0$). According to recent reports [19] tin is incorporated into In_2O_3 lattice as Sn^{4+} whose ionic radius (0.071nm) is less than that of indium. The increase in lattice parameter is attributed to the increase in repulsive forces arising from the extra positive charge of the tin cations. In the present work an increase in lattice constant with RF power was observed (Fig 5.4).

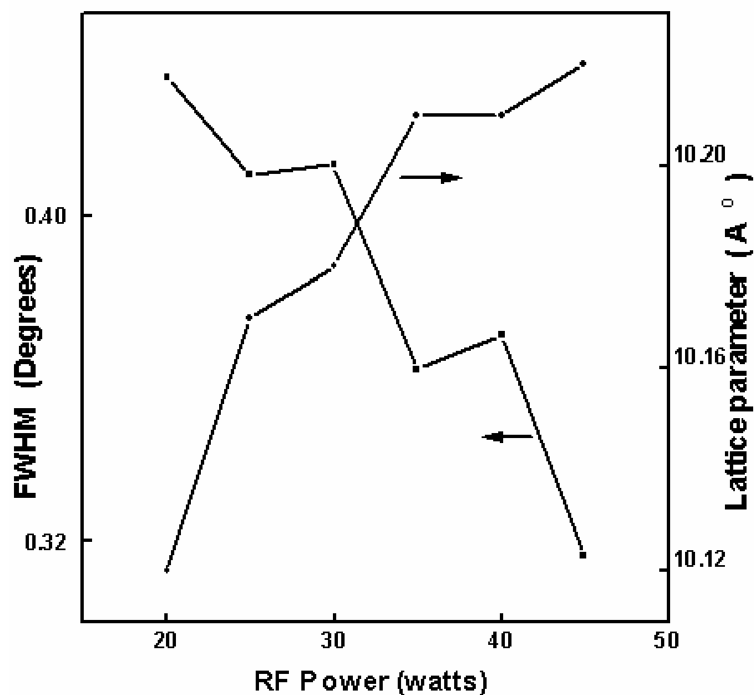

Figure 5.4. Variation of FWHM of (440) oriented grains and lattice parameter with RF power

The films were also deposited at a target to substrate spacing of 2cm under the same conditions mentioned above. The XRD pattern (Fig 5.5) shows that the films are polycrystalline and are oriented in the (100) direction. The films deposited at 20W were almost amorphous in nature. The (400) diffraction peak appeared at a sufficiently low RF power of 25W. The intensity of the (400) diffraction peak increase with increase in RF power. The appearance of the (400) diffraction peak at sufficiently lower RF power compared to the case with T-S spacing = 4 cm may be because of the sharp rise in temperature of the substrate during deposition which gives the sputtered particles the sufficient energy to orient in the (100) direction. (440) diffraction peak was also present in

the XRD pattern but with lesser intensity. Also the intensity of the (440) diffraction peak decreased with rise in RF power.

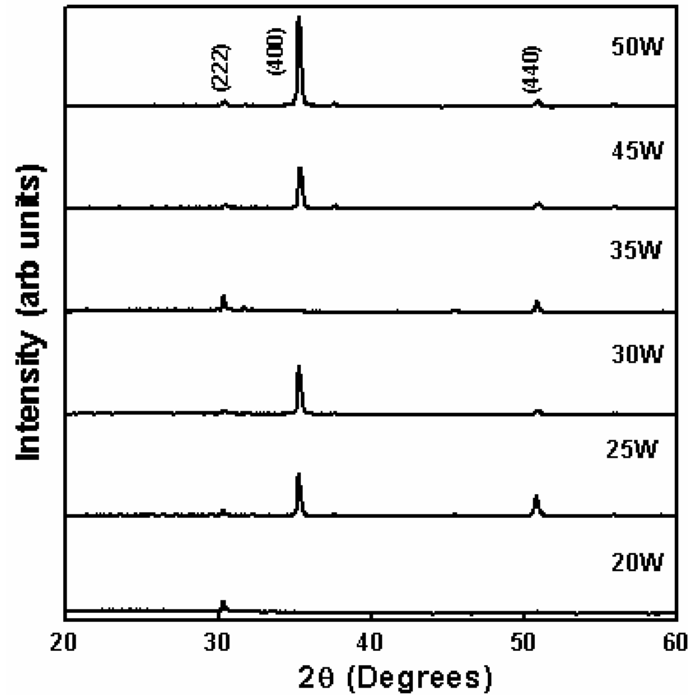

Figure5.5. XRD pattern of ITO thin films deposited at T-S spacing = 2cm and various RF powers

The influence of fluorine doping on the properties of ITO thin films were also studied. Fluorine doping was carryout by placing Indium fluoride pellets on the erosion zone of the target. The deposition was carried out at three different RF powers viz 30W, 40W and 50W at target to substrate distance 4cm. The films deposited at RF powers of 30W and 40W showed (440) diffraction peak at around $2\theta = 50.5^0$ indicating a preferred orientation in the [110] direction. As the power was increased to 50W the orientation of the films changed to [100] direction which can be inferred from the appearance of (400) diffraction peak in

the XRD pattern (Fig 5.6). Also we can see that the intensity of the (440) diffraction peak gets reduced as the RF power is increased from 30 to 50W.

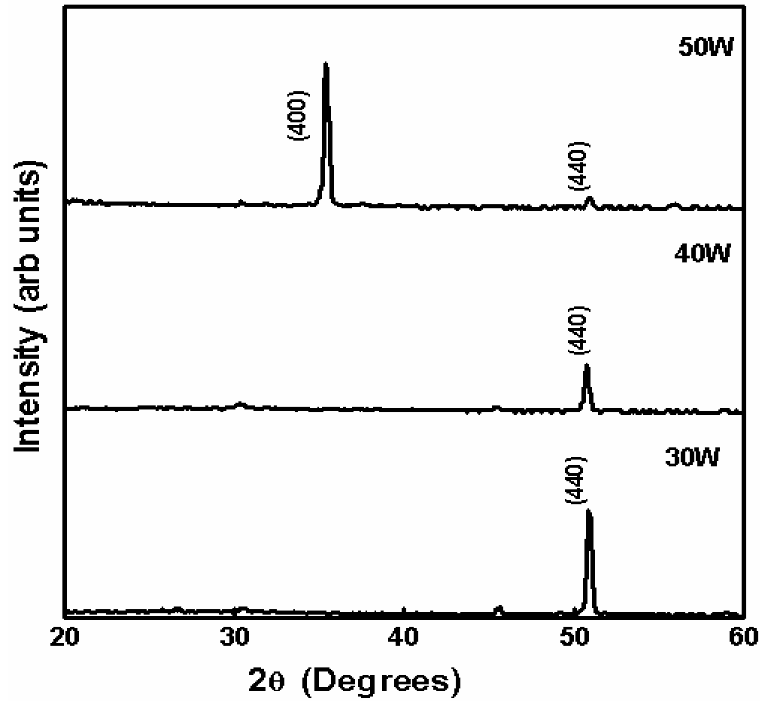

Figure 5.6. XRD pattern of Fluorine doped ITO thin films deposited at various RF powers

The FWHM of the (440) diffraction peak increased with increase in RF power, which indicate that the grain size of the (440) oriented crystallites gets reduced. Figure5.7 shows the variation in FWHM and intensity of (440) diffraction peak with RF power.

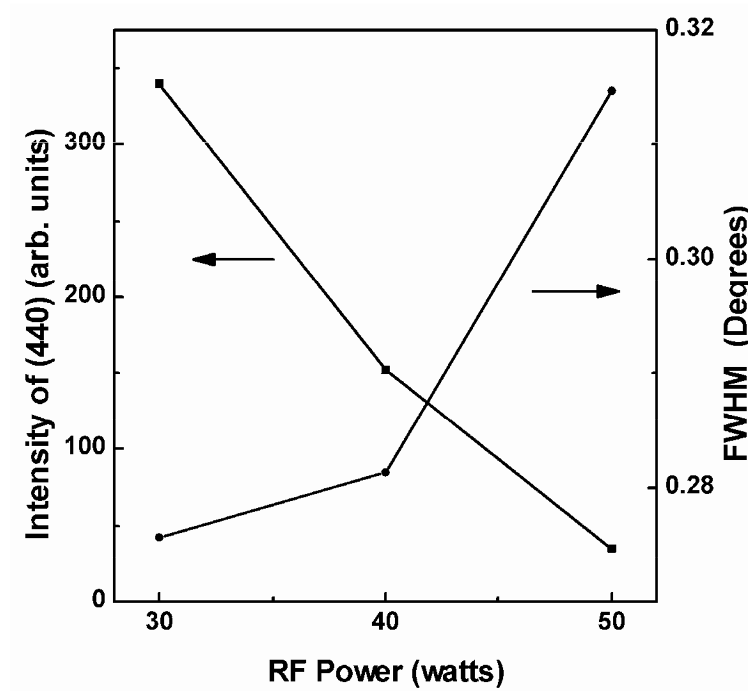

Figure5.7 Variation in FWHM and intensity of (440) diffraction peak with RF power

The alignment of the grains along (440) plane in the lower RF power range may be due to the lower energy of the sputtered particles reaching the substrate surface. Increase in RF powers gives additional energy to the sputtered particles, which enable them to orient in the [100] direction. Fluorine doping also favors the [100] orientation. It may be because of the replacement of some oxygen sites by fluorine ions since their radii are comparable [7].

5.4 Optical characterization

The transmission spectra of the ITO films grown at various RF powers are shown in figure 5.8. The films exhibited a strong absorption in the UV region. It is caused by the excitons across the fundamental bandgap E_g.

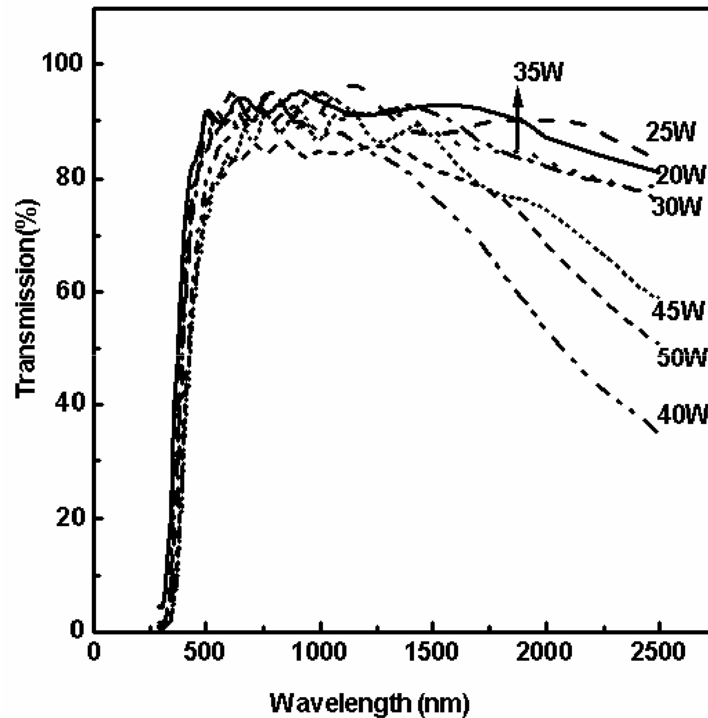

Figure 5.8.Transmission spectra of ITO thin films deposited at various RF powers

All the films were highly transparent in the visible region of the electromagnetic spectrum. The average transmission in the visible region of the electromagnetic spectrum was >80%. Films deposited at higher RF powers showed a decrease in transmission at higher wavelengths (in the near IR region).

In the near IR region, the free carrier absorption becomes important for the transmittance and reflectance of the ITO films [20]. The optical phenomena in this region can be explained on the basis of classical Drude theory. According to this theory, the transition from high transmittance to high reflectance will occur for films with higher carrier concentrations. Comparing the result of the present study with the theory, it can be concluded that the carrier concentration increases with increase in RF power.

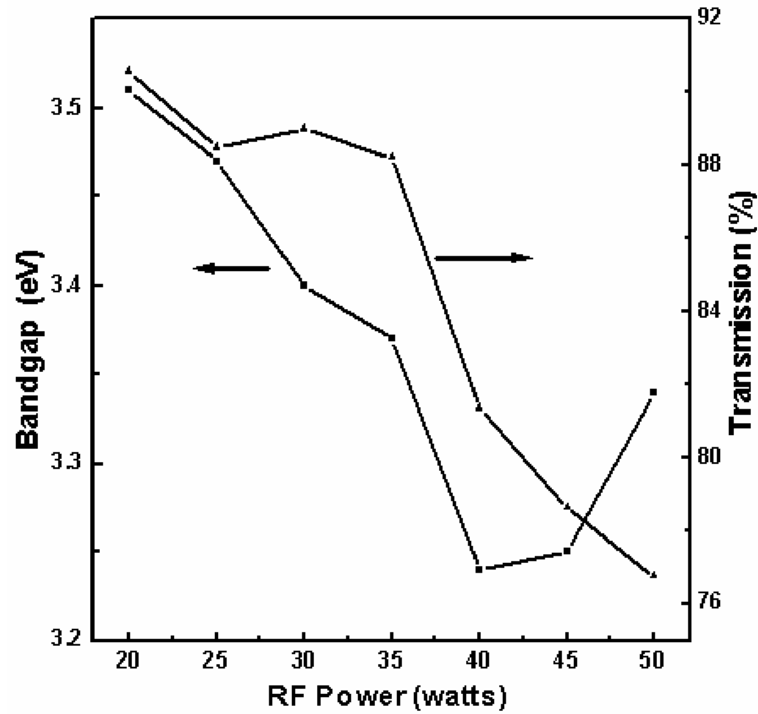

Figure5.9. Variation of bandgap and average transmission of ITO thin films as a function of RF power

The increase in carrier concentration with increase in RF power makes the transparent conductor to reflect the incident wavelengths in the IR region. The

average transmission in the visible range was found to decrease with increase in RF power (Fig5.9). According to Wu et al [21], the decrease in the value of transmission is related to the reduction of SnO_2 in ITO films.

The band gap of the ITO films were calculated from the transmission spectra. By assuming a parabolic band structure for the material, the absorption coefficient and bandgap can be related by the expression $\alpha h\nu = A(h\nu - E_g)^{1/N}$ where E_g is the band gap energy and α is the absorption coefficient corresponding to frequency ν. The constant N is equal to 2, for direct allowed transition. The bandgap of ITO films were determined from the plot of $(\alpha h\nu)^2$ vs $h\nu$ by extrapolating the linear portion of the curve to $\alpha h\nu$ equal to zero. In the present study, the bandgap decreased with increase in RF power (Fig 5.9) upto 40W and then increased. The increase in bandgap at higher RF powers can be attributed to Burstein - Moss effect which is a phenomenon that occurs at higher carrier concentrations. From the electrical measurements, a sharp increase in carrier density can be seen at higher RF powers which substantiate the increase in bandgap at high RF powers.

5.5 Electrical characterization

The resistivity of the films was determined by employing vander Pauw four probe technique. The resistivity of the films decreased with increase in RF power. Figure 5.10 shows the variation of resistivity and sheet resistance of ITO thin films with RF power for the films deposited at a target to substrate spacing of 4cm. The minimum resistivity of 1.27×10^{-3} Ω cm and sheet resistance of 208 Ω/square was obtained for the films deposited at an RF power of 50W. The mobility of the films increased upto 40 W and then decreased. The increase in mobility is related to the deposition rate [22]. As a result of high deposition rate at high RF powers, atoms do not have sufficient time to complete their bondings and it causes an increase in the number of oxygen vacancies. Increase in

mobility is also associated with the increase in grain size, which causes a reduction of scattering losses. The carrier density increased sharply at 50W (Fig 5.11a). The sharp increase in carrier density at 50W causes the decrease in mobility at that RF power.

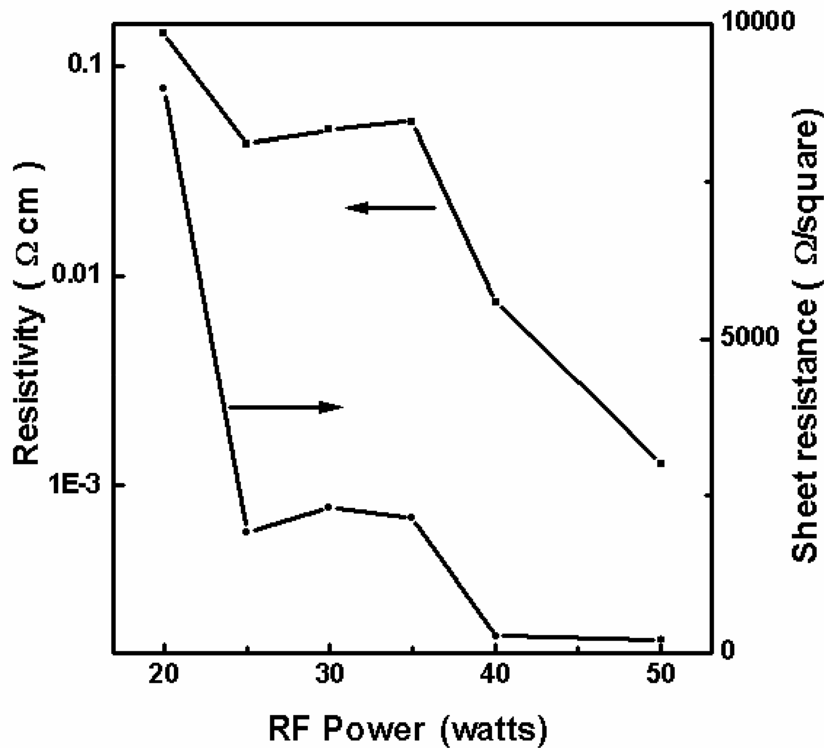

Figure 5.10. Variation of resistivity and sheet resistance of ITO thin films with RF power

In ITO, the magnitude of conductivity results from the ability of In_2O_3 lattice to incorporate substitutional tin atoms without major structural modifications as well as from the scattering mechanisms for free electrons [23]. The free electrons are liberated from the substitutionally entered tin atoms in the cation sub lattice and from doubly charged oxygen vacancies. When Sn^{4+} replaces In^{3+} in the In_2O_3 lattice, one free electron is created. Doubly charged oxygen vacancy

creates two free electrons. The increase in number of free carriers with increase in RF power reduces the resistivity of the films.

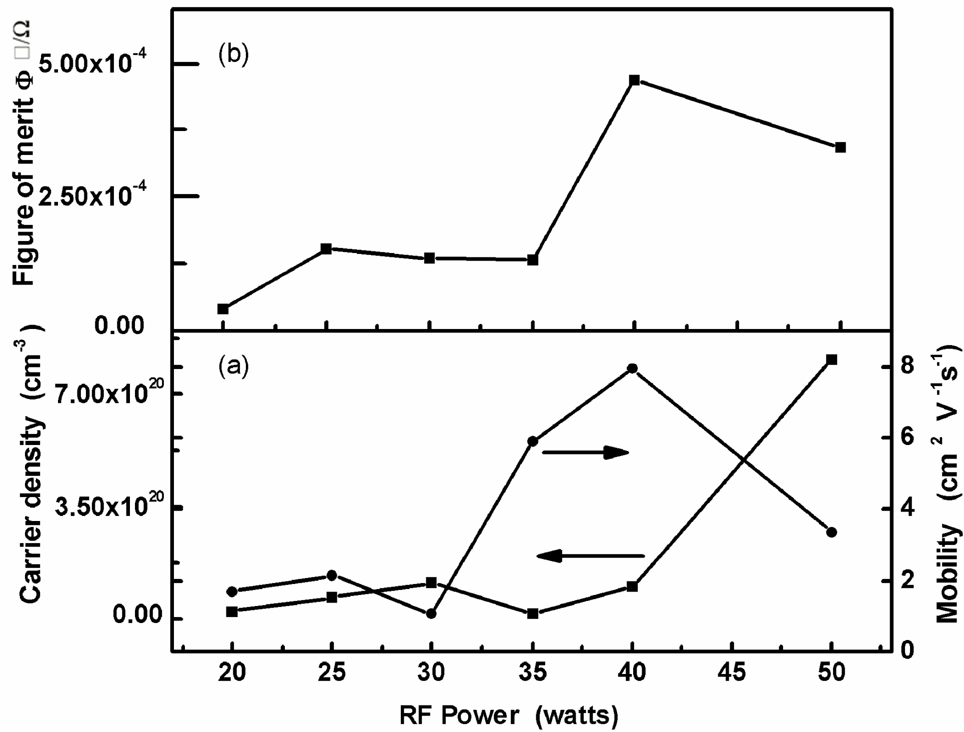

Figure 5.11. Variation in (a)mobility and carrier density and (b)figure of merit of ITO thin films with RF power.

The figure of merit of the films was determined using the relation deviced by Haacke[24]. The figure of merit increased with increase in RF power and showed a slight decrease corresponding to the RF power of 50W (Fig5.11b). This decrease is due to the decrease in the value of average transmission in the visible range corresponding to 50W.

The resistivity of the films deposited at a target to substrate spacing of 2cm also decreased with increase in RF power. It got almost saturated after 35W. But the minimum value of resistivity observed was less than that in the case of T-S = 4cm. The electrical properties of the fluorine doped ITO films also showed a similar trend with increase in RF power.

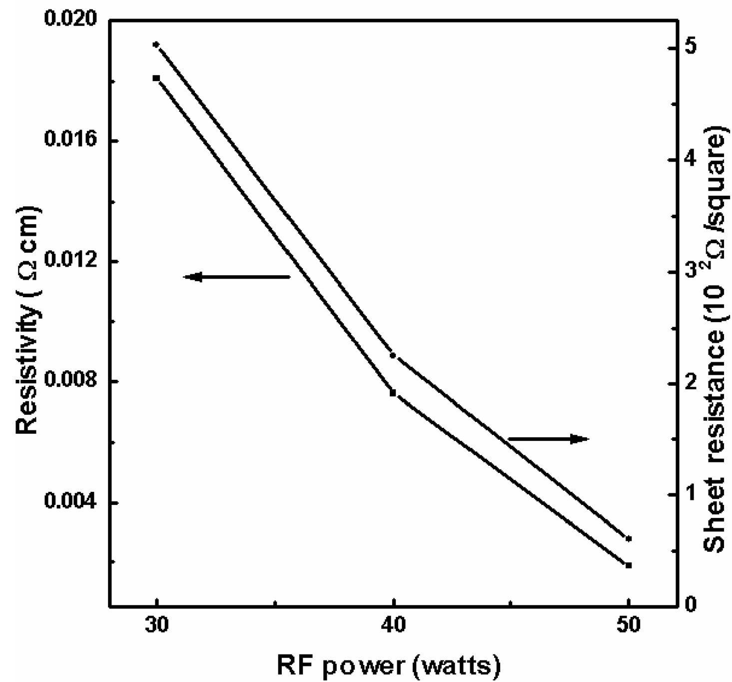

Figure 5.12. Variation of resistivity of ITO:F thin films with RF power.

Resistivity and sheet resistance decreased with increase in RF power (Fig 5.12) while mobility and carrier density increased with increase in RF power (Fig 5.13). However, there was much reduction in the value of sheet resistance for the

fluorine doped ITO films. A sheet resistance of 65 Ω/square was obtained when film deposition was carried out at an RF power of 50W.

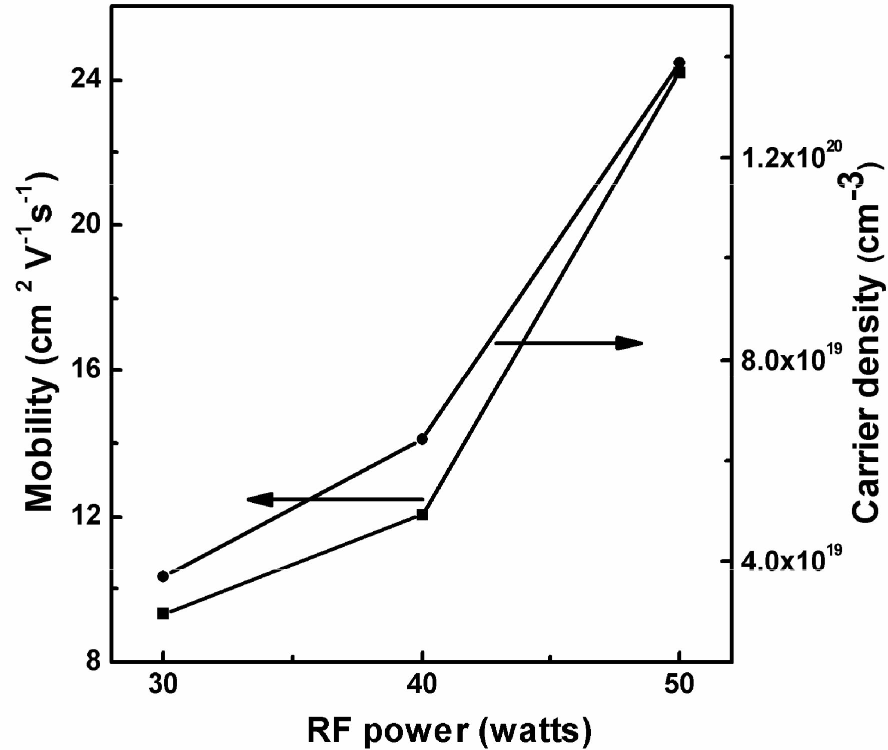

Figure 5.13. Variation of mobility and carrier density of ITO:F thin films with RF power

5.6 Plasma characterization

5.6.1 Langmuir Probe

Probe current (I) was measured for bias voltage (V) in the range –40 to +40V.The measurement was carried out at different RF powers ranging from 20W to 50W. Figure5.14 shows the probe I-V characteristics for an RF power of

20W with the probe placed at a distance of 4cm. This characteristics is normally determined by the plasma properties in the immediate vicinity of the probe [25].

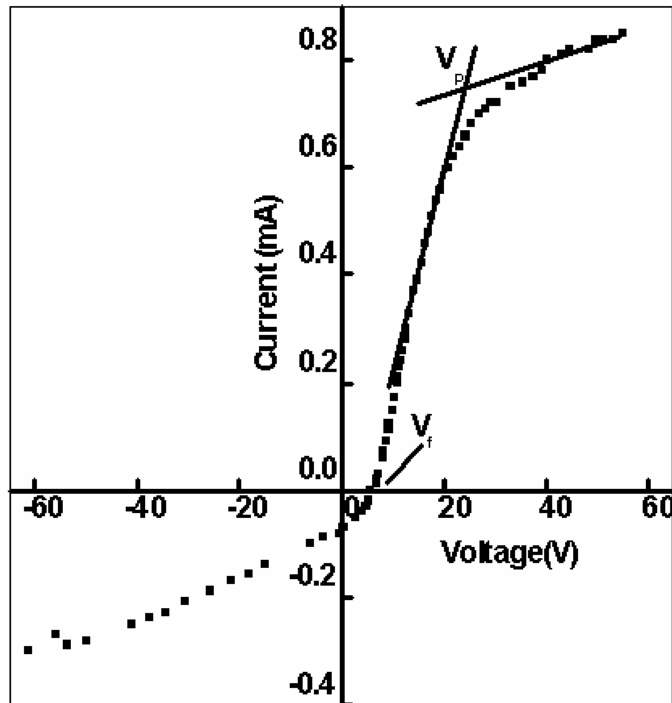

Figure 5.14. Langmuir probe I-V characteristics of RF plasma during the sputtering of ITO target (RF power = 20W)

As mentioned in section 3.5.1a three separate regions namely region I, region II and region III can be seen in the I-V characteristics. From the characteristics we can determine the plasma potential (V_p) and floating potential (V_f).The difference between plasma potential and floating potential ($V_p - V_f$) gives a measure of energy of the sputtered particles bombarding the substrate. $V_p - V_f$ is plotted in the figure 5.15 as a function of RF power. In the present investigation $V_p - V_f$ shows a slight decreases with increasing RF power.

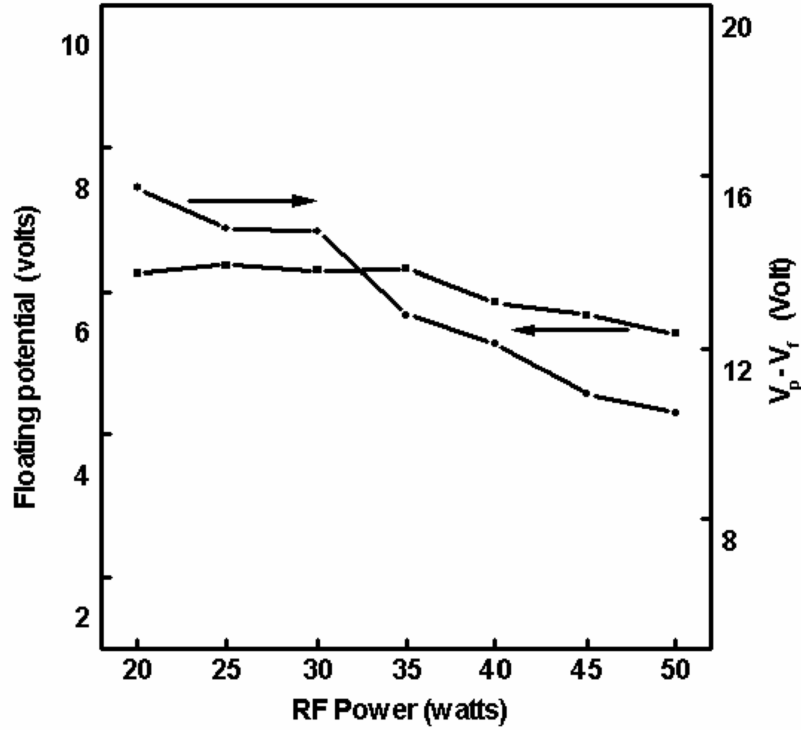

Figure 5.15. Variation of floating potential and V_p-V_f with RF power

5.6.1a Ion Density

The saturation ion portion of the characteristics is used to determine the ion density[26]. The ion current drawn by the probe is given by the equation

$$I_i = \frac{Ae^{3/2}N}{2\sqrt{\pi}}\left(\frac{3T_e}{m_i}\right)^{1/2}\left(1-\frac{V-V_f}{T_e}\right)^{1/2}, \qquad (5.3)$$

where A is the surface area of the probe, N is the plasma density, m_i is the ion mass and T_e is the electron temperature in electron volts. Taking the derivative of $I_i^{\,2}$ with respect to V and rearranging we get

$$n_i^{\,2} = \frac{4\pi m_i}{3A^2e^3}\left(\frac{\partial I_i^{\,2}}{\partial V}\right) \qquad (5.4)$$

Where n_i is the ion density, m_i is the ion mass and A is the collection area of probe which is given by

$$A = 2\pi rl + \pi r^2, \qquad (5.5)$$

where r is the radius of the probe (100 μm) and l is the probe length (5 mm). Ion mass was taken as m_i = 40m_p (where the m_p is the mass of the proton (1.667x10^{-27}Kg)), on the assumption that the major contribution of ions are given by Argon. This equation is based on the fact that n_i is equal to electron density n_e because plasma is neutral .

Figure 5.16 shows the dependence of ion density on RF power. Ion density is found to increase linearly with increase in RF power. The increase in ion density is due to the greater ionization resulting from collisions that may occur at higher RF power.

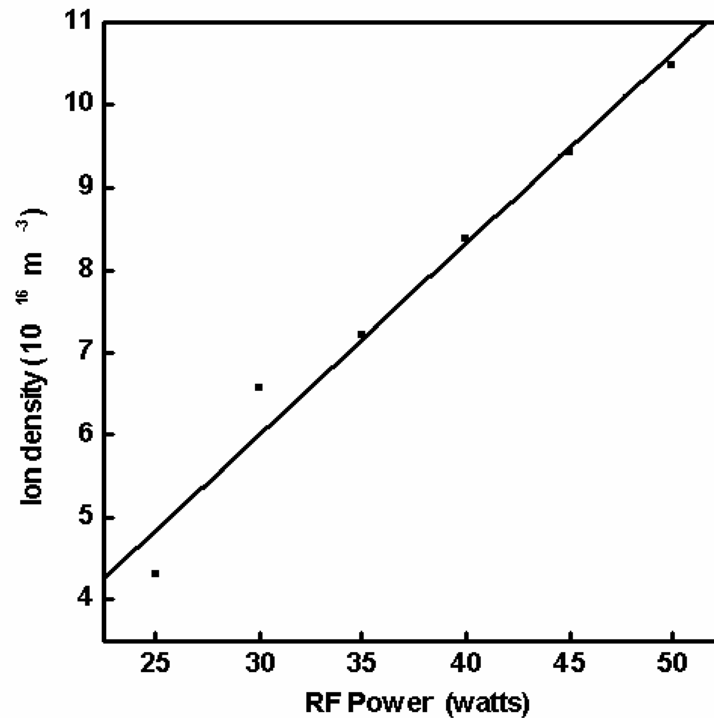

Figure 5.16. Variation of ion density as a function of RF power

5.6.1b Electron temperature

The state of plasma is essentially specified if the composition of the plasma is known and if the energy of each constituent can be determined. Electron temperature can be determined from the I-V characteristics [26]. The electron temperature can be determined from the plot of natural logarithm of current (ln I) versus probe voltage in the region between floating potential and plasma potential. The graph will be a straight line. The reciprocal of the slope of the straight line plot will give the value of kT_e. In the present investigation, electron temperature decreased with increase in RF power(Fig 5.17 (a)). The drop in electron temperature and V_p - V_f is due to the increase in ion density[27].

The electron velocity and ion velocity[28] were calculated using the equations,

$$v_e = \left(\frac{8kT_e}{\pi m_e} \right)^{1/2} \qquad (5.6)$$

$$v_i = \left(\frac{8kT_e}{\pi m_i} \right)^{1/2} \qquad (5.7)$$

where k is the Boltzmann constant, T_e is the electron temperature, m_e is the mass of electron and m_i is the ion mass.

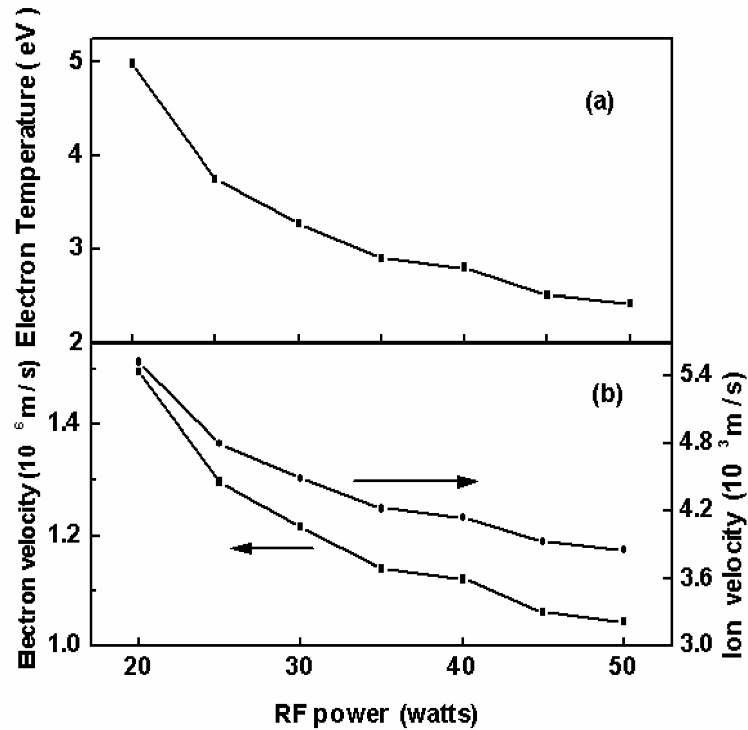

Figure 5.17. Variation of (a)electron temperatureand (b)electron and ion velocity with RF power

Ion velocity is of the order of 10^3m/s and electron velocity is of the order of 10^6m/s. Both ion velocity and electron velocity decreased with increase in RF power (Fig 5.17(b)). The variation of velocity with RF power showed a similar behaviour as that of electron temperature.

5.6.2 Optical Emission Spectral Studies

RF plasma generated during the sputtering of ITO target was analysed by recording the optical emission spectra, in order to identify the ionic species in the plume.

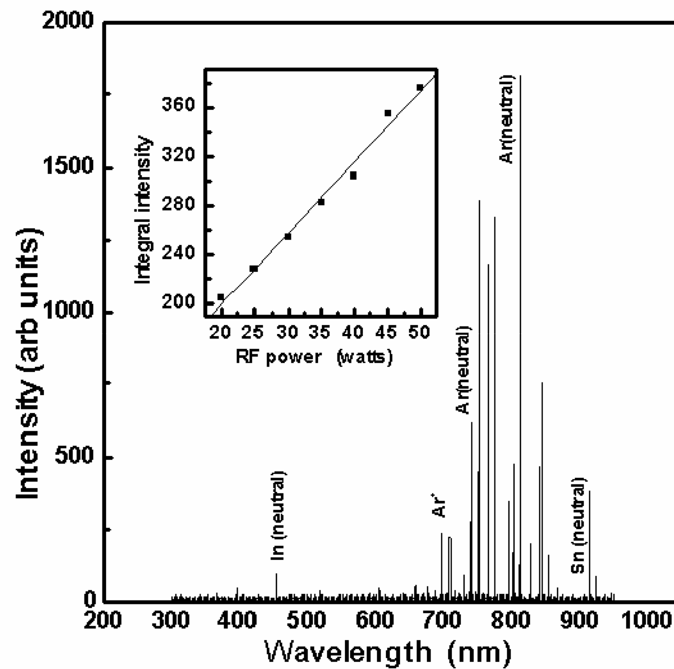

Figure 5.18. Optical emission spectrum of RF plasma generated with ITO target at an RF power of 20 W and at a distance of 4 cm from the target. Inset shows the variation of integral intensity of argon (I) at a wavelength of 811.5 nm with RF power

The spectral analysis revealed that the ionic species is mainly composed of argon ions. The identified species [29] essentially comprises argon neutrals (ArI), singly ionised argon (ArII), doubly ionised argon (ArIII), Indium neutral (InI), Oxygen neutral (OI) and tin neutral (SnI). Figure 5.18 gives a typical OES spectrum taken at an RF power of 20W. The spectral data is collected from the plasma at a distance of 4cm from the target.

The OES shows that the intensity of emission lines increases with increase of RF power. The variation of integral intensity of Argon (I) at a wavelength of 811.5nm with RF power is given in the inset of figure 5.18. The integral intensity is found to increase linearly with RF power. Increase of RF power causes more ionization, which in turn increases the population of various energy levels associated with the ions leading to the increase in integral intensity.

5.7 Conclusion

Highly transparent and conducting indium tin oxide thin films were deposited by RF magnetron sputtering at room temperature. The influence of RF power on the structural, electrical and optical properties were evaluated. Enhancement of crystallinity with increase in RF power was observed. The films deposited at an RF power of 50W were oriented in the (100) direction. An increase in lattice parameter with increase in RF power was also observed. The films were highly transparent in the visible range of the electromagnetic spectrum. The average transmission in the visible range was greater than 80%. The minimum resistivity of $1.25 \times 10^{-3} \Omega cm$ was obtained for the films deposited at an RF power of 50W. Langmuir probe and Optical Emission Spectroscopic (OES) studies were done to investigate the plasma parameters. Different ionic species in the plasma were identified from the spectrum. The plasma parameters such as electron temperature, electron & ion velocity and ion density were determined by the Langmuir probe technique for various RF powers. The observed plasma

parameters were correlated with the properties of thin films deposited under similar plasma conditions. The ion density and electron temperature was the highest for an RF power of 50W.

References

1. Aldrin Antony, Nisha M, Manoj R., M.K.Jayaraj, Appl.Surf.Sci. **225** (2004)294
2. J.O.Park, Thin Solid Films **474**(2005)127
3. I.L.Eisgruber, J.R.Engel, R.E.Hollingsworth, P.K.Bhat, R.Wendt, J.Vac.Sci.Technol.A **17**(1999) 190
4. JCPDS Card No.6-416
5. P.K.Song, Y.Shigesato, M.Kamei, I.Yasui, Jpn.J.Appl.Phys **38**(1999)2921
6. C.G.Choi, K.No, W.J.Lee, H.G.Kima, S.O.Jung, W.J.Lee, W.S.Kim, S.J.Kim , C.Yoon, Thin Solid Films **258** (1995)274
7. M.Nisha, S.Anusha, Aldrin Antony, R.Manoj, M.K.Jayaraj, Appl.Surf.Sci. **252**(2005)1430
8. F.El Akkad, A.Punnose, G.Prabu, J.Appl.Phys. A **71**(2000)157
9. P.K.Song, Y.Shigesato, I.Yasui, C.W.O. Yang and D.C.Paine, Jpn. J. Appl.Phys.**37**(1998)1870
10. R.W.Smith, J.Appl.Phys **81**(1997)1196
11. T.Q.Li, S.Noda, Y.Tsuiji, T.Ohsawa, H.Komiyama, J.Vac.Sci.Technol A **20**(2002)583
12. C.H.Yi et al, Jpn.J.Appl.Phys. **34**(1995)1638
13. Y.S.Jung, S.S.Lee, J.Crystal Growth **259**(2003)343
14. M.Ohring, The material science of thin films, Academic Press, Sandiago(1992)
15. K.F.Chiu, Z.H.Barber, Thin solid Films **358**(2000)264
16. A.Kachoune, M.Addou, A.Bougrine, B.Elidrissi et al, Mater.Chem and Phys. **70**(2001)285
17. T.Saitoh, X.Wang, H.Hashigami, T.Abe et al, Sol. Energy.Mater.Sol. cells **65**(2001)285

18. G. G.Gonzalez, J.B.Cohen, J.H.Hwang, T.O.Mason, J.Appl.Phys. **87**(2001)2550
19. A.Grill, Cold Plasma in Material Fabrication, IEEE press, New York(1994)
20. L.J.Meng, M.P.dos Santos, Thin Solid Films **322**(1998)56
21. W.F.Wu, B.S.Chiou, Thin solid Films **247**(1994)201
22. M.A.Martinez, J.Herrero, M.T.Gutierrez, Thin solid Films**269**(1995)80
23. C.G.Granqvist, A.Hultaker, Thin solid Films **411** (2002)1
24. G. Haake, Appl. Phys. **47**(1976)4086
25. H.R.Griem, Plasma Spectroscopy, McGraw-Hill, New York (1964)
26. J.E.Heidenreich, J.R.Paraszczak, M.Moison, G..Suave, J.Vac.Sci.Technol. B **5**(1987)347
27. K.Deenamma Varghese, G.Mohan Rao, Rev.Sci.Instrum **71**(2000)467
28. J.M.Hendron, C.M.O.Mahony, T.Morrow, W.G. Graham, J.Appl.Phys **81**(1997)2131
29. J.R.Fuhr, W.L.Wiese, Handbook of Chemistry and Physics, 79th ed.CRC, Boca Raton, FL (1998)

CHAPTER 6

Influence of Bias Voltage on the Properties of ITO Thin Films Grown on Flexible Substrates

Abstract

Transparent conducting Indium tin oxide thin films were deposited on polyimide substrates by RF bias sputtering of ITO target. The influences of bias voltage on the structural and electrical properties of the films were investigated. In order to correlate the material characteristics with the plasma parameters during sputtering, we employed Langmuir probe and Optical Emission Spectral studies. The films deposited onto positively biased substrates were poorly crystalline. An improvement in crystallinity was observed with increase in negative bias. The films deposited at a bias voltage of –20V showed a preferred orientation in the [111] direction and a minimum resistivity of $2.24 x 10^{-2} \Omega cm$.

6.1 Introduction

Liquid crystal display technology has dominated the flat panel display market for many years. This technology involves complex film growth process of the component layers on rigid and brittle substrates such as silicon wafers[1]. The advent of organic light emitting devices has given a new opportunity for the development of flexible display technology. Devices on flexible substrates have many advantages such as being lightweight, unbreakable and conveniently portable [2]. A flexible organic light-emitting device has a layer of transparent conducting oxides (TCO) the anode. Among the various TCO materials, Indium Tin Oxide (ITO) thin films is the most widely used one because of its low resistivity[3-8], high transmission and high work function. Because of the poor thermal endurance of the organic substrates, it is necessary for ITO films to be deposited at lower substrate temperatures. Also low substrate temperature deposition can improve the quality and efficiency of semiconductor devices.

Reports show that the effect similar to that of substrate heating can be achieved by ion bombardment of the growing film during deposition [9]. In a sputtering system, this can be achieved by biasing the substrate during deposition. This chapter presents the dependence of the ITO film properties on the bias voltage. Analysis of the plasma parameters using Langmuir probe technique is also discussed in the chapter.

6.2 Experimental

ITO films were deposited on polyimide (Kapton VN 500) substrates by RF magnetron sputtering of ITO target containing 95wt% of In_2O_3 and 5wt% of SnO_2. The base pressure used for sputtering was $1x10^{-5}$mbar and the deposition was carried out at an argon gas pressure of 0.01 mbar. The substrate was kept at a distance of 4cm from the target. The RF power used for sputtering was kept

constant at 30 W. The film deposition was carried out at various negative and positive bias voltages using an external DC power supply. Indium electrodes in the form of strips (1cm x 0.1cm) were coated on the polyimide substrates for biasing. The thickness of the ITO films was determined using Tolansky interference technique. All the films used for the present study were about 250nm thick. The crystallinity of the films was analyzed using an X-ray diffractometer using the Cu-Kα radiation (1.5414 A^0). The electrical characterization was done using Keithley Source Measure Unit. Surface morphology of the films were analysed using Scanning Electron Microscopy (SEM).

To obtain the information about the ions in the plasma, Langmuir probe technique was used [10]. Probe current was measured for bias voltages in the range of - 60 to + 60 V. The probe voltage – current (V – I) characteristics were plotted for different bias voltages by keeping the RF power constant at 30W. Great care was taken to prevent the probe feed wires being exposed to the plasma since this will contribute to the measured probe current. The ionic species present in the RF plasma were analyzed by taking the optical emission spectra (OES) of plasma plume generated by RF sputtering of ITO target using a 0.32m monochromator and charge coupled device (CCD) detector. The spectral studies were carried out for different bias voltages, keeping the RF power a constant.

6.3 Results and discussion

6.3.1 Structural characterisation

The X-ray Diffraction (XRD) pattern (Fig 6.1) of the films show that the films deposited at a bias voltage of + 20 V is amorphous in nature. When a bias voltage of +10V was given to the substrate the film showed (222) diffraction peak [11]. The intensity of the (222) diffraction peak increased with increase in

negative bias voltage up to –20V. The films deposited at negative bias voltages greater than 40V were poorly adhesive. The films appeared powdery and it easily peeled off from the substrate. This may be due to the increase in stress in the films due to ion bombardment.

The bombardment of cations on the growing film caused by the negative bias give additional energy to the molecules and clusters condensed on substrate [12], which will make the growing film crystalline. With further increase in negative bias the film orientation changed to (211) plane. The change in orientation at higher negative bias voltages may be due to the deviation from stoichiometry resulting from the decrease in packing density [13].

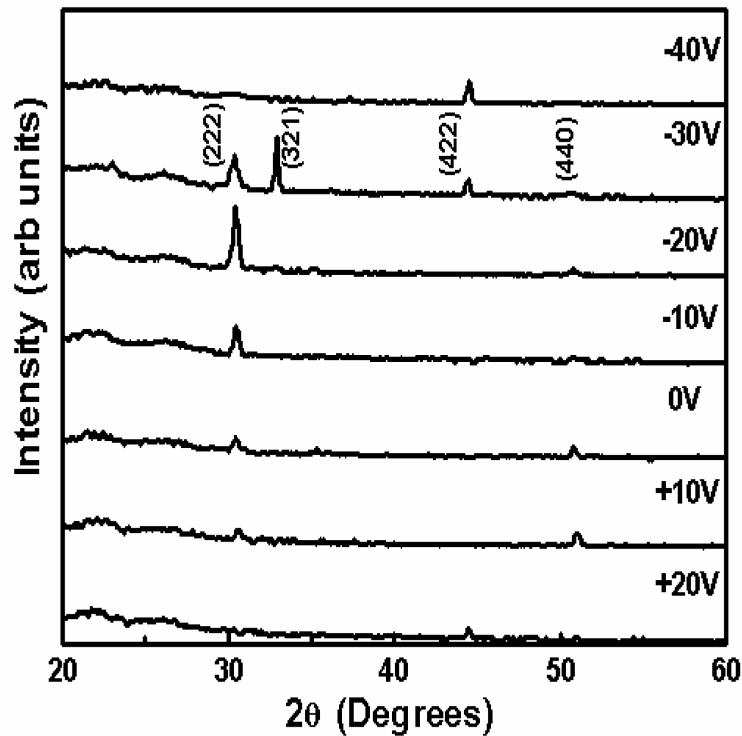

Figure 6.1. XRD pattern of ITO thin films deposited at various bias voltages

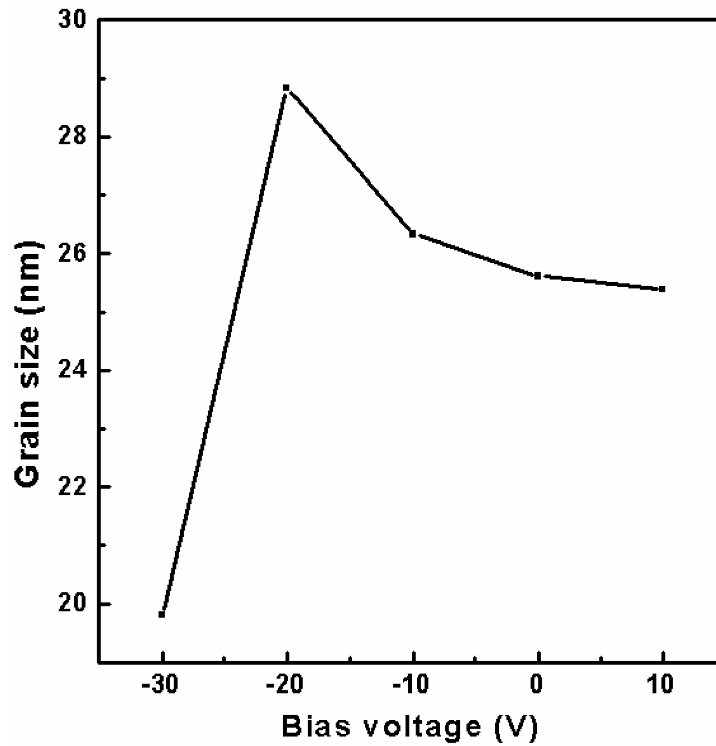

Figure 6.2. Variation of grain size of ITO thin films with bias voltage

The grain size of the (222) oriented grains was determined using Scherrer formula by finding the full width at half maximum of the peak (Fig 6.2). The grain size was maximum for the films deposited onto substrates biased at –20V. The degradation of crystallinity at higher negative biases causes a decrease in grain size due to the resputtering.

6.3.2 Electrical Characterisation

The resistivity of the films was found to decrease when the bias voltage was varied from +20V to –30V (Fig 6.3). The high value of resistivity at positive bias voltages is due to the poor crystallinity of the films. The resistivity was

minimum for a bias voltage of –20V. This may be due to the better crystallinity of the films as seen from the XRD pattern. The preferential orientation of the films in the [111] direction at this particular voltage may also contribute to the minimum resistivity [14]. One of the reasons for the increase in resistivity at higher substrate biases may be the entrapment of argon ions in the films. At lower substrate biases, only loosely held surface contaminants are resputtered while at higher substrate biases, there is possibility of resputtering from the deposited film, which causes a nonstoichiometry of the films. This factor also contributes to the degradation in film properties at higher substrate biases.

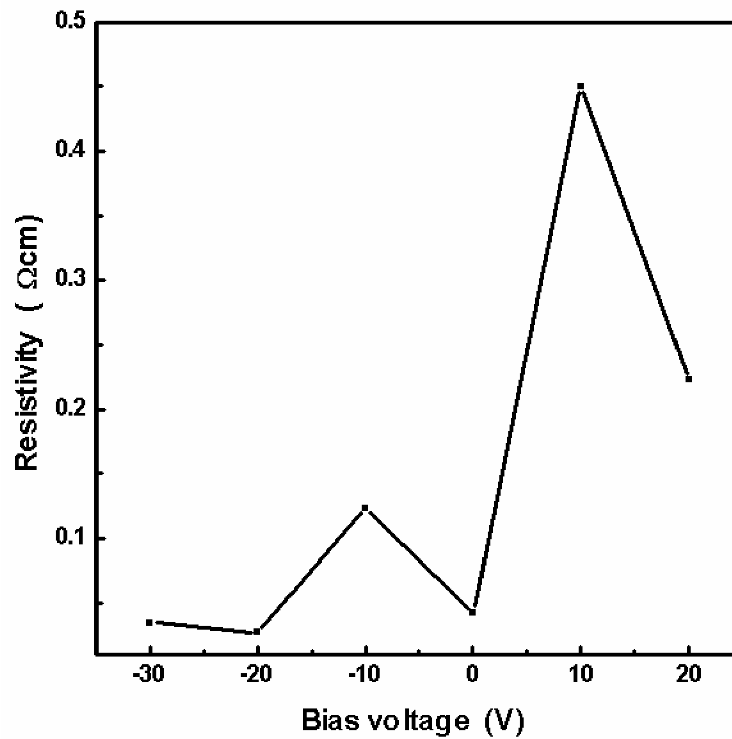

Figure 6.3. Variation of resistivity of ITO thin films with bias voltage

Figure 6.4 shows the SEM pictures of the ITO films deposited at –20 V, 0 and +20 V respectively. It can be seen that the films deposited at negative and zero bias voltage has got smooth surface while the films deposited at positive substrate bias is having a rough surface. This may be due to the bombardment of the substrate by energetic electrons during positive biasing.

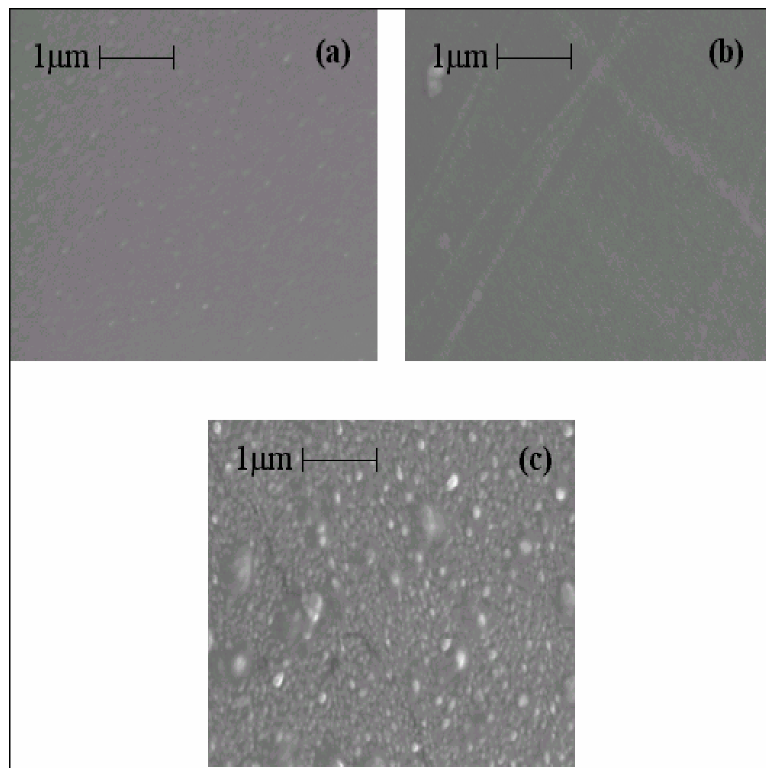

Figure 6.4. SEM picture of ITO thin films deposited at (a)-20V, (b)0V and (c) +20V

6.3.3 Langmuir probe analysis

To understand the growth and film properties of ITO thin films during bias sputtering, Langmuir probe and optical emission spectroscopic studies were carried out during sputtering. A typical Langmuir probe I – V characteristics for an RF power of 30W and bias voltage of –20 V is shown in figure 6.5.

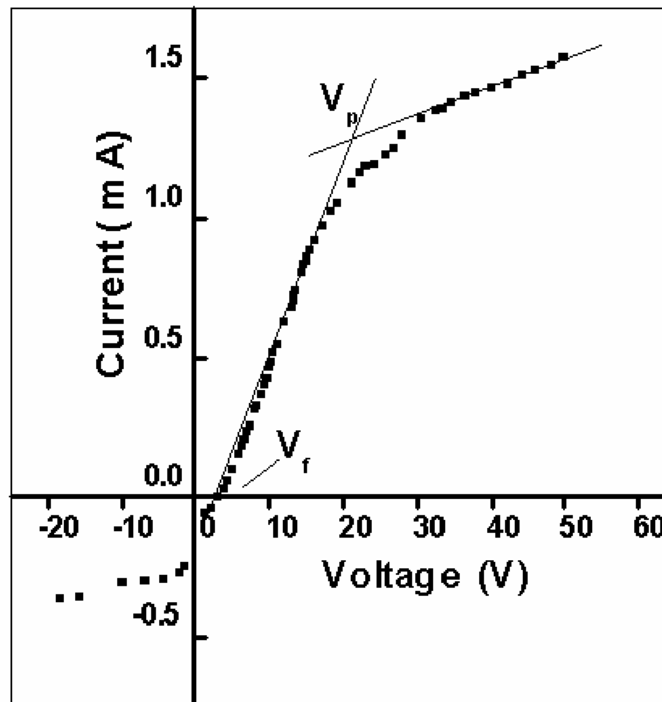

Figure 6.5. Typical Langmuir probe I – V characteristics of the plasma generated during sputtering of ITO target. RF power = 30W and bias voltage = -20V

The floating potential (V_f) and plasma potential (V_p) are determined from the Langmuir probe I-V plots as shown in the figure6.5. The difference between plasma potential and floating potential ($V_p - V_f$) is plotted in figure6.6 as a

function of bias voltage. It is found that $V_p - V_f$ is maximum in the unbiased condition. With increase in positive and negative bias, the value of $V_p - V_f$ decreases. $V_p - V_f$ is a measure of the energy of the sputtered particles reaching the substrate surface. The lower value of $V_p - V_f$ at higher bias voltages may be due to a decrease in energy of the particles reaching the substrate surface.

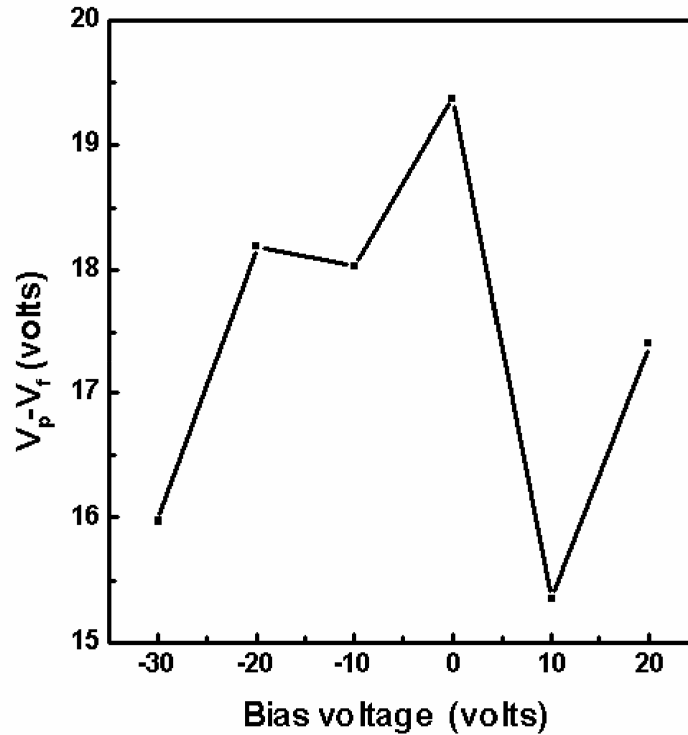

Figure 6.6 Variation of $V_p - V_f$ with RF power

The saturation ion portion of the characteristics is used to determine the ion density. The ion current drawn by the probe is given by the equation

$$I_i = \frac{Ae^{3/2}N}{2\sqrt{\pi}}\left(\frac{3T_e}{m_i}\right)^{1/2}\left(1-\frac{V-V_f}{T_e}\right)^{1/2}, \quad (6.1)$$

where A is the surface area of the probe, N is the plasma density, m_i is the ion mass and T_e is the electron temperature in electron volts[15]. Taking the derivative of I_i^2 with respect to V and rearranging we get

$$N_i^2 = -\frac{4\pi m_i}{3A^2 e^3}\left(\frac{\partial I^2}{\partial V}\right), \qquad (6.2)$$

The electron temperature is determined from the slope of the *ln (I) – V* curve of the probe in the region between V_f and V_p by the equation

$$T_e = \frac{\partial V}{\partial \ln(I)}, \qquad (6.3)$$

where I is the electron current[16].

Figure6.7 shows the dependence of ion density on bias voltage. Ion density is found to be of the order of $10^{16}\,m^{-3}$.

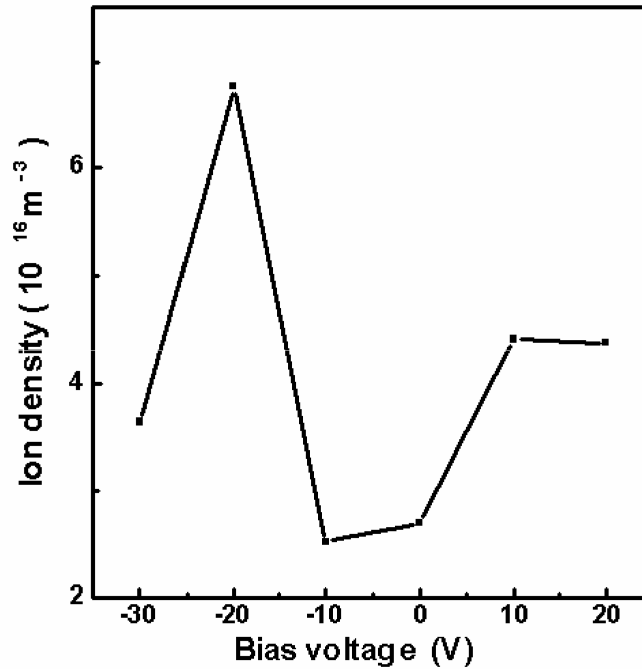

Figure 6.7. Variation of ion density with RF power

With increase in bias voltage, both for positive and negative biases, an increase in ion density was observed except for -30V. It was maximum for a bias voltage of –20V. The maximum value for ion density was observed for a bias voltage of -20V. This may be due to the greater growth rate at that bias voltage. The reduced growth rate at -30V caused a decrease in ion density. Best film properties such as good crystallinity and better conductivity were observed corresponding to a bias voltage of -20V.

Figure 6.8 shows the variation of electron temperature with bias voltage. The electron temperature increased when the bias voltage was decreased from +20V to 0V and then to –20V.

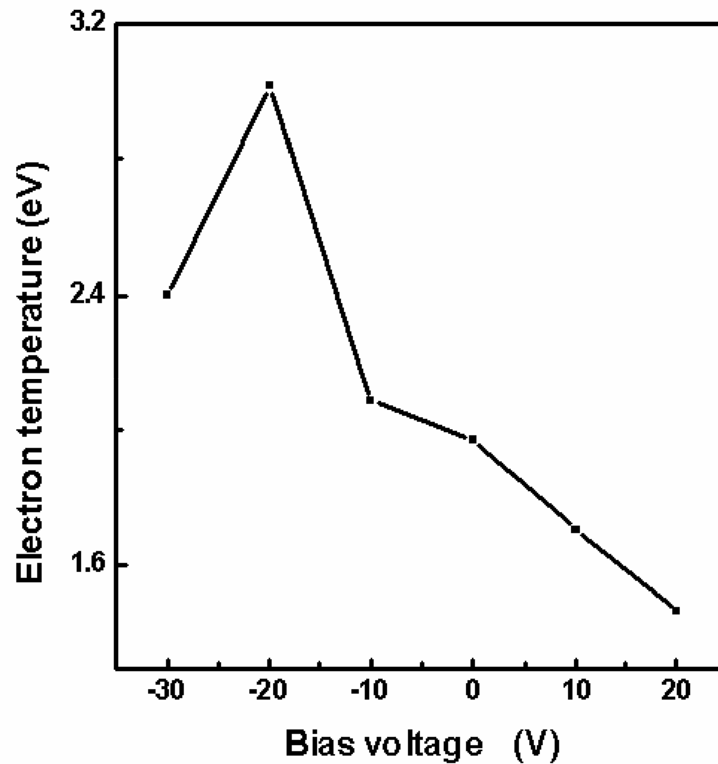

Figure 6.8. Variation of electron temperature with RF power

The maximum value of electron temperature was observed for a bias voltage of –20V. When the bias voltage was further made to decrease to –30V the electron temperature decreased. Variation of ion and electron velocity is shown in figure 6.9. Velocity of electrons is found to be of the order of 10^6 ms^{-1} while that of ions is of the order of 10^3 ms^{-1}. Both ion velocity and electron velocity attained a maximum value for a bias voltage of -20V. The degradation in film properties at higher negative biases may be due to resputtering effects.

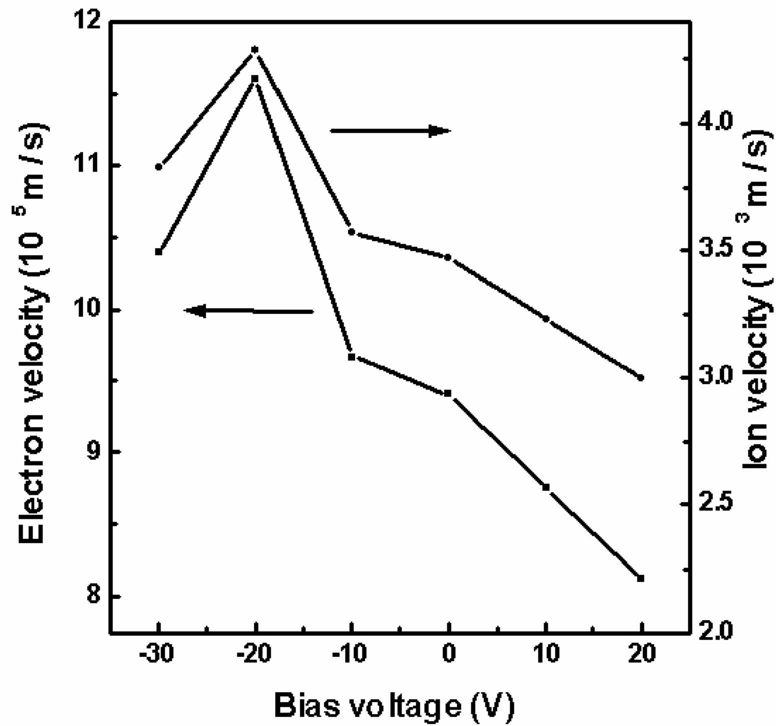

Figure 6.9. Variation of electron and ion velocity with RF power

6.3.4 Optical Emission spectral Studies

RF plasma generated during the sputtering of ITO target was analysed by recording the optical emission spectra to identify the ionic species in the plume. The spectral analysis revealed that the ionic species is mainly composed of argon ions[16]. The identified species essentially comprises argon neutrals (Ar I), singly ionised argon (Ar II), doubly ionised argon (Ar III), indium neutral (InI), oxygen neutral(OI) and tin neutral (SnI). Figure 6.10 gives a typical OES spectrum taken at an RF power of 20W. The spectral data is collected from the plasma at a distance of 4cm from the target.

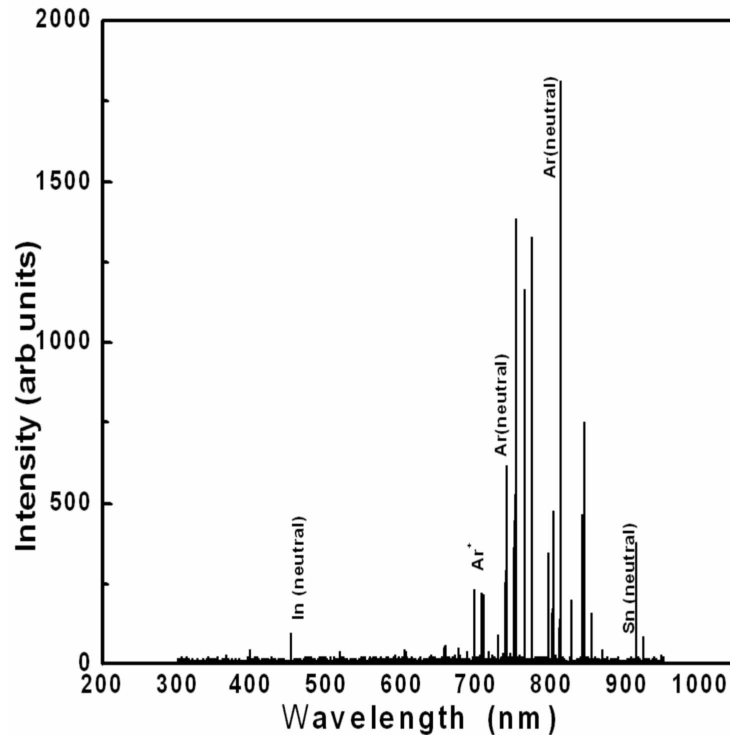

Figure 6.10 Typical optical emission spectrum of the plasma generated during the sputtering of ITO target. RF power = 30W and bias voltage = -20V

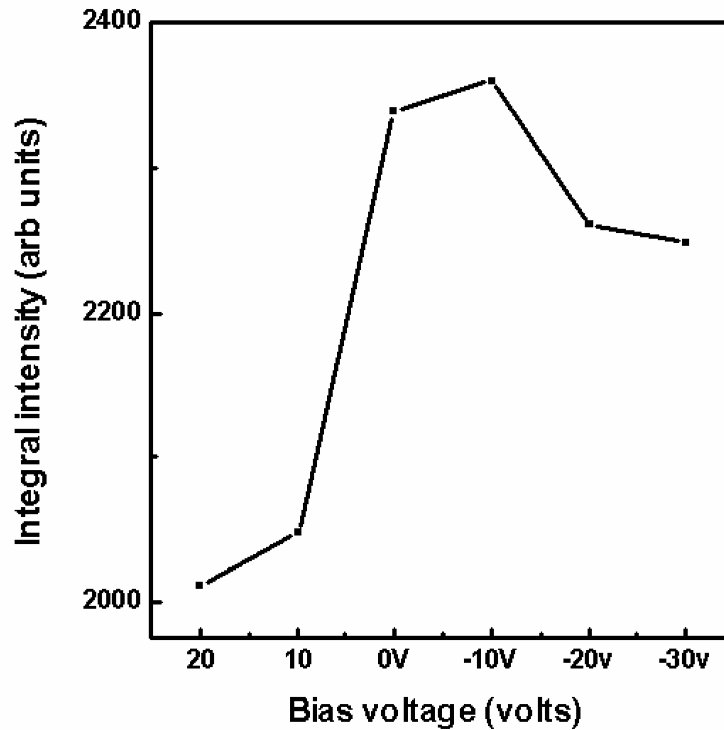

Figure 6.11. Variation of integral intensity of the spectral line at 751.5nm with RF power.

The integral intensity of the emission line at 751.5nm was evaluated by integrating the peak. The variation of integral intensity with bias voltage is plotted in figure 6.11. It is found that integral intensity is greater when the substrate is biased negatively. With increase in positive bias the integral intensity is found to reduce considerably.

6.4 Conclusion

ITO films were prepared at room temperature by RF bias sputtering on polyimide substrates. The influence of bias voltage on the structural and

electrical properties was investigated. The films deposited at negative bias voltages showed a preferred orientation along [111] direction while positive bias voltages resulted in poorly crystalline films. The maximum grain size of about 28nm and a minimum resistivity of 2.24×10^{-2} Ωcm were obtained for the film deposited onto substrates biased at –20V. The plasma parameters during the deposition was analyzed using Langmuir probe technique and the observed plasma parameters were correlated with the film characteristics.

References

1. F.L.Wong, M.K.Fung, S.W.Tong, C.S.Lee, S.T.Lee, Thin Solid Films **466**(2004)225
2. Z.Yang, S.Han, T.Yang, L.Ye, H.Ma, C.Cheng, Appl. Surf.Sci **161** (2000)279
3. A.Salehi, Thin Solid Films **214**(1998)324
4. S.Seki, Y.Sawada, T.Nishide, Thin Solid Films **388**(2001)22
5. H.Kim, J.S.Horwitz, G.Kushto, A.Pique, Z.H.Kafafi, C.M.Gilmore, D.B.Chrisey,J.Appl.Phys. **88**(2000)6021
6. Y.Shigesto, D.C.Paine, Thin Solid Films **238**(1994)44
7. D.Kim, Y. Han, Jun-Sik Cho, Seok-Keun Koh, Thin Solid Films, **377-378**(2000)81
8. F.L.Akkad,A.Punnose, J.Prabu, J.Appl.Phys.A **71**(2000)157
9. Z.W.Yang, S.H.Han,T.L.Yang, Lina Ye, D.H.Zhang, H.L.Ma, C.F.Cheng, Thin Solid films **366**(2000)4
10. R.Huddlestone , S.L.Leonard, Plasma diagnostic techniques Academic Press, London (1995)
11. Joint Committee on Powder Diffraction Standards,Powder Diffraction File Card No.6-416, ASTM, Philadelphia,PA (1967)
12. H.L.Ma, X.T. Hao, J.Ma et al, Surf. And Coat.Technol **161**(2002)58
13. M.Lavanya, O.N.Balasundaram, G.Mohan Rao, Proceedings of NACTTA-2002, edited by O.N.Balasundaram et. al (2002)77
14. Aldrin Antony, Nisha M., Manoj R., M.K. Jayaraj, Appl. Surf. Sci. **225** (2004) 294
15. J.E.Heidenreich III, J.R.Paraszczak, M.Moisan, G.Suave, J.Vac.Sci.Technol. B. **5**(1987) 347.
16. J.R.Fuhr, W.L.Weise, Handbook of Chemistry and Physics, 79th Edn, edited by D.R.Lide , CRC, Boca Raton, FL(1998)10

CHAPTER 7

Summary and Outlook

7.1 Summary

Transparent conducting oxides occupy an important role in various fields of research and industry. Recent trends in transparent electronics show that these materials are essential parts of various devices. The development of p and n-type TCOs has made possible the fabrication of various transparent devices such as transparent diodes, thin film transistors and field effect transistors. Among the various n-type TCOs, tin doped indium oxide (ITO) is an attractive material for various optoelectronic applications because of its properties such as high transmittance in the visible region and high electrical conductivity. Since the properties of ITO film strongly depend on the deposition conditions, the optimisation of the process parameters is an essential factor. With this outlook we have optimized the process parameters for the deposition of ITO thin films by RF magnetron sputtering.

RF magnetron sputtering was employed for the deposition because of the possibility of getting films with the same composition as the target. Also, the relatively high growth rate during sputtering process minimizes the possibility of incorporation of impurities in the grown films. Sputtering also helps to deposit films on large area substrates. Different characterisation tools such as, X-ray diffraction, optical transmission studies, electrical resistivity measurements, energy dispersive x-ray analysis, scanning electron microscopy etc. were used to analyse the structure, morphology, composition, electrical and optical properties of the materials prepared. Another important aspect of the present study is the analysis of RF plasma during the sputtering process. This was carried out by employing Langmuir probe and optical emission spectral studies.

The ITO thin films were optimized by depositing the films under various conditions. The post deposition heat treatment of the films under high vacuum conditions improved the transparency and conductivity of the film. An annealing temperature of 250^0C was found to be optimum for getting best figure of merit.

Substrate temperature is another important parameter that influences the properties of ITO thin films. The studies on ITO thin films deposited at various substrate temperatures revealed that increase in substrate temperature upto a certain value favors the growth of crystalline films with better electrical and optical properties. In the present study, a substrate temperature of 150^0C was found to be the optimum temperature. The influence of RF power on the properties of the films were also investigated. Films deposited at an RF power of 40watts showed the greater figure of merit. A simultaneous measurement of the plasma parameters were also carried out and the film properties were correlated with the plasma parameters [1].

Flexible devices are now becoming an integral part of research and industry. The deposition on flexible substrates will require lower processing temperature. This can be achieved by biasing the substrate. The substrate bias will be providing the effect similar to that of heating the substrate. In the present investigation, ITO thin films were grown on flexible substrates by bias sputtering. A bias voltage of -20V provided films with better crystallinity and conductivity. The analysis on plasma parameters also showed a correlation with the observed film properties. The optimized ITO thin films can be used for various device applications. It can be used as transparent electrode in various display devices, thin film transistors and transparent thin film field effect transistors. The possibility of deposition over plastic substrates at relatively lower temperatures opens up a new window in the field of flexible devices.

References

1. M.Nisha, K.J.Saji, R.S.Ajimsha, N.V.Joshy, M.K.Jayaraj, J.Appl.Phys. **99** (2006) 033304